AN ABSTRACT OF THE THESIS OF

Khavinet Lourvanij for the degree of Doctor of Philosophy in Chemical Engineering presented on May 8, 1995. Title: Partial Dehydration of Glucose to Oxygenated Hydrocarbons in Molecular-Sieving Catalysts.

Redacted for Privacy

Abstract approved: _____

Gregory L. Rorrer

Molecular-sieving catalysts have the potential to selectively promote the production of oxygenated hydrocarbons from glucose, a renewable chemical feed stock. Solid-acid molecular-sieves, including HY-zeolite, microporous pillared montmorillonite, and mesoporous MCM catalysts, possess pore diameters ranging from 7 to 40 Å and acid activity ranging from 0.5 to 1.0 mmol H^+/g-catalyst. A pore size of at least 10 Å allows the 8.6 Å glucose molecule to diffuse and react directly within the pores of the catalysts.

Reactions of 0.75 M glucose solution with catalyst powder were conducted in a well-mixed batch reactor at 130 to 190°C. The Fe-pillared montmorillonite had the highest glucose conversion rate (k_{app} = 0.427 h^{-1}), the lowest selectivity of reaction intermediate HMF (0.04 mol/mol glucose reacted), and the highest selectivity of formic acid (0.6 mol/mol glucose reacted) at an optimum temperature of 150°C.

A reaction model was developed for the dehydration of glucose to organic acids by solid-acid, molecular-sieving catalysts. Kinetic parameters proposed by the model were estimated from glucose conversion and product formation rates for HY-zeolite, Al-pillared

montmorillonite, MCM-20, and MCM-41 catalysts under conditions where mass transfer resistances were minimized. Rate constants for the dehydration of glucose to HMF and rehydration of HMF to organic acids were maximized at a 10 to 30 Å pore size range, whereas rate constants for the competing parallel reactions of glucose isomerization to fructose and fructose dehydration to HMF were minimized. The final organic acid product yields were low due to significant coke formation. The predicted coke formation from HMF and organic acids was also minimized at a 10 to 30 Å pore size range. The model consistently over predicted the coke formation relative to the measured coke, suggesting the formation of water-soluble humic solids.

The deactivation of HY-zeolite was due to the blockage of acid sites by product molecules adsorbed on catalyst pore wall. The decrease in reaction activity for both glucose isomerization to fructose and fructose dehydration to HMF was due to an anti-selective poisoning process which assumed a homogeneous site blockage. The reaction activity of HMF rehydration to organic acids was not, however, influenced by catalyst deactivation.

Partial Dehydration of Glucose to Oxygenated Hydrocarbons in Molecular-Sieving Catalysts

by

Khavinet Lourvanij

A THESIS

submitted to

Oregon State University

in partial fulfillment of
the requirements for the
degree of

Doctor of Philosophy

Completed May 8, 1995
Commencement June 1995

Doctor of Philosophy thesis of Khavinet Lourvanij presented on May 8, 1995

APPROVED:

Redacted for Privacy

Major Professor, representing Chemical Engineering

Redacted for Privacy

Chair of Department of Chemical Engineering

Redacted for Privacy

Dean of Graduate School

I understand that my thesis will become part of the permanent collection of Oregon State University libraries. My signature below authorizes release of my thesis to any reader upon request.

Redacted for Privacy

Khavinet Lourvanij, Author

TABLE OF CONTENTS

TABLE OF CONTENTS (Continued)

LIST OF FIGURES

LIST OF FIGURES (Continued)

LIST OF TABLES

LIST OF APPENDICES

LIST OF APPENDIX FIGURES

LIST OF APPENDIX FIGURES (Continued)

LIST OF APPENDIX TABLES

LIST OF APPENDIX TABLES (Continued)

LIST OF APPENDIX TABLES (Continued)

LIST OF APPENDIX TABLES (Continued)

NOMENCLATURE

$\boldsymbol{A_i}$	Jacobian matrix of component "*i*"
$A_{C,i}$	peak area of component "*i*" by calibration, counts-sec
A_S	peak area of internal standard, counts-sec
A_p	external surface area of catalyst particle, cm^2/g
a_X	acid activity, mmol H^+/g-catalyst
$a_{X,f}$	acid activity after 24 h reaction, mmol H^+/g-catalyst
$\boldsymbol{C}$	vector of concentration C_G, C_H, C_F, C_{FA}, C_{OA}, C_X, and $C_{v,X}$
$C_{C,i}$	concentration of component "*i*" by calibration, mg/mL
C_{cat}	catalyst loading, g catalyst/L
C_i	bulk liquid phase concentration of component "*i*", mol/L
$C_{i,l}$	calculated liquid phase concentration of component "*i*" at "*l*", mol/L
$C^*_{i,l}$	experimental liquid phase concentration of component "*i*" at "*l*", mol/L
$C_{i,p}$	concentration at outer surface of particle for component "*i*", mol/cm^3
$C_{i,X}$	concentration of component "*i*" adsorbed on catalyst surface, mol/L
$C_{T,G,0}$	initial concentration of glucose loaded to the reactor, mol/L
$C_{T,i}$	total concentration of component "*i*", mol/L
$C_{v,X}$	concentration of vacant acid sites on catalyst surface, mol H^+/L
C_X	concentration of total acid sites on catalyst surface, mol H^+/L
D	sum of gas molecule and sample molecule diameters, Å
DA	diameter of gas molecule, Å
DS	diameter of sample molecule, Å

$D_{G,e}$	effective diffusion coefficient of glucose within the catalyst, cm^2/s
D_G	molecular diffusivity of glucose in water, cm^2/s
D_I	impeller diameter, cm
D_ρ	density conversion factor, cm^3 liquid/cm^3 STP
d_{001}	basal spacing, Å
d_p	particle size of catalyst, μm
d_{pore}	pore diameter of catalyst, Å
$d_{pore,A}$	adjusted pore diameter, Å
E_{Sj}	activation energy of surface reaction "j", kcal/mol
E_{app}	apparent activation energy, kcal/mol
F_{sj}	activity ratio of surface reaction "j"
g_i	rate equation of component "i", mol/L-h
HETP	height equivalent to a theoretical plate, cm
h	total number of liquid phase components
IP	interaction parameter, 10^{-43} ergs-cm^4
K	Avogadro's number, 6.023 x 10^{23} molecules/mol
K_i	adsorption equilibrium constant of component "i", L/mol
K_{Sj}	equilibrium constant of surface reaction "j"
$\boldsymbol{k}$	vector of model parameters: k_{S1}, k_{S2}, $1/K_{S1}$, k_{S3}, k_{S4}, k_{S5}/C_X, k_{S6}, k_{S7}, K_G, K_H, K_F, K_{FA}, and K_{OA}
k_{Sj}	forward reaction rate constant of surface reaction "j", 1/h
k_c	mass transfer coefficient, cm/s

k_{app}	apparent rate constant, 1/h
$ln(A)$	Arrhenius constant
$m_{I,i}$, $m'_{I,i}$	parameter # I using in the Runge-Kutta method for component "i"
$m_{C,i}$	mass of component "i" using in an instrument calibration, mg
m_S	mass of internal standard, mg
N	impeller speed, rps
N_p	power number
n_i	total number of experimental data points for component "i"
P	power input, erg/s
p	equilibrium pressure, mm Hg
p_o	saturated pressure, mm Hg
R	gas constant, 8.314 x 10^7 ergs/mol-K
Re	Reynolds number
$R_{F,i}$	response factor of component "i"
$r_{i,app}$	pseudo-homogeneous reaction rate (apparent rate), mol/cm^3-s
$r_{i \cdot X}$	surface reaction rate, mol/cm^2-s
S	BET surface area, m^2/g
SSR_I	weighted sum of squared residuals at iteration "I"
Sh	Sherwood number
$S_{p,i}$	maximum selectivity of component "i", mol of "i"/mol glucose reacted
t	reaction time, h
T	absolute temperature, K
t_0	initial value of reaction time, h

t_f	final value of reaction time, h
Δt	increment of time, h
W	mass of liquid in slurry, g
w_i	weighting factor corresponding to component "i"
X_G	glucose conversion
U	interstitial velocity, cm/min
V_{CUM}	cumulative pore volume, cm^3/g
V_G	molar volume of glucose, cm^3/mol
V_l	measured volume of gas at point "l" for Horvath-Kawazoe calculation, cm^3
V_p	volume of catalyst particle, cm^3/g
ZA	gas equilibrium diameter at zero interaction energy, Å
ZS	sample equilibrium diameter at zero interaction energy, Å

Abbreviations

F	fructose
FA	formic acid
G	glucose
H	5-hydroxymethylfurfural (HMF)
OA	4-oxopentanoic acid
R_i	coke or carbon complex from component "i"
X	acid site on catalyst surface

Greek Symbols

αI	diagonal matrix used in the Marquardt method
δ	gas-solid nuclear separation at zero interaction energy, Å
Φ_T	Thiele modulus
Φ_W	Weisz modulus
γ	ratio of glucose conversion rate to external mass transfer rate
η	effectiveness factor
λ_i	ratio of long axis of component "i" to mean pore size diameter
μ	corrected first moment, min
μ_L	viscosity of liquid, cp
ν	kinemetic viscosity, cm^2/s
θ	deactivation ratio of acid sites on catalyst surface
ρ_L	density of liquid, g/cm^3
ρ_p	density of catalyst particle, g/cm^3
σ^2	corrected second moment, min^2
σ^2_i	variance for each vector of the "i" component
ω	energy dissipation rate, erg/s-g
ζ	Eddy size, μm

PARTIAL DEHYDRATION OF GLUCOSE TO OXYGENATED HYDROCARBONS IN MOLECULAR-SIEVING CATALYSTS

Chapter 1

INTRODUCTION

Glucose is a inexpensive, abundant, and renewable resource obtained from plant biomass. Therefore it is attractive feedstock for production of useful organic chemicals. Fermentation is the most common process for converting glucose to value oxygenated hydrocarbons such as alcohols, organic acids, and ketones. However, fermentation-based processes for production of oxygenated hydrocarbons are often not economically viable due to inherent process limitations, including long residence times, low yields, and narrow range of process conditions. Also, significant amounts of carbon in the feed are lost to carbon dioxide.

To address the problems of fermentation processes, alternative processes using solid inorganic catalysts for production of industrially-significant chemicals from glucose need to be explored. It is well known that catalysts generally improve reaction rates under a broad range of process conditions. Furthermore, solid-liquid system using the catalyst as the solid phase can solve problems involving the reuse of catalyst, conversion of reactants, and separation of products. In particular, the use of solid-acid catalysts to promote reaction of glucose to oxygenated hydrocarbons deserves consideration.

Molecular sieves such as zeolite and pillared clays can serve as solid-acid catalysts. These molecular-sieving catalysts can improve the yield and selectivity of chemical reactions. The molecular-sized channels within these catalysts control the access of molecules of a desired size and shape to active sites within the porous matrix of the catalyst. Since it is well established that glucose can be dehydrated by mineral acids, it is appropriate to explore how solid-acid, molecular-sieving catalysts can promote selectivity to reaction products. The partial dehydration of glucose to organic acids at temperatures low enough to prevent coke formation is of special interest.

The partial dehydration of glucose to organic acids within a molecular-sieving catalyst is proposed in Figure 1-1. The glucose molecules diffuse into the pores and are dehydrated by acid sites to 5-hydroxymethylfurfural (HMF) molecules. The acid-catalyzed rehydration of HMF yields the linear molecules of formic acid and 4-oxopentanoic acid. A shape-selective reaction process for organic acids production can be promoted by trapping the large molecule of HMF within the porous matrix, while allowing smaller organic acid products to diffuse out of the porous matrix.

In this research, the feasibility of using solid-acid, molecular-sieving catalysts for conversion of glucose to oxygenated hydrocarbons is studied. Molecular-sieving catalysts including Y-zeolite, pillared clay, and mesoporous MCM catalysts are prepared and characterized. The reaction of aqueous glucose with these solid-acid catalyst powders are studied in a well-mixed batch reactor by measuring the conversion of glucose and the yield of oxygenated hydrocarbon products as a function of reaction time, process conditions, and catalyst properties.

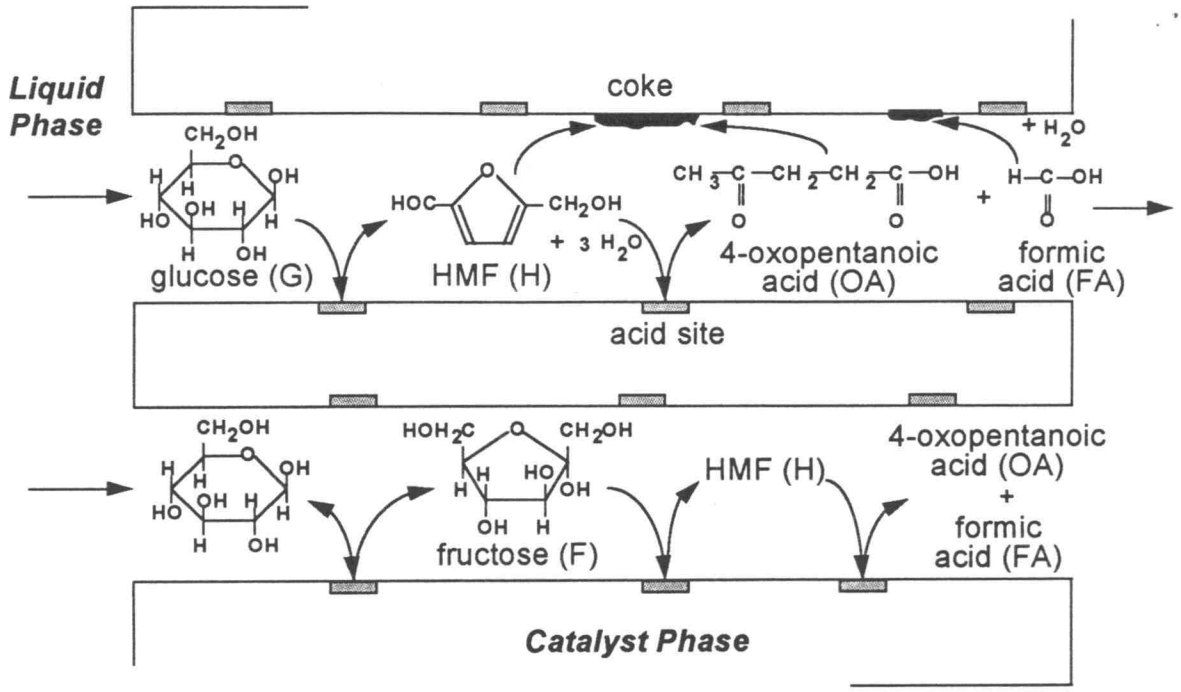

Figure 1-1. Proposed intraparticle diffusion and reaction scheme of glucose within porous matrix of the molecular-sieving catalyst.

A kinetic model and the rate equations for partial dehydration of glucose to organic acids are developed based on a heterogeneous system of first-order reaction processes. Model parameters, including reaction rate constants and adsorption equilibrium constants for each reaction step, are estimated from the glucose conversion and product formation data by non-linear regression. The kinetic model parameters are correlated to the properties of each catalyst. From this information, a concept for shape-selective dehydration of glucose to organic acids within solid-acid, molecular-sieving catalysts can be proposed.

This research has two major goals. The first goal is to explore the feasibility of using solid-acid, molecular-sieving catalysts to promote the shape-selective reactions of glucose to oxygenated hydrocarbons with a high yield and selectivity at fairly low temperatures (100 to 190°C). Molecular-sieving catalysts with pore sizes larger than glucose molecule (9 Å) in the microporous to mesoporous range of 10 to 50 Å are of particular interest. The second goal is to elucidate the reaction kinetics and transport processes associated with the partial dehydration of glucose to organic acids in molecular-sieving catalysts and to develop kinetic model which describes these processes. The effect of reaction and catalyst parameters on the dehydration of glucose and product selectivity are studied. Catalyst parameters of interest include type of the molecular-sieving catalyst, pore size of the catalyst, and acid activity of the catalyst.

There are five specific objectives of this research:

1. Synthesize solid-acid, molecular-sieving materials with pore size from 10 to 50 Å (pillared clay and mesoporous MCM catalysts);
2. Characterize the internal surface area, pore size distribution, and acid activity of the synthesized catalysts;
3. Conduct batch-reactor experiments with aqueous glucose solution for each of the synthesized catalysts, and determine the effect of reaction parameters and catalyst properties to the shape-selective dehydration from glucose conversion and product formation;

4. Develop a kinetic model and rate equations for partial dehydration of glucose to organic acids within aluminosilicate, molecular-sieving catalysts under conditions where mass transfer processes are minimized; and

5. Estimate kinetic model parameters, including rate constants and adsorption equilibrium constants for each reaction step, and correlate to the reaction parameters and catalyst properties, especially, mean pore size.

Chapter 2

LITERATURE REVIEW

Previous work has established the feasibility of glucose dehydration to oxygenated hydrocarbons using various kinds of acid catalysts. It is well known that the sequential dehydration of glucose to furan derivatives and organic acids is promoted by mineral acids (Kuster and Van der Baan, 1977; Baugh and McCarty, 1988) and acidic ion exchange resins (Schraufnagal and Rase, 1975). However, the dehydration of glucose with solid-acid catalysts has not been well studied. Previous studies on the reaction of glucose or other carbohydrates with solid-acid catalysts focused on hydrocarbons production at high temperatures. For example, the dehydration of glucose over HZSM-5 zeolite catalyst of 5 Å nominal pore diameter was studied at temperatures of 300°C and greater ((.en et al., 1986; Haniff and Dao, 1988). These studies did not attempt to investigate the molecular-sieving capability of zeolite for the selective reaction of glucose because the high reaction temperature could promote the complete dehydration and coke formation.

Recently, the reaction kinetics of the partial dehydration of glucose to organic acids was studied at moderate temperatures of 110 to 160°C using solid-acid Y-zeolite catalysts (Lourvanij and Rorrer, 1993). This catalyst promoted partial dehydration of glucose to 5-hydroxymethylfurfural (HMF) and the subsequent rehydration of HMF to formic acid and 4-oxopentanoic acid. Thus, the reaction system did not fully exploit the molecular-sieving properties of this catalyst because the 8.6 Å glucose molecule could not directly diffuse in the 7.4 Å microporous matrix of the Y-zeolite. This prior work

suggests that other microporous catalysts with pore sizes large enough to accommodate the 8.6 Å glucose molecule for direct intraparticle reaction may improve both glucose reaction rate and product selectivity. In this regard, solid-acid pillared clays and mesoporous crystalline materials are attractive molecular-sieving catalysts for promoting acid-catalyzed partial dehydration of glucose.

Pillared clay catalysts typically consist of layered montmorillonite sheets propped up by intercalated metal-polyoxycation pillars. This arrangement provides a lamellar, microporous structure consisting of slit-like pores which provide internal surface areas as large as 300 m^2/g and gallery height of 10 Å or greater. For example, iron-pillared montmorillonite and chromium-pillared montmorillonite have nominal pore slit widths of 12 to 19 Å (Rightor et al., 1991; Pinnavaia et al., 1985). Clays pillared by polyoxycations can be converted upon dehydration and dehydroxylation to intercalates containing molecular-size oxide aggregates and protons which provide Bronsted acid activity (Pinnavaia et al., 1985). For intraparticle diffusion and reaction of glucose, the aluminum-, chromium-, and iron-pillared montmorillonites are of particular interest. These catalysts possess pore sizes large enough to accommodate the 8.6 Å glucose molecule for direct intraparticle diffusion and reaction. However, the pore size distribution is still microporous so that molecular-sieving reactions can be promoted.

Mesoporous Crystalline Materials (Mobil MCM), a family of mesoporous alumino-silicates, recently synthesized by the liquid crystal templating technique of Beck et al. (1992). This mesoporous MCM catalyst possesses uniform mesopores, which can vary from 20 Å to 65 Å depending on the molecular size of the template, and also possesses

large surface areas of 500 m^2/g or greater. The synthesis of MCM using an alkaline aluminate source and a two-step calcination in nitrogen and air stream reduces the degree of dealumination. Therefore, thermal stability, textural properties, and proportion of Bronsted acid sites are improved (Corma et al., 1994). The hexagonal array of uniform channels within the MCM catalysts can accommodate a glucose molecule for intraparticle reactions and possibly promote shape-selective reactions. The large channel size can also accommodate catalytically-active components such as carbonyl metal clusters $M_3(CO)_{12}$ (M = Ru, Os) for Fischer-Tropsch catalysis (Giannelis et al., 1988) embedded inside these channels without losing the effective pore size. The mesoporous MCM has the potential to be applied to other catalytic reactions as well.

Reaction kinetic models and rate equations have been developed for the reaction of monosaccharides and polysaccharides with mineral acids in a homogeneous reaction system (Kuster, 1977; Baugh and McCarty, 1988; Baugh et al., 1988). The series reaction model of sugars to furan derivatives and furan derivatives to organic acids was proposed. The humic solid formation was also considered as parallel reactions of sugars and furan derivatives. First-order rate equations for each reaction step were analytically solved with the rate constants correlated to the pH and the concentration of acid in the reaction. Unfortunately, this study did not consider the heterogeneous reaction mechanism and kinetic model for the partial dehydration of glucose to organic acids within molecular-sieving catalysts.

In this research, the series reactions for partial dehydration of glucose to organic acids are studied to explore how selectivity can be promoted by molecular-sieving

catalysts. Such reactions must be carried out a temperatures below 200°C in order to prevent total dehydration of glucose to hydrocarbons and coke. A kinetic model and rate equations for partial dehydration of glucose within molecular-sieving catalysts are developed to characterize this particular heterogeneous reaction system.

Chapter 3

EXPERIMENTAL METHODS AND DATA ANALYSIS

3.1 Catalyst Preparation

3.1.1 Y-zeolite Catalysts

Ultrastable Y-zeolite powder in hydrogen form was obtained from the PQ Catalyst Corporation under the product label VALFOR CP300-35. This solid-acid HY-zeolite is a Faujasite aluminosilicate possessing a unit cell size of 24.35 Å, SiO_2/AlO_3 molar ratio of 6.5, and Na_2O composition of 0.18 wt%. The Y-zeolite pore matrix consists of 7.4 Å diameter pores connected to 13 Å diameter cages arranged in cubic symmetry.

3.1.2 Pillared Clay Catalysts

Sodium montmorillonite, a smectite clay with sodium (Na) exchange sites, was obtained from Southern Clay Products (Gonzales, TX). Pillared clay catalysts were synthesized by propping up the montmorillonite sheets with metal-polyoxycation pillars to form intercalated clay materials with microporous structure. The gallery height, or pore slit width between montmorillonite layers, is dependent on the type of metal-polyoxycation pillar and the synthesis conditions used to prepare the pillaring agent. The gallery height is also dependent on the conditions of drying and/or calcination.

A series of pillared montmorillonite catalysts were prepared. Preparation of iron-pillared montmorillonite (FPM), adapted from Rightor et al. (1991) is briefly described

here to illustrate the basic procedures. First, the pillaring agent was prepared by hydrolyzing 0.2 M $FeCl_3$ with Na_2CO_3. The amount of Na_2CO_3 added to the 0.2 M $FeCl_3$ solution corresponded to ratio of 1.5 mole equivalents of hydroxyl ion per mole of metal ion at 25°C. This reaction was carried out for 24 h to polymerize the iron hydroxy cation according to the reaction: $[Fe(OH)_2^+]_n + Fe^{+3} + 2H_2O \rightarrow [Fe(OH)_2^+]_{n+1} + 2H^+$. After polymerization, the solution was sparged with nitrogen gas to remove dissolved CO_2. Sodium montmorillonite powder was mixed into the pillaring agent solution until a ratio of 70 mmole iron per mole-equivalents of montmorillonite (empirical formula $Na[Si_{13.09}Al_{4.10}Mg_{0.58}Ca_{0.17}K_{0.03}Ti_{0.01}O_{34.47}Fe_{0.57}]$) was established. The slurry was stirred at 25°C for 4 h to insert the metal-polyoxycations between the montmorillonite sheets. The pillared clay material was centrifuged and then washed in water at least 10 times to promote final hydrolysis of the clay-bound iron-polyoxycations and to provide a uniform gallery height (Rightor et al., 1991). The material was then dried in air, and degassed at 110°C for 10 h prior to surface area and pore-size distribution measurements. The dried pillared clay was ground in a mortar and pestle and sieved to a 100 μm powder.

Chromium-pillared montmorillonite (CPM) was prepared as described by Pinnavaia et al. (1985) and aluminum-pillared montmorillonite (APM) was prepared according to Doblin et al. (1991).

The unpillared sodium montmorillonite (HM) was converted to its solid-acid form by treatment with 0.1 N HCl at room temperature for 12 h. During this process, sodium atoms in the aluminosilicate clay matrix were exchanged with hydronium ions to form Bronsted solid-acid sites.

3.1.3 Mesoporous MCM Catalysts

Mesoporous crystalline material (Mobil MCM-41) was synthesized by the liquid-crystal templating technique of Beck et al. (1992). Specifically, an aqueous solution of 29 wt% cetyltrimethylammonium chloride surfactant ($C_{16}H_{33}(CH_3)_3NCl$) was exchanged with IRA-400 (OH) resin (4 meq/g). Then, 100 g of the surfactant solution was mixed with 2.2 g sodium aluminate, 50 g tetramethyl ammonium silicate, and 12.5 g silica powder at 120°C for 24 h within a glass-lined Parr autoclave reactor at 350 rpm. The solid fraction was filtered from the slurry, washed with distilled water, and calcined sequentially in flowing N_2 and air at 540°C. The MCM-20 was prepared by the same procedures except for the surfactant solution. In the MCM-20 preparation, 50 wt% dodecyltrimethylammonium chloride ($C_{12}H_{25}(CH_3)_3NCl$) was used as the surfactant solution. The acidic activity of MCM-20 was increased by treating the catalyst powder in an aqueous slurry with a 0.1 N HCl solution until pH was equal to 2.0 at room temperature for 12 h.

3.2 Catalyst Characterization

Surface area and pore size distribution measurements were performed on a Micromeritics ASAP-2000 Surface Area and Porosimetry Analysis System. The BET surface area of the pillared clay catalysts was determined by static nitrogen physisorption at 77 K. Each sample was degassed at 110°C for 10 h prior to analysis. The micropore distribution was determined by pore-filling with increasing partial pressures of argon at

87.3 K. Each sample was degassed at 110°C for 10 h prior to analysis. The micropore analysis control module dosed the argon gas onto the degassed sample (0.1 g) in very small volumes so that detailed pore distribution data was obtained for micropore sizes less than 15 Å. The smallest pore diameter which could be conveniently analyzed was 5 Å, although 3.5 Å was the lower limit of resolution. The software provided with the ASAP-2000 estimated the micropore diameters by the Horvath-Kawazoe method of analysis (Horvath and Kawazoe, 1983) using the interaction parameter (I.P.) computed for Ar adsorbed on aluminosilicate (I.P. = 3.19 x 10^{-43} ergs-cm^4). The Horvath-Kawazoe method of analysis assumes the micropores have a slit geometry, which approximates the pore geometry in pillared clay, and MCM catalysts.

The pillared clay catalysts possessed micropores in the 5 to 20 Å range and both pillared clay and MCM catalysts possessed mesopores greater than 20 Å. The pore size distribution analysis was focused on micro- and mesopores in the 5 to 50 Å range. The upper limit of 50 Å was chosen for two reasons. First, the differential pore volume was less than 10% of the peak value at pore sizes above 50 Å. Second, about 50 Å was the maximum pore size which could be reasonably computed from argon pore-filling data given the equipment and methods employed. The mean micropore size over the pore size distribution range of 5 to 50 Å was computed by numerical integration of

$$\bar{d}_{pore} = \frac{\int_{d_{pore,1}}^{d_{pore,2}} d_{pore}\, f(d_{pore})\, d(d_{pore})}{\int_{d_{pore,1}}^{d_{pore,2}} f(d_{pore})\, d(d_{pore})} \qquad (3\text{-}1)$$

where $\overline{d}_{pore}$ is the is the mean pore size between limits $d_{pore,1}$ (5 Å) and $d_{pore,2}$ (50 Å) and $f(d_{pore})$ is the pore size distribution, obtained by differentiation of pore volume vs. pore size data.

The acid activity, expressed as the Bronsted acid site concentration (mmol H^+/g), was measured by a non-aqueous titration technique as described by Lourvanij and Rorrer (1993). The particle size distribution of each catalyst was measured by a Horiba CAPA-700 centrifugal automatic particle size distribution analyzer. The catalyst powder was sieved to the range of 20 to 100 μm prior to the particle size distribution measurement. The mean particle size of each catalyst was estimated by the integral average of the particle size distribution.

The effective diffusion coefficient of aqueous glucose within each catalyst at 30°C was measured by a liquid chromatography technique (Awum et al., 1988 and Ma et al., 1988). Detailed experimental procedures and data analysis techniques for the present measurements are given by Netrabukkana (1994).

The details of each catalyst preparation technique and catalyst properties are provided in Appendix A.

3.3 Molecular Dimensions

The molecular dimensions of glucose, HMF, formic acid, and 4-oxopentanoic acid were computed using Hyperchem Software (Version 2, Autodesk, Inc.). The critical molecular dimensions of each compound were determined from the least-hindered

conformation using bond angles, bond lengths, and Van der Waals radii. The largest long axis and short axis of each molecule are provided in Table 3-1.

Table 3-1. Molecular dimensions.

Molecule	Long Axis (Å)	Short Axis (Å)
Glucose	8.6	8.4
Fructose	9.8	8.5
HMF	9.3	5.9
Formic Acid	4.6	4.6
4-Oxopentanoic Acid	10.3	5.7

3.4 Batch Reactor Studies

A 300-mL stirred Parr autoclave reactor and control instrumentation was used for all reaction studies. In all experiments, 150 mL of 12 % wt (0.74 M) glucose solution and 5 g of catalyst powder were charged to the 300 mL reactor vessel. The mixing speed was fixed at 400 rpm and the temperature was set at either 130, 150, 170, or 190°C. Details on reactor operation and liquid phase sampling are described by Lourvanij and Rorrer (1993).

The concentration of sugars and oxygenated hydrocarbons in the liquid phase were determined by High Performance Liquid Chromatography, HPLC (Lourvanij and Rorrer, 1993). Since 4-oxopentanoic acid was not well resolved by HPLC, the concentration of

4-oxopentanoic acid was determined by gas chromatography (GC) using a Hewlett Packard HP 5890-II GC equipped with a flame ionization detector (FID). The samples were separated on a HP-FFAP capillary column (10 m x 0.53 mm x 1.0 μm) at a linear temperature program of 25°C/min. The initial temperature was 90°C and the final temperature was 180°C. The sample inlet temperature and detector temperature were 220°C and 240°C respectively. The carrier gas was helium at 10 mL/min. The retention time of 4-oxopentanoic acid was 11.2 min under these analysis conditions. The concentration of each identified component was quantified by the internal standard method of data analysis using butyric acid as the internal standard with a retention time of 6.1 min.

The amount of solid residue and the carbon content of the solid residue (coke) on the catalyst after a 24 h reaction time were gravimetrically determined (Lourvanij and Rorrer, 1993).

3.5 Apparent Rate Constant Estimation

The apparent rate constant for glucose conversion (k_{app}) at each temperature was obtained by fitting conversion (X_G) vs. time (t) data to a pseudo first-order rate equation of the form

$$ln\left(\frac{1}{1-X_G}\right) = k_{app} \cdot t \qquad (3\text{-}2)$$

The apparent activation energy (E_{app}) was obtained from the least-squares slope of an Arrhenius plot of $ln(k_{app})$ vs. reciprocal of temperature, $1/T$. The Arrhenius constant, $ln(A)$, was also obtained from the intercept of the fitting.

Chapter 4

EXPERIMENTAL RESULTS AND DISCUSSION

4.1 Catalyst Characterization

Pore size distributions in the range of 5 to 50 Å for aluminum-pillared montmorillonite (APM), chromium-pillared montmorillonite (CPM), iron-pillared montmorillonite (FPM), and unpillared montmorillonite (HM) catalyst powder are compared in Figure 4-1A. Pillaring montmorillonite with the metal-polyoxycations greatly opened up the micropore structure relative to unpillared montmorillonite. This result is also reflected in the large BET internal surface areas of the pillared montmorillonites relative to unpillared montmorillonite, as shown in Table 4-1. Solid-acid activities of CPM and FPM were comparable to HM. The APM had a solid-acid activity comparable to HY-zeolite. Rightor et al. (1991) pointed out that the air-dried form of the large-gallery catalyst is labile over prolonged periods at 25°C, with some loss of d_{001} ordering after three months. However, in our experiments, the pillared clay catalysts were always used for reaction studies within one week of preparation.

Pore size distribution in the range of 5 to 50 Å for MCM-20 and MCM-41 catalysts are compared in Figure 4-1B. The large differential pore volume of MCM-20 and MCM-41 catalysts are clearly in the mesopore size range and show a uniform pore size distribution. The BET surface area of MCM catalysts is large relative to pillared montmorillonite catalysts, as shown in Table 4-2. The peak for the MCM pore size

distribution within the range of 5 to 10 Å is attributed to the tiny imperfections in the crystalline structure of the pore wall itself.

The relatively broad micropore size distribution of the pillared clay catalysts relative to the HY-zeolite and MCM catalysts is most likely result of uneven polymerization of the hydroxy metal cations during the pillaring process (Rightor et al., 1991).

Table 4-1. Catalyst properties. The standard deviation for each catalyst property refers to replicate batches for catalyst preparations, except for HY-zeolite catalyst, where the standard deviation refers to repeated measurements on the same sample.

Catalyst	HY-zeolite	HM	APM	CPM	FPM
Mean Pore Diameter, $\bar{d}_{pore}$ 5 to 50 Å range (Å)	6.8 ± 0.2	17.2 ± 0.1	10.8 ± 0.6	12.0 ± 0.3	14.9 ± 0.7
BET Surface Area, S (m^2/g)	645.1 ± 3.0	40.9 ± 8.1	134.3 ± 3.9	249.6 ± 21.7	230.9 ± 7.0
Acid Activity, a_X (mmol H^+/g)	0.52 ± 0.01	0.90 ± 0.07	0.52 ± 0.01	0.98 ± 0.17	0.93 ± 0.15
Micropore Volume, V_{CUM} 5 to 50 Å range (mL/g)	0.243 ± 0.003	0.017 ± 0.001	0.057 ± 0.005	0.108 ± 0.003	0.122 ± 0.004
Percent of Accessible Volume in 10 to 50 Å	0.0	--	35	50	64

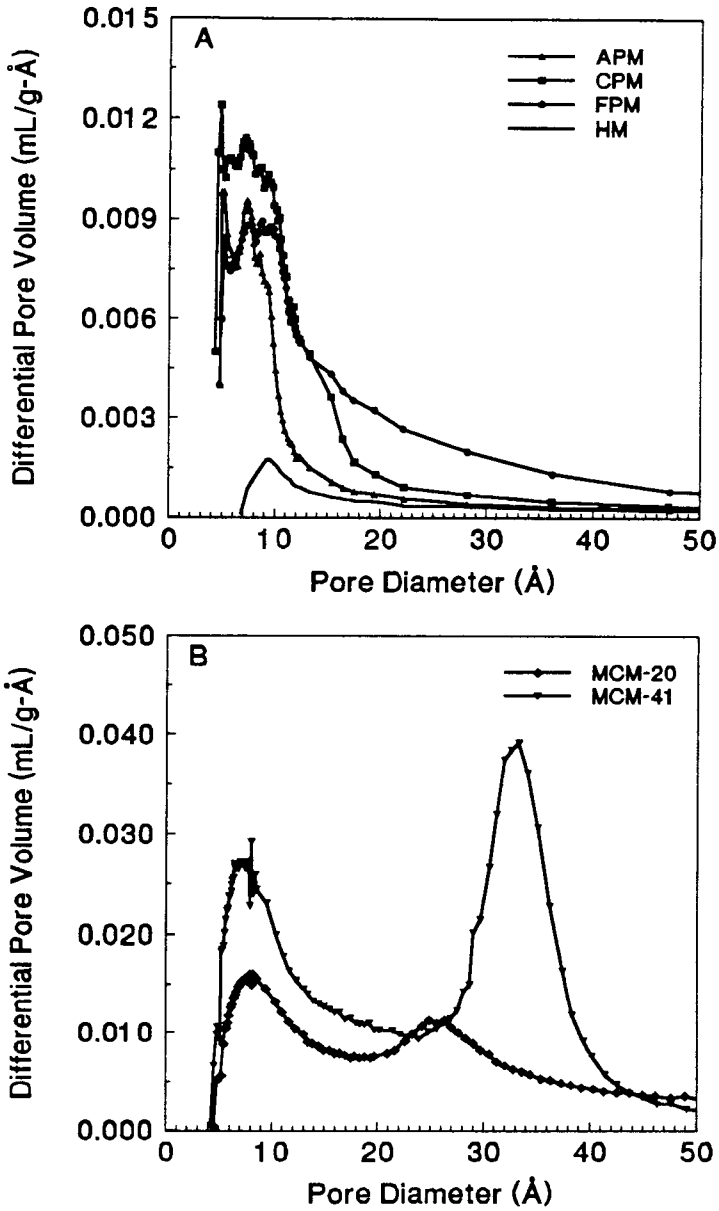

Figure 4-1. Pore size distribution in the 5 to 50 Å range for HM, APM, CPM, FPM, MCM-20, and MCM-41 catalysts.

Table 4-2. Properties of the molecular-sieving catalysts used in the kinetic modeling study. The standard deviation for each catalyst property refers to replicate batches for catalyst preparations, except for HY-zeolite and MCM-20 catalysts, where the standard deviation refers to repeated measurements on the same sample.

Catalyst	Pore Geometry	Mean Pore Diameter $\bar{d}_{pore}$ (Å)	BET Surface Area S (m^2/g)	Mean Particle Size $\bar{d}_p$ (μm)	Acid Activity a_X (mmol H^+/g)	Effective Diffusion Coefficient[(a)] $D_{G,e}$ (cm^2/s)
HY-zeolite	pores connected to cages in cubic symmetry	6.8 ± 0.2	645.1 ± 3.0	23.7	0.52 ± 0.01	1.77×10^{-9} ± 0.02×10^{-9}
APM	silicate sheets supported by Al-pillars	10.8 ± 0.6	134.3 ± 3.9	20.3	0.52 ± 0.01	2.83×10^{-9} ± 0.50×10^{-9}
MCM-20	hexagonal array of cylindrical pores	27.4 ± 0.3	541.8 ± 6.3	29.7	0.31 ± 0.02	9.09×10^{-9} ± 0.17×10^{-9}
MCM-41	hexagonal array of cylindrical pores	32.8 ± 0.5	799.8 ± 5.7	22.0	0.46 ± 0.01	17.10×10^{-9} ± 0.90×10^{-9}

[(a)] Glucose at 30°C

The calculated mean pore sizes in the range of 5 to 50 Å are also compared in Tables 4-1 and 4-2. Note that the FPM catalyst has the largest nominal mean pore size among the pillared clay catalysts, due primarily to the large fraction of pores in the 10 to 50 Å range. Since the pore size distribution plots for pillared clays are skewed toward the right, the mean pore sizes are best interpreted as relative values within a series of different catalysts. Furthermore, the mean pore size is very sensitive to the pore size distribution.

In order to promote intraparticle diffusion and reaction of the 8.6 Å glucose molecule, the micropores should be at least 10 Å because the first stable reaction product, HMF, has a nominal molecular dimension of 9.3 Å. In this regard, the MCM-41 has the most open pore structure in the 10 to 50 Å range, followed by the MCM-20, FPM, CPM, and APM respectively (Figure 4-1). The FPM and CPM pore size distributions are comparable between 5 and 12 Å, but FPM possesses a broader distribution in the 12 to 50 Å range. In contrast, the HY-zeolite, MCM-20, and MCM-41 catalysts are mono-disperse and possess a mean pore diameter of 6.8, 27.4, and 32.8 Å respectively. The MCM-20 and MCM-41 also possess a large pore volume per unit mass relative to other catalysts.

As shown in Table 4-2, the MCM-20 and MCM-41 catalysts have an acid activity comparable to APM and HY-zeolite catalysts.

4.2 Batch Reactor Studies

Reactions of aqueous glucose solution with HY-zeolite, pillared clay and MCM catalyst powder were carried out in a well-mixed, 300 mL Parr autoclave reactor. In all

experiments, the following process parameters were fixed: 1) initial glucose concentration of 12 wt% (0.75M or 20 g in 150 mL water solvent); 2) catalyst loading of 33 g/L (5 g in 150 mL reactor liquid volume); and 3) mixing speed of 400 rpm, which was sufficient to minimize external mass transfer resistances. The conversion of glucose and yield of selected products, including HMF, fructose, formic acid, and 4-oxopentanoic acid, were followed as a function of reaction time at temperatures ranging from 130 to 170°C. Batch reactor data for glucose conversion and product formation kinetics from HY-zeolite, pillared clay, and MCM catalysts are provided in Appendix F. Details on the effect of the catalyst type and the reaction temperature are provided below.

4.2.1 Effect of Catalyst Type

The effect of pillared clay catalyst type on the glucose conversion kinetics at 150°C is shown in Figure 4-2 for HM, CPM, and FPM powder. For comparison, glucose conversion kinetics at the same reaction conditions for HY-zeolite, APM, MCM-20, and MCM-41 powder are also provided in Figure 4-2. The glucose conversion rate was highest for the FPM. The pseudo-first order rate constant (k_{app}) for each catalyst was obtained by fitting glucose conversion vs. time data to a first-order rate equation. The apparent rate constants at 150°C are compared in Table 4-3. The FPM catalyst had the highest glucose conversion rate of the seven catalysts tested at 150°C.

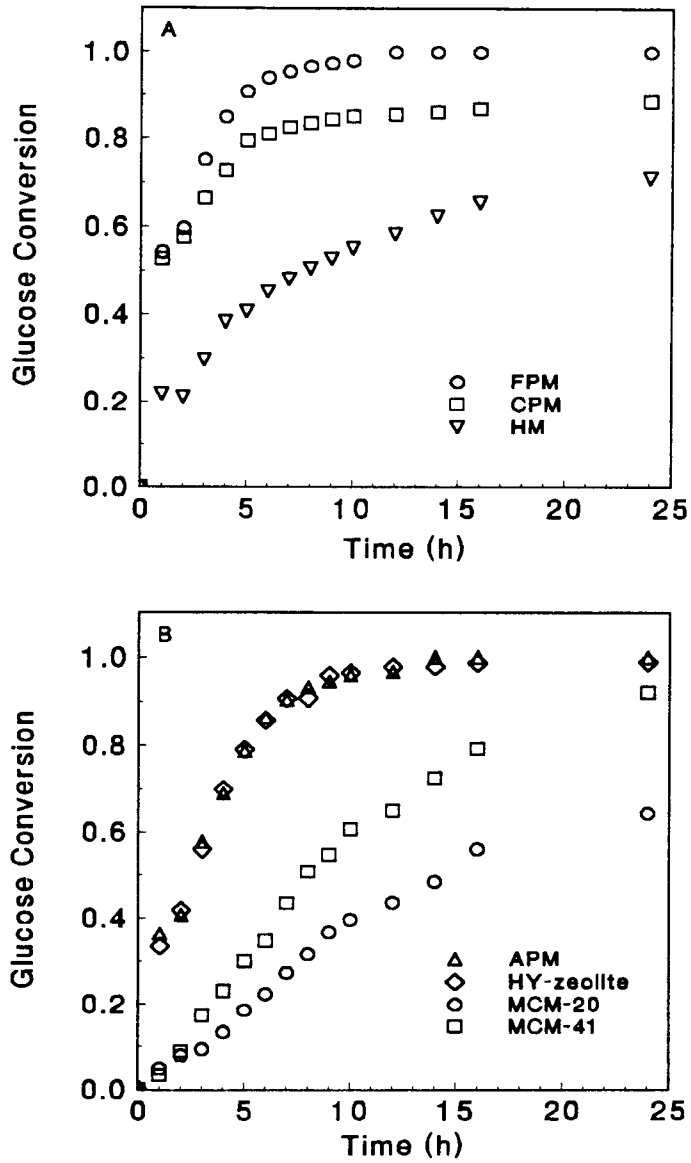

Figure 4-2. Glucose conversion vs. reaction time at 150°C for HY-zeolite, HM, APM, CPM, FPM, MCM-20, and MCM-41 catalysts.

Table 4-3. Apparent rate constants based on glucose conversion kinetics at 150°C for HY-zeolite, HM, APM, CPM, FPM, MCM-20, and MCM-41 catalysts.

Catalyst	k_{app} (1/h, ±1s)
HY-zeolite	0.256 ± 0.015
APM	0.313 ± 0.007
HM	0.068 ± 0.004
CPM	0.292 ± 0.022
FPM	0.427 ± 0.011
MCM-20	0.043 ± 0.001
MCM-41	0.096 ± 0.003

In our previous study (Lourvanij and Rorrer, 1993), a heterogeneous reaction scheme for dehydration of glucose with HY-zeolite catalyst powder in aqueous solution was proposed. The reaction scheme involved partial dehydration of glucose to HMF, rehydration of HMF to formic acid and 4-oxopentanoic acid, isomerization of glucose to fructose, and carbonization of reaction products to water-insoluble residue. In this present study, the same liquid-phase reaction products were obtained for unpillared montmorillonite, pillared montmorillonite, and MCM catalysts. In addition, seven other minor reaction products were isolated by HPLC but not chemically identified. However, no gas-phase reaction products detected in the reactor headspace for any of the catalysts tested.

The type of catalyst had a significant effect on the distribution of the reaction products (Figures 4-3 and 4-4). In order to more concisely compare the effect of catalyst type on product distribution, the maximum selectivity of each product, defined as

$$S_{p,i} = \frac{moles\ of\ product\ (i)\ formed}{moles\ of\ glucose\ reacted} \tag{4-1}$$

was determined for each of the seven catalysts listed in Table 4-1 and 4-2. A bar graph comparison of the maximum measured selectivity for each catalyst at 150°C is shown in Figure 4-5 for HMF, the intermediate reaction product, and formic acid, one of the final organic acid reaction products. Of seven catalysts tested, the FPM offered the lowest selectivity of HMF in the liquid phase ($S_{p,HMF} = 0.04$) and the highest selectivity of formic acid ($S_{p,FA} = 0.60$) in the liquid phase.

The amount of coke deposited on the catalyst after a 24 h reaction time at 150°C was significant for all five of the catalysts tested (Figure 4-6). Coking amounts were comparable for the HY-zeolite, CPM, and FPM. At 150°C, coke deposition was highest for APM, and was lowest for the MCM-20 and MCM-41.

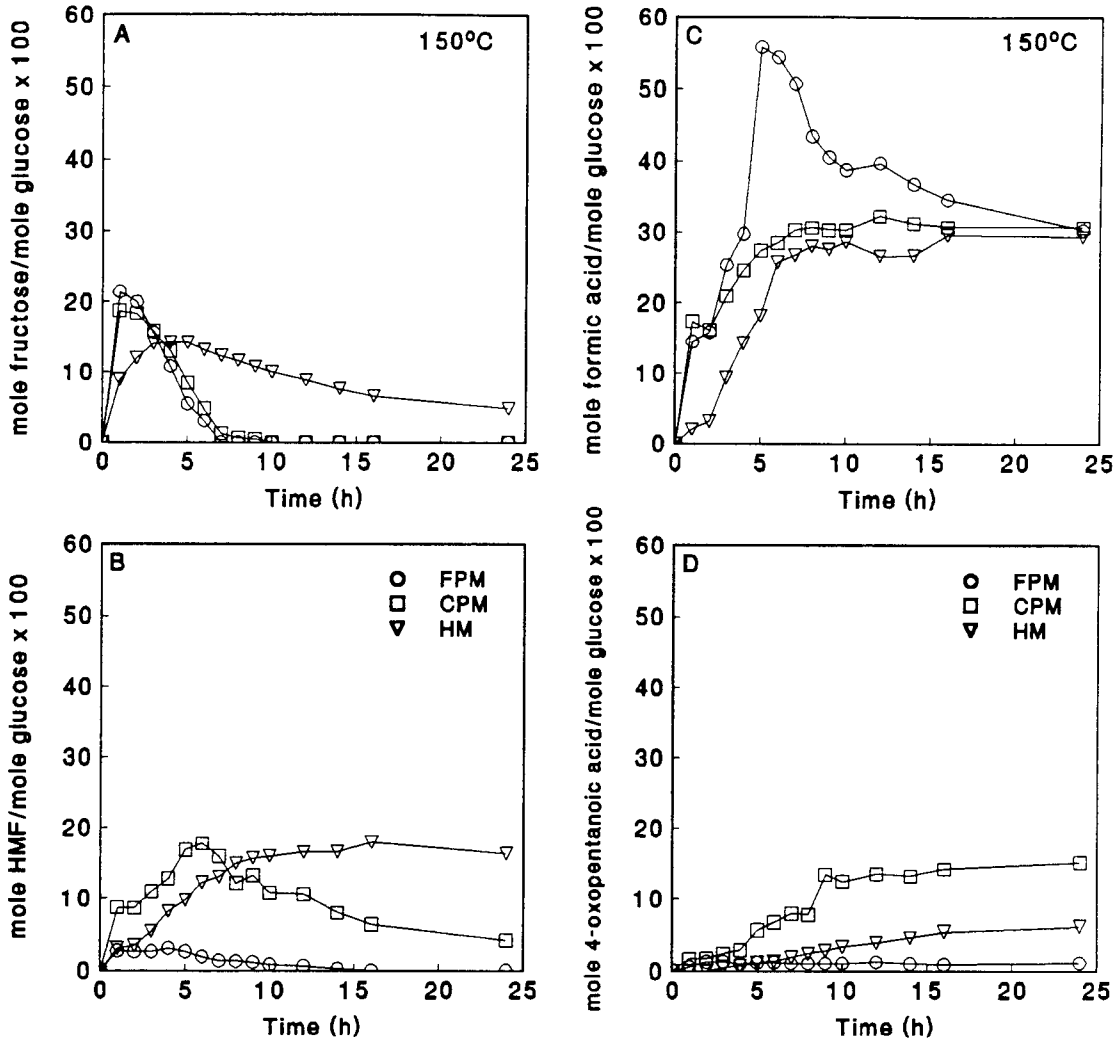

Figure 4-3. Product yield vs. reaction time at 150°C for HM, CPM, and FPM catalysts.

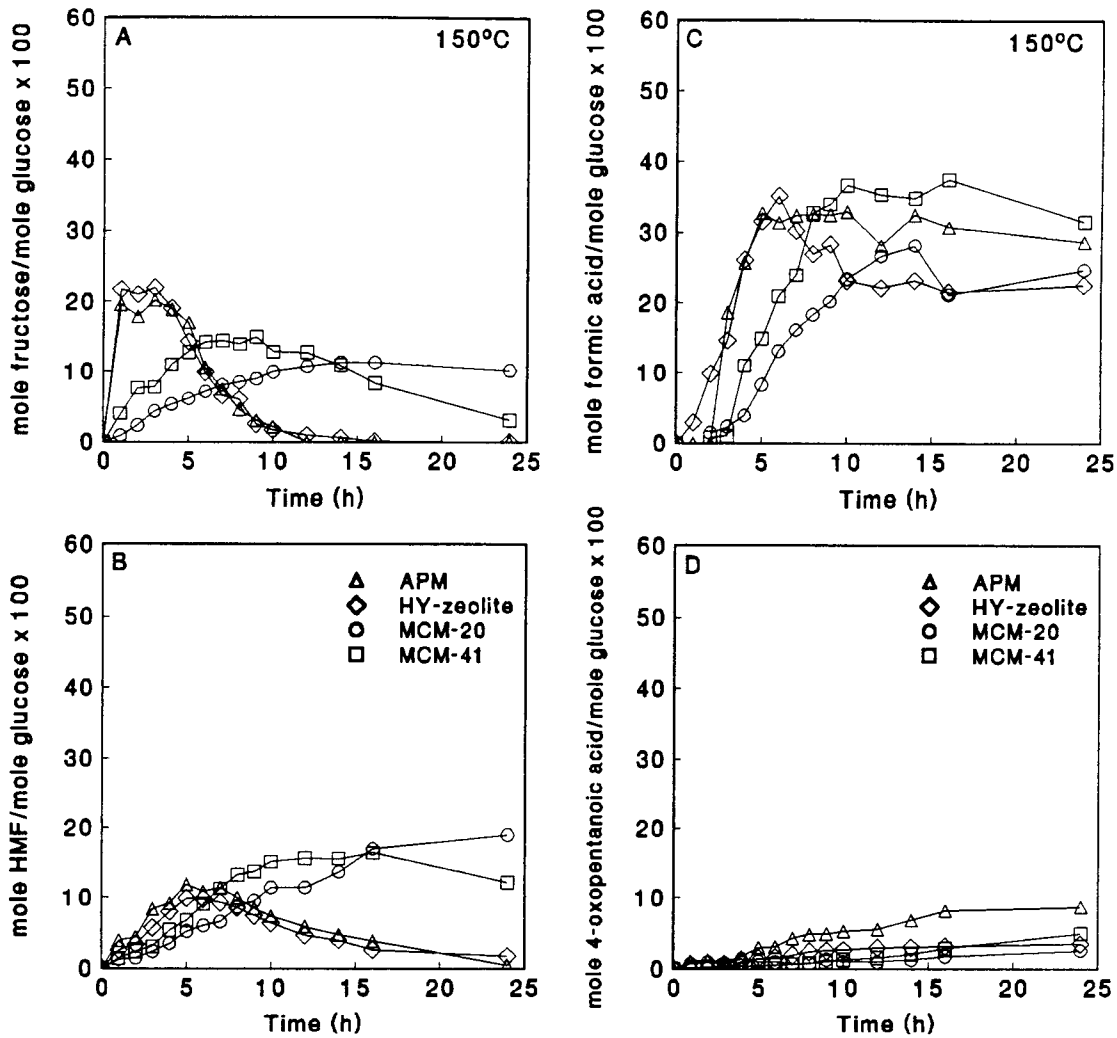

Figure 4-4. Product yield vs. reaction time at 150°C for HY-zeolite, APM, MCM-20, and MCM-41 catalysts.

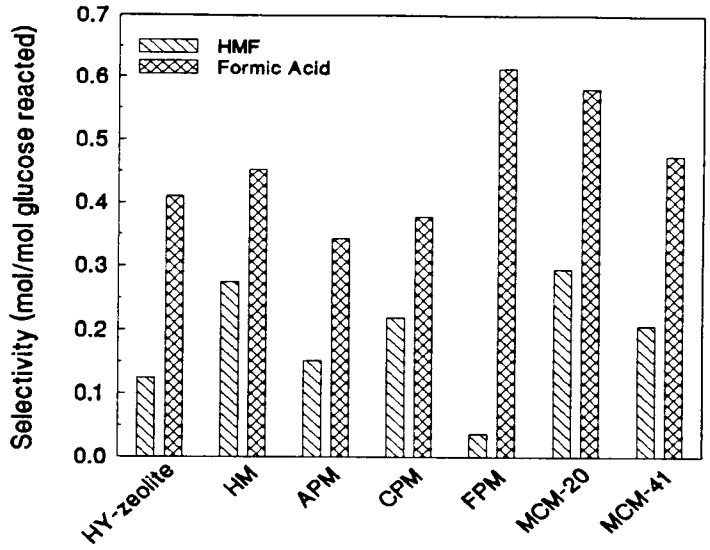

Figure 4-5. Comparison of the maximum selectivity for HMF and formic acid at 150°C for HY-zeolite, HM, APM, CPM, FPM, MCM-20, and MCM-41 catalysts.

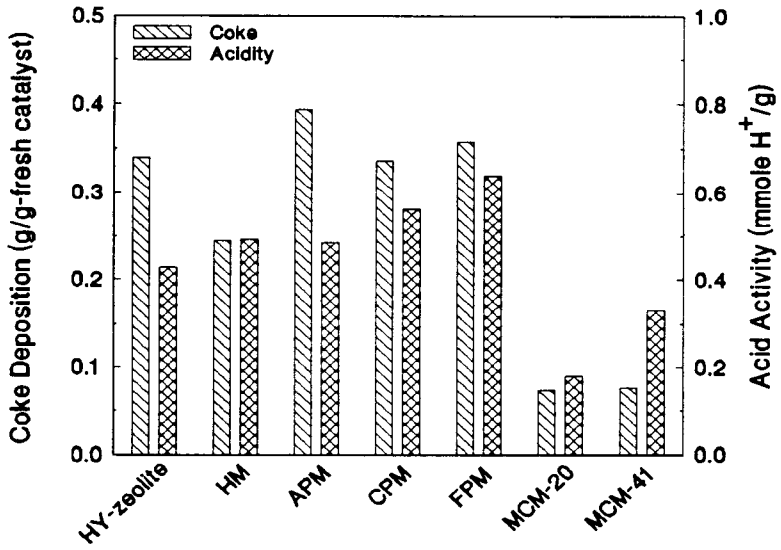

Figure 4-6. Coke formation and catalyst acid activity after 24 h reaction time at 150°C for HY-zeolite, HM, APM, CPM, FPM, MCM-20, and MCM-41 catalysts.

4.2.2 Effect of temperature

Glucose conversion and product yield vs. reaction time data at 130 to 170°C were obtained for APM, CPM, FPM, HM, and MCM-41 catalyst powder. For the FPM, APM, and HY-zeolite catalysts, 100% glucose conversion occurred only at temperatures of 150°C or greater. However, the CPM and MCM-41 catalysts required a temperature of 170°C for 100% glucose conversion.

Glucose conversion vs. time data for iron-pillared montmorillonite (FPM) and unpillared montmorillonite (HM) at temperatures of 130 to 170°C are presented in Figure 4-7. The FPM and HM catalysts are compared to demonstrate the difference in catalytic activity between the pillared and unpillared clay catalysts. Since both catalysts have a similar acid activity of 1.0 mmol H^+/g-catalyst, the catalytic activity really depends on the pillaring of clay sheets with the metal-polyoxycations.

The glucose conversion rate for FPM catalyst was significantly higher than the glucose conversion rate for HM catalyst. For the HM catalyst, 100% conversion required a temperature of greater than 170°C. For the FPM catalyst, 100% conversion is obtained at temperatures of 150°C and greater. However, at 130°C the conversion leveled off at 80% of theoretical, and the conversion rate dropped off sharply at 70% conversion, resulting in a poor fit of conversion vs. time data to a pseudo first-order rate equation.

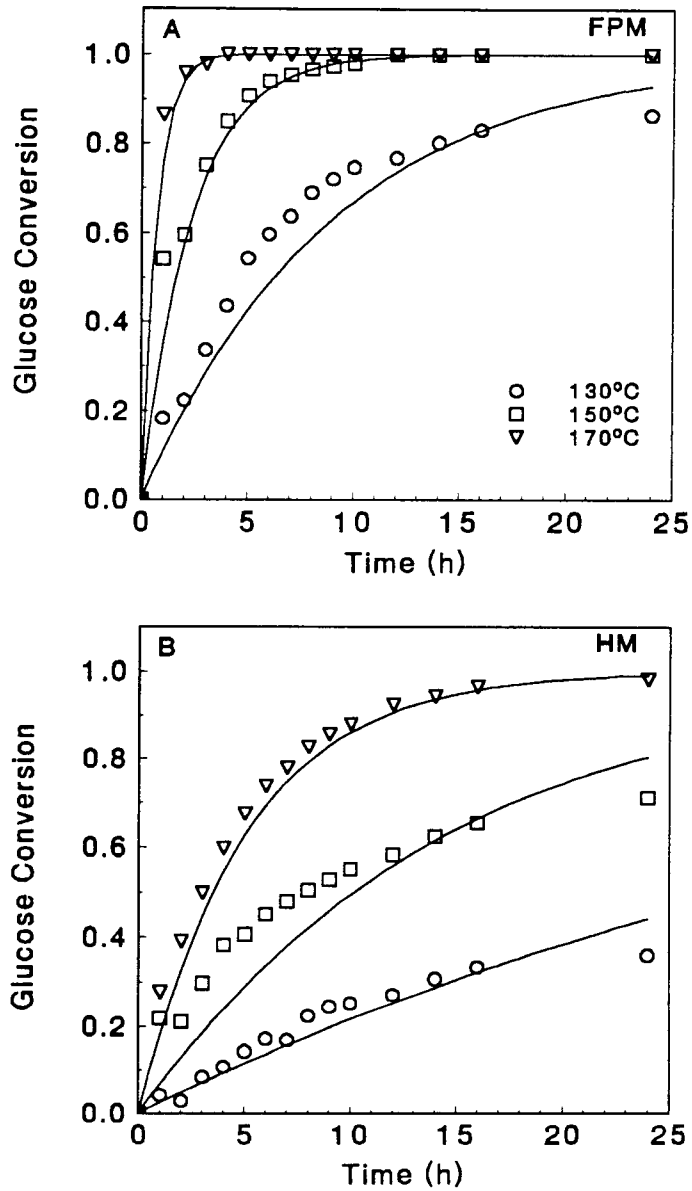

Figure 4-7. Glucose conversion vs. reaction time at 130 to 170°C for FPM and HM catalysts.

Based on glucose conversion data from 130 to 170°C, the apparent activation energy, E_{app}, and Arrhenius constant, $ln(A)$, for the pillared montmorillonite and MCM-41 catalysts were estimated (Table 4-4). The term E_{app} was estimated from the least-squares slope of an Arrhenius plot of $ln(k_{app})$ vs. $1/T$, whereas $ln(A)$ was computed from the least-squares intercept. The apparent activation energies were comparable for all the catalysts.

Table 4-4. Apparent activation energy and Arrhenius constants for glucose conversion catalyzed by HM, APM, CPM, FPM, and MCM-41 catalysts.

Catalyst	Activation Energy, E_{app} (kcal/mole ± 1s, n=3)	Arrhenius Constant, $ln(A)$
HM	18.5 ± 0.6	19.4
APM	20.7 ± 2.3	23.3
CPM	18.9 ± 3.1	21.1
FPM	22.6 ± 0.2	26.1
MCM-41	24.6 ± 1.5	26.8

Increasing the temperature increased the rate of product formation, and had a pronounced effect on the water-soluble product distribution of HMF and organic acids. Also, the yield of fructose decreased significantly with increasing temperature, because it was converted to HMF and organic acid products along with glucose. For example, the yield of selected products from the FPM catalyst at temperatures of 130 to 170°C are compared in Figure 4-8. The same trends in product release with increasing temperature of 130 to 170°C were also observed for the CPM catalyst (data in Appendix F).

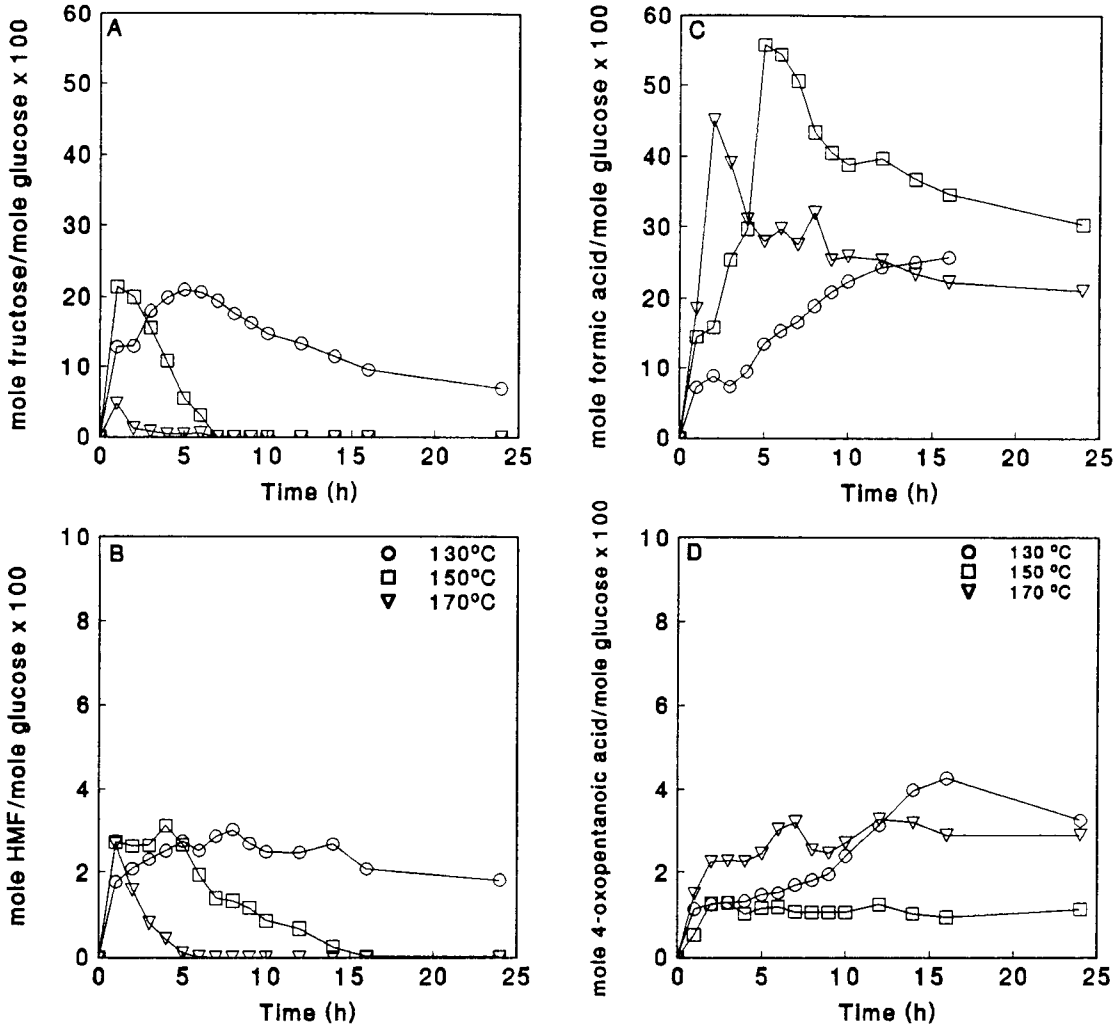

Figure 4-8. Product yield vs. reaction time at 130 to 170°C for FPM catalyst.

A bar graph comparison of the maximum measured selectivity for HMF and formic acid at temperatures of 130 to 170°C are shown in Figure 4-9 for HM, APM, CPM, FPM, and MCM-41 catalysts.

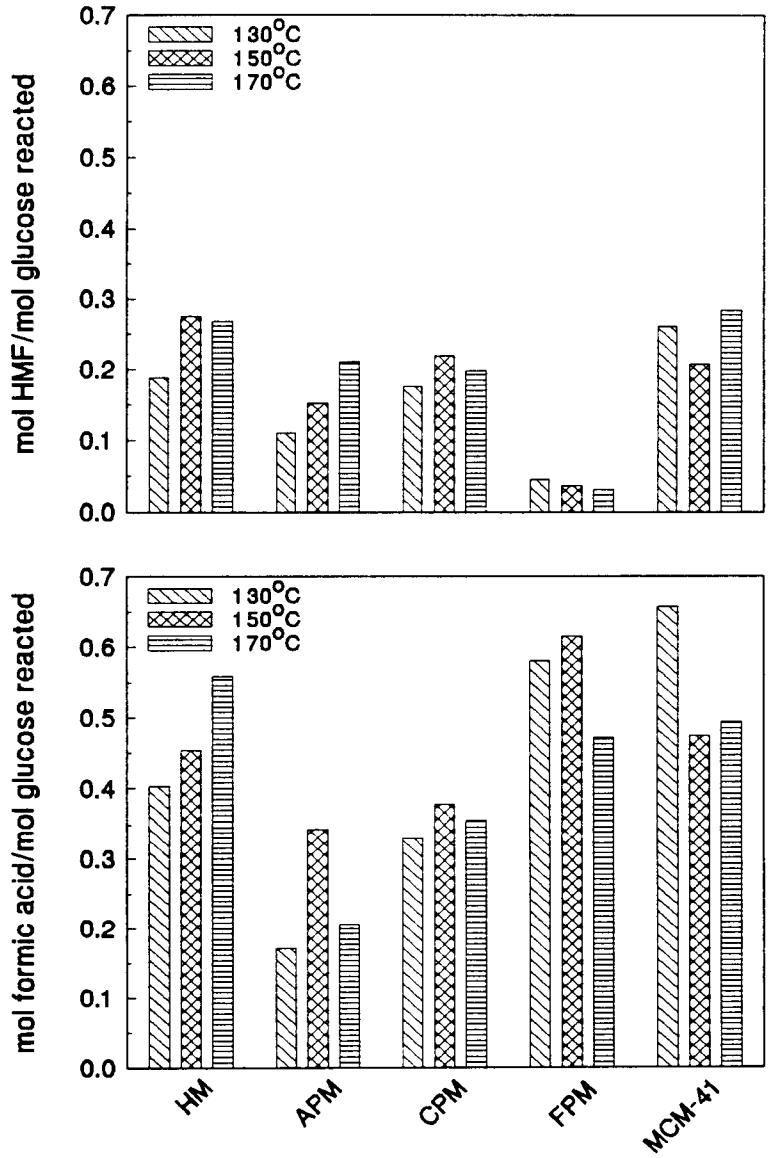

Figure 4-9. Comparison of the maximum selectivity of HMF and formic acid at 130 to 170°C for HM, APM, CPM, FPM, and MCM-41 catalysts.

Temperature had a significant effect on the amount of coke deposited on the catalyst after a 24 hr reaction time (Figure 4-10).

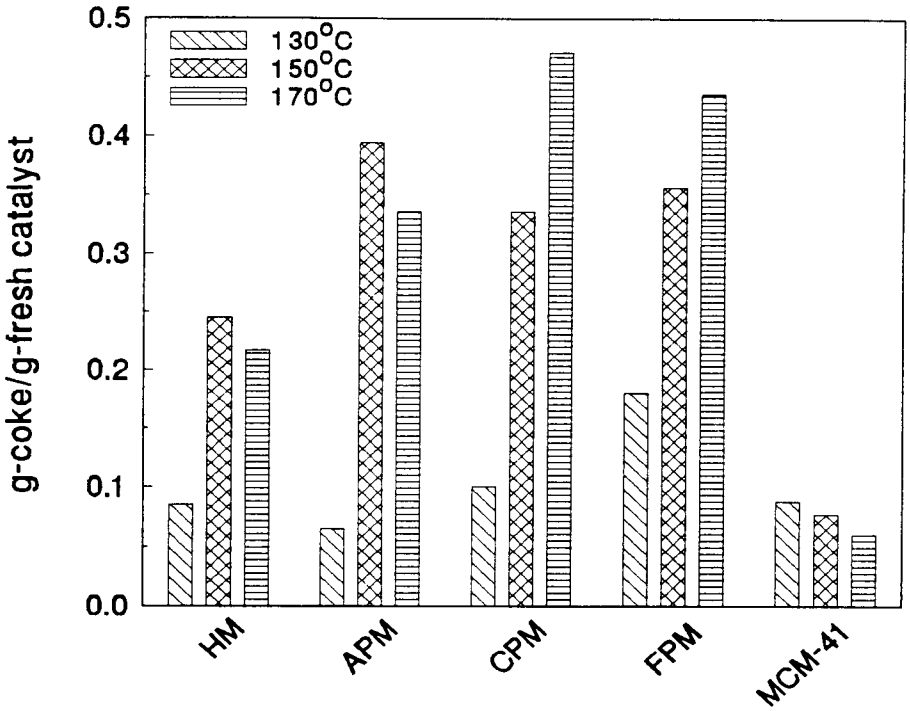

Figure 4-10. Coke formation after 24 h reaction time at 130 to 170°C for HM, APM, CPM, FPM and MCM-41 catalysts.

4.3 Discussion

Pillared clay and MCM catalysts promoted the shape-selective dehydration of glucose to formic acid but not to 4-oxopentanoic acid. The low selectivity of HMF in the liquid phase and the high selectivity of formic acid provided evidence for molecular-sieving reactions. In particular, the low selectivity of HMF in the liquid phase implied that the bulky, 9.3 Å HMF molecule was trapped within the porous matrix of the catalyst, or at least diffused very slowly through the pore matrix. This molecular entrapment gave HMF sufficient opportunity to rehydrate to formic acid and 4-oxopentanoic acid. These linear molecules, in particular formic acid, which has small molecular dimensions (Table 3-1) relative to the size of the pores, diffused out more readily into the liquid phase. The solid-acid pillared clay and MCM catalysts also promoted the reversible isomerization of glucose to fructose, which was subsequently converted to HMF and organic acids.

Glucose conversion rates, product yields, and product selectivity were affected by the properties of the pillared clay catalyst. The pore size distribution and the type of metal-polyoxycation pillar had the most significant effects. The APM, CPM, and FPM all possessed a distribution of pores below 10 Å and a distribution pores above 10 Å, as shown in Figure 4-1. However, as shown in Table 4-1, the order of accessible pore volume of pillared clay catalysts in the 10 to 50 Å range was: FPM > CPM > APM >> HM, HY-zeolite. Both the FPM and CPM had higher glucose conversion rates and product yields than the HM catalyst of comparable acid-activity. The FPM catalyst, which offered the largest pore distribution 10 to 50 Å range, also offered the highest glucose conversion rate, the lowest selectivity of HMF in the liquid phase, and the highest

selectivity of formic acid in the liquid phase for the seven catalysts tested at 150°C. In comparing the catalyst properties, one sees that although FPM and CPM have a comparable internal surface area and catalyst acid-activity, CPM has a smaller distribution of pores in the 10 to 50 Å range. This could explain why the CPM had a lower glucose conversion rate, a much higher selectivity of HMF, and a somewhat lower selectivity of formic acid relative to FPM. These results also suggest that in order to promote shape-selective conversion of glucose to organic acids, the catalyst must possess a significant fraction of micropores of at least a 10 Å nominal size so that the 8.6 Å glucose molecule can diffuse directly into the microporous matrix, gain access to intraparticle solid-acid catalytic sites, and then react to form the 9.3 Å HMF molecule within the pores.

Recently, Baksh et al. (1992) provided evidence that the *inter-pillar* spacings represent a more accurate picture of the microporous structure of the pillared clay. This suggests that the type of pillar and spacings between pillars also determine the molecular-sieving characteristic for the shape-selective reactions, in addition to the spacing between the clay layers.

The alumino-silicate catalysts considered by this study, including HY-zeolite, APM, MCM-20, and MCM-41, have a comparable acid activity of 0.5 mmol H^+/g-catalyst. However, the pore size and pore structure of each catalyst is different. Therefore, the effect of catalyst pore size and pore structure on the reactions is studied by considering these catalysts. The glucose conversion rates for the HY-zeolite and APM catalysts were higher relative to the MCM-20 and MCM-41 catalysts. The product yields for HY-zeolite, APM, MCM-20, and MCM-41 were nominally the same, resulting in

higher product selectivities of MCM-20 and MCM-41. Although the HY-zeolite, APM, MCM-20, and MCM-41 catalysts had a similar acid activity, the internal surface area and accessible pore volume were significantly different. The APM catalyst had a much lower internal surface area compared to the HY-zeolite, MCM-20, and MCM-41 catalysts. The measured HY-zeolite pore diameter was uniform at 6.8 Å, and therefore was too small to accommodate the 8.6 Å glucose molecule for direct intraparticle diffusion and reaction. Also, the APM possessed only a very small fraction of micropores in the 10 to 50 Å pore size range accessible to the 8.6 Å glucose molecule. In contrast, MCM-20 and MCM-41 possessed a large mesopore volume which was highly accessible to the glucose molecule.

The shape-selective dehydration of glucose to HMF and organic acids can directly occur on Bronsted acid sites within the mesoporous matrix of the MCM catalyst. Thus, both the HY-zeolite and the APM may have promoted the non shape-selective dehydration of glucose by Bronsted acid sites on the outer surface of the catalyst particle. The large mesopores of MCM catalysts, however, allow intermediate products, including fructose and HMF, to easily diffuse through the porous matrix, resulting in the higher yields and selectivities of fructose and HMF compared to other catalysts.

Although the product distribution data suggests that pillared montmorillonite and MCM catalysts can promote shape-selective, intraparticle dehydration of glucose to organic acids (particularly formic acid), the yields of organic acid products, particularly for 4-oxopentanoic acid, were low. For example, the maximum yield of formic acid FPM was 56 mole%, then rapidly decreased to 30 mole% between 6 and 24 h of reaction time. The maximum yield of 4-oxopentanoic acid was only 1.2 mole% after 24 h at 150°C. For

MCM-41, the maximum yield was 30 mole% for formic acid and 5 mole% for 4-oxopentanoic acid after 24 h at 150°C, which is surprising when one considers that formic acid and 4-oxopentanoic acid should be theoretically produced in equimolar amounts.

With respect to temperature, the product yields and selectivities obtained from pillared montmorillonites had maximum values at 150°C. The product yields and selectivities from HM increased with increasing temperature from 130 to 170°C. In contrast, the product yields and selectivities from MCM-41 catalyst had minimum values at 150°C. Furthermore, coke formation on the pillared montmorillonites was significant and increased from 130 to 170°C. Thus, the temperature optima in organic acids production can be explained by carbonization of HMF and organic acid products to water-insoluble coke within the micropores of the pillared montmorillonite, which was shown to become very significant at 170°C. Coke formation on the MCM-41 was significantly lower than the coke formation on other catalysts and decreased from 130 to 170°C. In contrast, for the MCM catalysts, glucose and products easily diffused through the pore matrix. Therefore, the molecules were not as readily trapped inside the catalyst, which decreased the subsequent dehydration of reaction products to coke.

Carbonization of organic acid reaction products may also explain the reaction time optima in formic acid yield for the iron-pillared montmorillonite (FPM). Finally, the lowered yield of 4-oxopentanoic acid relative to formic acid may be again due to product degradation. This is because the molecular dimensions of 4-oxopentanoic acid are much larger than formic acid (Table 3-1) and in fact approach the molecular dimensions of the

pores. Thus 4-oxopentanoic acid diffuses slowly out of the porous matrix relative to formic acid, allowing more time for degradation.

The discussion of reaction selectivity given above assumes that the metal-polyoxycation pillars did not possess any catalytic activity in the temperature range of 130 to 170°C, and that the catalyst acid-activity was provided solely by Bronsted acid sites imbedded in the montmorillonite sheets. Chromium-oxide and iron-oxide catalysts promote a variety of reactions (Kung, 1989), but usually not in aqueous solvent systems at the low reaction temperatures of 130 to 170°C defined by this study. However, aluminum-oxide catalysts can promote acid-catalyzed dehydration reactions.

Chapter 5

REACTION MODELING

5.1 Reaction Mechanism

A reaction scheme for the partial dehydration of glucose to organic acids within a molecular-sieving catalyst is proposed in Figure 1-1. The glucose molecule diffuses into the pores of catalyst, then reacts on solid acid sites within the pores. The products diffuse out of the pores. The reaction model is developed by assuming that the external and internal mass transfer resistances are negligible, so that surface reactions on the catalyst are the rate-limiting processes.

The detailed surface reaction mechanism is proposed in Figure 5-1. Glucose from the liquid phase adsorbs onto the acid sites on the catalyst surface. The adsorbed glucose partially dehydrates to HMF or reversibly isomerizes to fructose. Fructose also dehydrates to HMF or desorbs to the liquid phase. HMF is cleaved on the catalyst surface and then rehydrates to 4-oxopentanoic acid and formic acid. HMF can also completely dehydrate to coke and deposit on the catalyst phase, or desorb to the liquid phase. Finally, the adsorbed 4-oxopentanoic acid and formic acid products can also completely dehydrate to coke or desorb to the liquid phase.

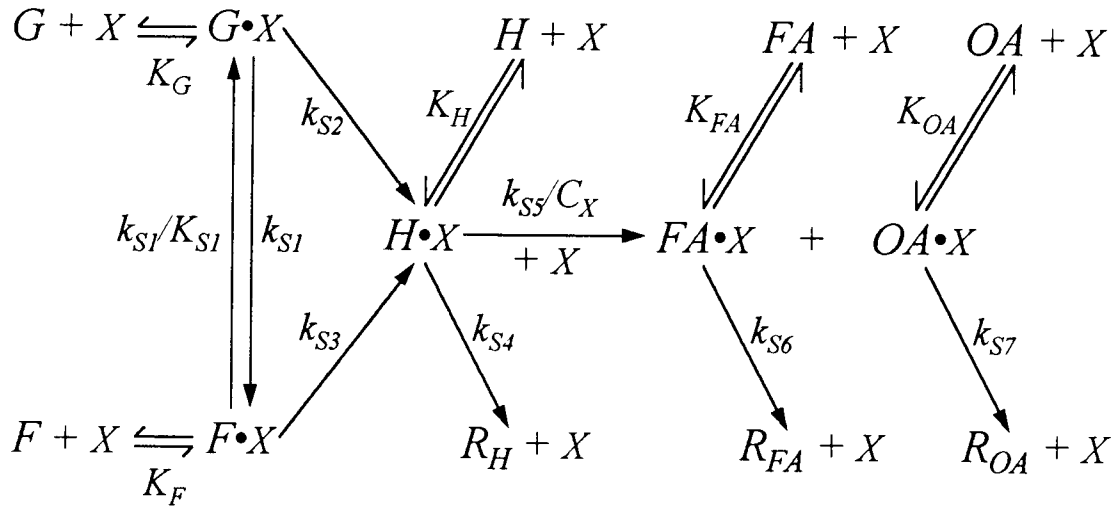

Figure 5-1. Proposed surface reaction model consisting of adsorption/desorption processes and surface reaction processes. G = glucose, H = HMF, F = fructose, FA = formic acid, OA = 4-oxopentanoic acid, R = coke, and X = acid site.

5.2 Rate Equations

Five major assumptions are made for the development the isothermal surface reaction model. First, external and internal mass and heat transfer resistances are negligible. Second, the rate equations are formulated by assuming that the surface reactions shown in Figure 5-1 are all first-order with respect to the concentration of each species. Third, the total number of acid sites on catalyst surface is assumed to be constant. Under this assumption, coke formation does not block the acid sites. Fourth, the adsorption and desorption processes are at equilibrium relative to the surface reaction processes. Finally, no gas-phase reaction products (e.g. CO_2) are produced, an assumption verified by reaction experiments described in Chapter 4.

Based on the above assumptions, the surface concentration of each specie "i" ($C_{i,X}$) can be expressed in terms of its liquid phase concentration (C_i)

$$C_{G\cdot X} = K_G C_X C_G \tag{5-1}$$

$$C_{H\cdot X} = K_H C_X C_H \tag{5-2}$$

$$C_{F\cdot X} = K_F C_X C_F \tag{5-3}$$

$$C_{FA\cdot X} = K_{FA} C_X C_{FA} \tag{5-4}$$

$$C_{OA\cdot X} = K_{OA} C_X C_{OA} \tag{5-5}$$

The total acid site concentration on the catalyst surface can also be expressed as the sum of the surface concentrations of each component ($C_{i,X}$) and vacant acid site concentration ($C_{v,X}$)

$$C_X = \sum_i C_{i\cdot X} + C_{v,X} = C_{G\cdot X} + C_{H\cdot X} + C_{F\cdot X} + C_{FA\cdot X} + C_{OA\cdot X} + C_{v,X} \tag{5-6}$$

The total acid site concentration (C_X) is obtained by experiment from

$$C_X = C_{cat}\, a_X \tag{5-7}$$

where C_{cat} is the catalyst loading (g catalyst/L), and a_X is the acid activity of the catalyst (mmol H^+/g-catalyst).

If the surface reaction rates are the rate-limiting processes, then the rate equations derived from the surface reaction mechanism in terms of liquid phase concentrations are

$$\frac{dC_{T,G}}{dt} = \frac{dC_{G\cdot X}}{dt} = -k_{S2} K_G C_X C_G - k_{S1}\left(K_G C_X C_G - \frac{K_F C_X}{K_{S1}} C_F\right) \tag{5-8}$$

$$\begin{aligned}\frac{dC_{T,H}}{dt} = \frac{dC_{H\cdot X}}{dt} &= k_{S2} K_G C_X C_G + k_{S3} K_F C_X C_F - k_{S4} K_H C_X C_H \\ &\quad - \frac{k_{S5}}{C_X} K_H C_X C_H C_{v,X}\end{aligned} \tag{5-9}$$

$$\frac{dC_{T,F}}{dt} = \frac{dC_{F\cdot X}}{dt} = -k_{S3}K_F C_X C_F + k_{S1}(K_G C_X C_G - \frac{K_F C_X}{K_{S1}} C_F) \tag{5-10}$$

$$\frac{dC_{T,FA}}{dt} = \frac{dC_{FA\cdot X}}{dt} = \frac{k_{S5}}{C_X} K_H C_X C_H C_{v,X} - k_{S6} K_{FA} C_X C_{FA} \tag{5-11}$$

$$\frac{dC_{T,OA}}{dt} = \frac{dC_{OA\cdot X}}{dt} = \frac{k_{S5}}{C_X} K_H C_X C_H C_{v,X} - k_{S7} K_{OA} C_X C_{OA} \tag{5-12}$$

$$\frac{dC_{R,H}}{dt} = k_{S4} K_H C_X C_H \tag{5-13}$$

$$\frac{dC_{R,FA}}{dt} = k_{S6} K_{FA} C_X C_{FA} \tag{5-14}$$

$$\frac{dC_{R,OA}}{dt} = k_{S7} K_{OA} C_X C_{OA} \tag{5-15}$$

The surface concentration ($C_{i\cdot X}$) is also related to the liquid phase concentration (C_i) by

$$C_{i\cdot X} = C_{T,i} - C_i \tag{5-16}$$

where $C_{T,i}$ represents the total concentration of each species "i" in both catalyst and liquid phases. The kinetic parameters in equations (5-8) to (5-15) are defined in Figure 5-1. The initial conditions at $t = 0$ are

$$C_{G,0} = C_{T,G,0} \tag{5-17}$$

$$C_{H,0} = C_{F,0} = C_{FA,0} = C_{OA,0} = 0 \tag{5-18}$$

$$C_{T,H,0} = C_{T,F,0} = C_{T,FA,0} = C_{T,OA,0} = 0 \tag{5-19}$$

$$C_{R,H,0} = C_{R,FA,0} = C_{R,OA,0} \tag{5-20}$$

The numerical solution of the coupled set of first-order differential equations predicts glucose conversion by equation (5-8), product yield formation by equations (5-9) to (5-12), and coke formation by equations (5-13) to (5-15) as a function of reaction time

and catalyst concentration (C_X) under isothermal conditions where mass transfer resistances are minimized. The numerical solution is detailed in Appendix G.

5.3 Mass Transfer Resistances

The significance of external and internal mass transfer resistances were considered. External mass transfer resistances were evaluated by the ratio of glucose conversion rate to convective mass transfer rate (γ)

$$\gamma = \frac{k_{app} d_p}{6 k_c} \tag{5-21}$$

as described by Petersen (1965). The parameter (γ) was determined from the mean particle size given in Table 4-2 and mass transfer coefficient (k_c) given in Table 5-1. The mass transfer coefficient was estimated from the Sherwood number (Sh) for convective flow around a spherical particle (Cussler, 1984), given by

$$Sh = \frac{k_c d_p}{D_G} = 2.0 + 0.6(Re)^{1/2}\left(\frac{\nu}{D_G}\right)^{1/3} \tag{5-22}$$

where D_G is the molecular diffusivity of glucose in water (3.75 x 10^{-5} cm^2/s at 150°C), estimated by the Hayduk and Laudie correlation. The Reynolds number (Re), defined in terms of the energy dissipation rate (ω), is described by Smith (1981) as

$$Re = \left(\frac{\omega \cdot d_p^4}{\nu^3}\right)^{1/3} \tag{5-23}$$

The energy dissipation rate was calculated by

$$\omega = \frac{N_p \rho_L N^3 D_I^5}{W} \tag{5-24}$$

where D_I is the impeller diameter (3.5 cm), ρ_L is the density of liquid (g/cm^3), N is the impeller speed (6.67 rps or 400 rpm), W is the mass of liquid in slurry (g), and N_p is the power number, which is equal to 10. If γ is below 1, then the process is not controlled by the external mass transfer. As shown in Table 5-1, values of γ for each catalyst were on the order of 10^{-7} due to the small catalyst particle size of 20 μm. Therefore, glucose conversion rates were not influenced by external mass transfer resistance at a mixing speed of 400 rpm. This result was confirmed by a previous study (Lourvanij and Rorrer, 1993), which considered the effect of mixing speed on the rate of glucose dehydration by HY-zeolite catalyst powder.

Table 5-1. Estimation of mass transfer resistances.

Catalyst	k_{app} [(a)] (1/h)	k_C (cm/s)	γ	Φ_W
HY-zeolite	0.256	0.094	2.98×10^{-7}	0.0063
APM	0.313	0.103	2.85×10^{-7}	0.0048
MCM-41	0.096	0.098	0.99×10^{-7}	0.0002

[(a)] at 150°C

The internal mass transfer resistance for diffusion of glucose within the catalyst particle was evaluated by the Weisz Modulus (Φ_W), given by

$$\Phi_W = \frac{k_{app}\left(d_p/6\right)^2}{D_{G,e}} \tag{5-25}$$

The effective diffusion coefficient ($D_{G,e}$) for aqueous glucose in each catalyst is given in Table 4-2. Although the values for $D_{G,e}$ were on the order of 10^{-9} cm^2/s, the catalyst particle size was also very small. If the Weisz Modulus (Φ_W) is below 0.15, then the process is not controlled by internal mass transfer (Levenspiel, 1993). As shown in Table 5-1, values of Φ_W for each catalyst were on the order of 10^{-3}. Therefore, glucose conversion rates were not influenced by internal mass transfer resistances as well.

5.4 Kinetic Parameter Estimation

The numerical method for non-linear regression of differential equations described by Constantinides (1987) was used to estimate kinetic parameters proposed by the rate equations (5-8) to (5-15). First, the system of ordinary differential equation representing the rate equations was solved by the 4th order Runge-Kutta method using initial guess values for each model parameter and initial reactant and product concentrations given by equations (5-17) to (5-20). Second, the sum of squared residuals were calculated from the difference of the model predictions and data for the liquid phase concentration of glucose, HMF, formic acid, and 4-oxopentanoic acid at each time point over the 24 h reaction period. Finally, the total sum of squared residuals was iteratively minimized by the Marquardt method until the sum of squared residuals varied by no more than 0.1%

between iterations. All data points were weighted equally at 1.0. The details of non-linear regression using the Marquardt technique are provided in Appendix G.

Glucose conversion and product formation vs. time data of fructose, HMF, formic acid, and 4-oxopentanoic acid for the HY-zeolite, APM, MCM-20, and MCM-41 catalysts are presented in Figures 5-2 and 5-3. This series of HY-zeolite, APM, MCM-20, and MCM-41 catalysts are all alumino-silicates and possess a similar acid activity of 0.5 mmol H^+/g-catalyst. Only the structure and pore size of each catalyst is different. Therefore, these catalysts are used to study the specific effect of pore size on the reaction kinetics. In contrast, HM, CPM, and FPM catalysts possess different catalyst compositions due to the pillaring agents, and also possess a much higher acid activity of 1.0 mmol H^+/g-catalyst. Therefore, these pillared clay catalysts are not selected for this analysis.

The solid lines represent the non-linear, least-square fit of the data to the surface reaction model given by equations (5-8) to (5-12). The estimated model parameters at 150°C are summarized in Table 5-2. All reactions were conducted with an initial glucose concentration of 0.74 M and catalyst loading of 33 g/L within a well-mixed, 300 mL Parr reactor at 150°C and mixing speed of 400 rpm.

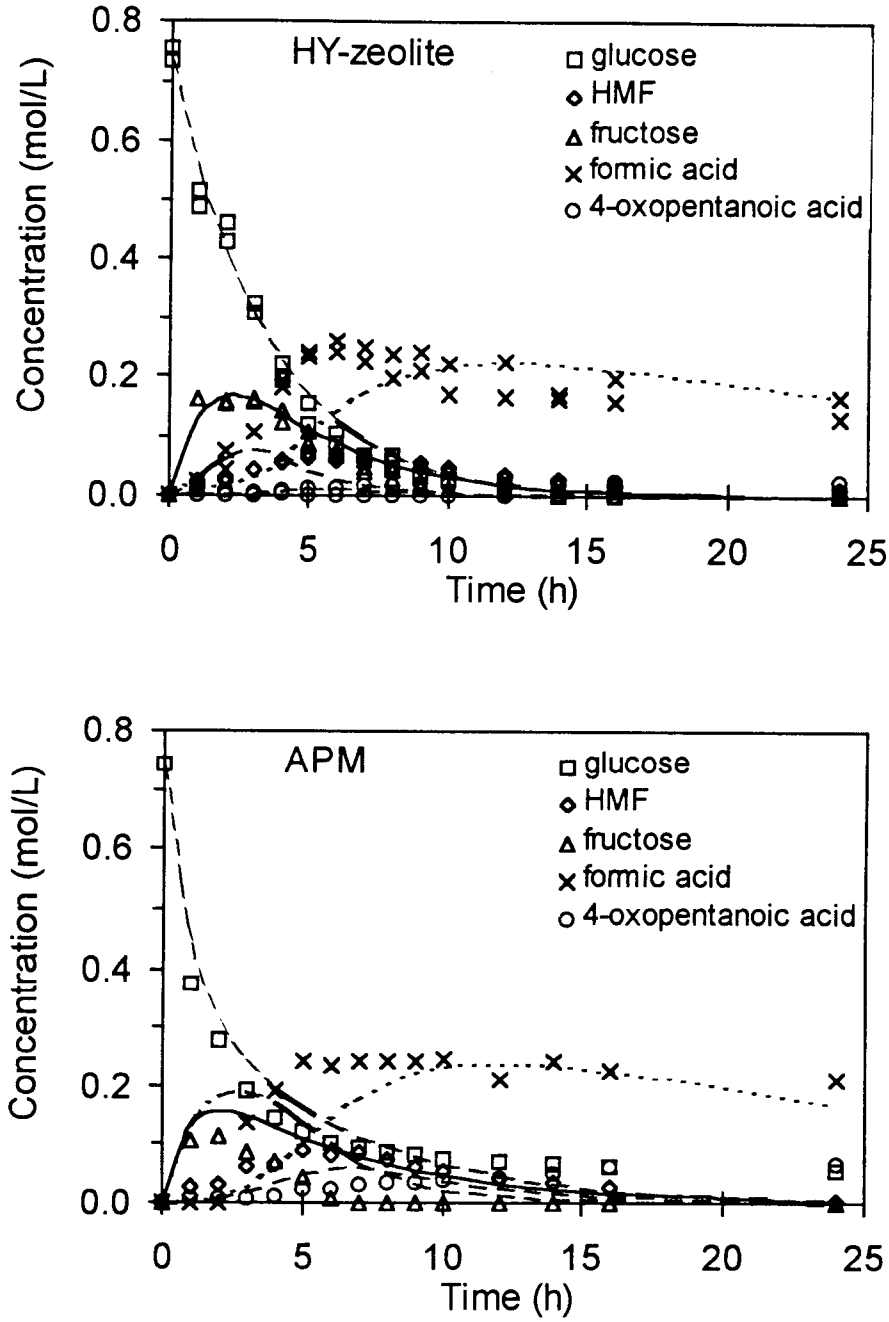

Figure 5-2. Glucose conversion and product distribution vs. reaction time at 150°C for HY-zeolite and APM catalysts.

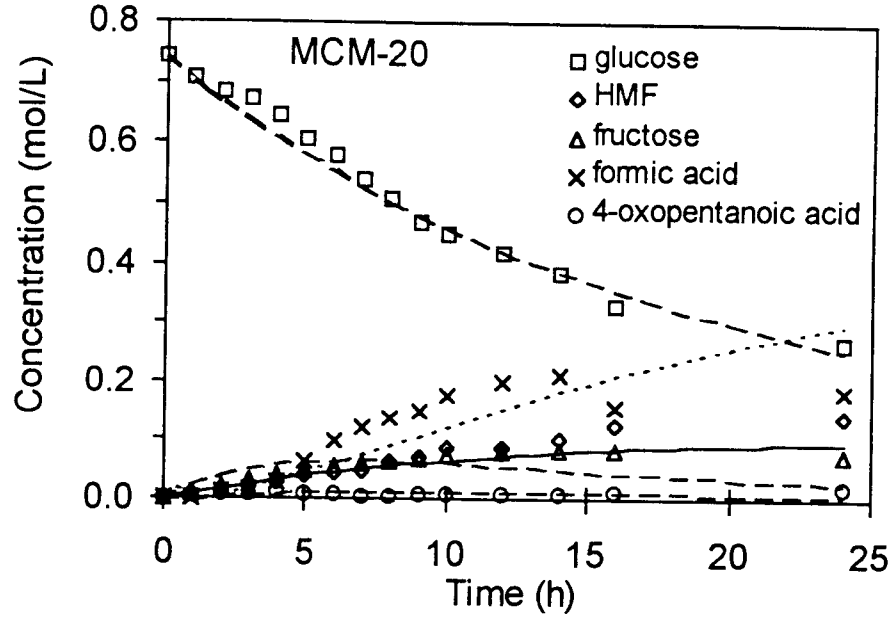

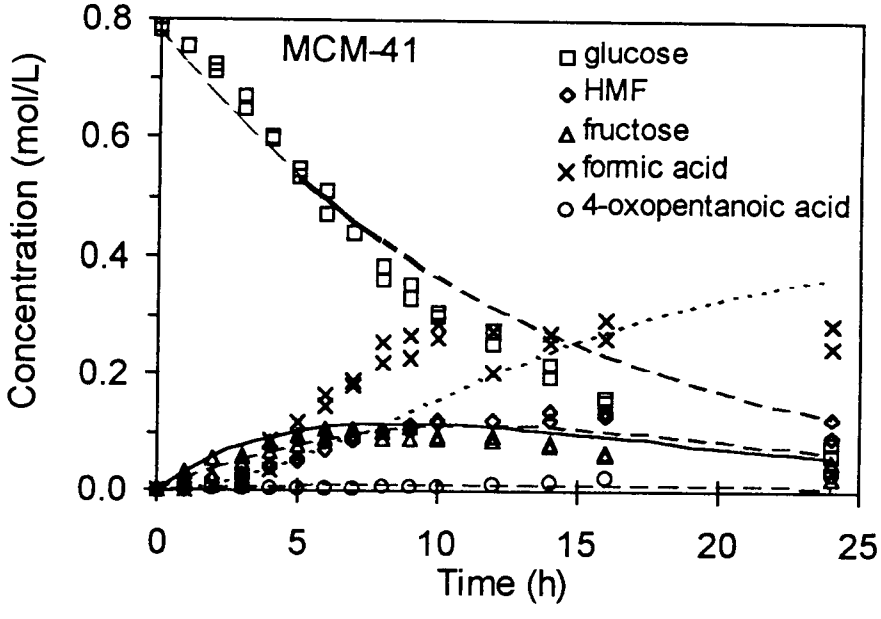

Figure 5-3. Glucose conversion and product distribution vs. reaction time at 150°C for MCM-20 and MCM-41 catalysts.

Table 5-2. Estimated model parameters at 150°C for the HY-zeolite, APM, MCM-20, and MCM-41 catalysts.

Catalyst	HY-zeolite	APM	MCM-20	MCM-41
Pore Size (Å)	7.4	10.8	27.4	32.8
k_{S1} (1/h)	18.043	14.350	1.977	8.287
k_{S2} (1/h)	0.065	11.985	5.745	4.681
$1/K_{S1}$	0.000	3.950	6.634	0.000
k_{S3} (1/h)	29.476	2.775	0.000	27.385
k_{S4} (1/h)	13.244	7.167	6.049	0.000
k_{S5} (1/h)	30.305	33.839	43.598	21.189
k_{S6} (1/h)	4.546	5.716	0.000	4.648
k_{S7} (1/h)	95.963	29.412	49.407	52.890
K_G (L/mol-h)	0.946	1.342	0.624	0.373
K_H (L/mol-h)	4.937	2.257	0.945	13.262
K_F (L/mol-h)	1.315	0.643	0.195	0.397
K_{FA} (L/mol-h)	0.455	0.571	0.000	0.465
K_{OA} (L/mol-h)	2.399	1.415	2.471	2.545

The surface reaction model fitted the glucose conversion and product formation kinetic data reasonably well. For all catalysts, the surface reaction model underestimated the formic acid formation during the first 10 hours of reaction time. The model also predicted a maximum in the yield of the reaction intermediate HMF at lower reaction times. These two discrepancies in the model predictions may be due to the assumption of constant acid sites on the catalyst surface. In the real situation, the acid sites could be partially blocked by coke or unknown products. If the total acid site concentration decreases during reaction, then the dehydration rates of glucose and fructose to HMF would decrease, and the rehydration rate of HMF to organic acids would also decrease.

Recall from Chapter 4 that the dehydration of glucose with solid-acid, molecular-sieving catalysts yielded much more formic acid than 4-oxopentanoic acid. Theoretically, formic acid and 4-oxopentanoic acid are produced in equimolar amounts from the cleavage and rehydration of HMF. The lowered yield of 4-oxopentanoic acid relative to formic acid is due to subsequent reactions of this product to coke or unknown products. The predicted amounts of HMF and organic acid degradation to coke will be discussed later in section 5.6 (Coke Formation).

Arrhenius plots for the dehydration of glucose to HMF within HY-zeolite, APM, and MCM-41 catalysts are presented in Figure 5-4. All of the estimated model parameters for each of these three catalysts at 110 to 190°C are summarized in Tables 5-3, 5-4, and 5-5 respectively. The relatively high value of the activation energy (> 20 kcal/mol) further confirms that glucose conversion to HMF in each catalyst was reaction limiting rather than mass transfer limiting.

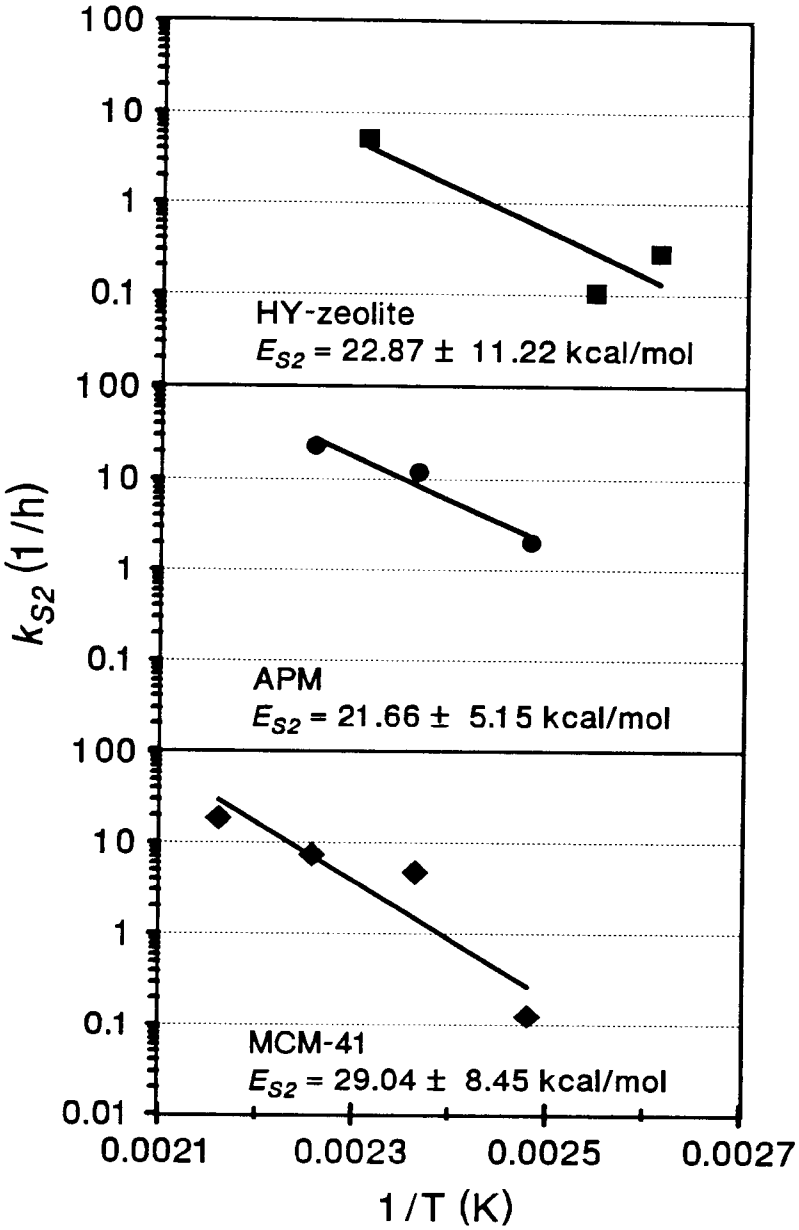

Figure 5-4. Arrhenius plot and activation energy for glucose dehydration to HMF within HY-zeolite, APM, and MCM-41 catalysts.

Table 5-3. Estimated model parameters at 110 to 160°C for the HY-zeolite catalyst.

Temperature (°C)	110	120	130	160
k_{S1} (1/h)	0.850	2.765	5.989	10.445
k_{S2} (1/h)	0.281	0.105	0.000	5.215
$1/K_{S1}$	0.000	0.617	0.000	0.000
k_{S3} (1/h)	0.000	5.167	7.431	23.538
k_{S4} (1/h)	13.610	11.403	19.551	19.865
k_{S5} (1/h)	12.478	12.906	29.447	24.936
k_{S6} (1/h)	0.000	0.000	2.559	3.220
k_{S7} (1/h)	4.541	6.567	8.261	6.106
K_G (L/mol-h)	0.551	0.559	0.506	1.115
K_H (L/mol-h)	1.095	1.291	0.899	4.599
K_F (L/mol-h)	0.000	0.451	0.769	1.282
K_{FA} (L/mol-h)	0.000	0.000	0.256	0.321
K_{OA} (L/mol-h)	0.376	0.378	0.413	0.299

Table 5-4. Estimated model parameters at 130 to 170°C for the APM catalyst.

Temperature (°C)	130	150	170
k_{S1} (1/h)	3.598	14.350	46.825
k_{S2} (1/h)	2.033	11.985	23.014
$1/K_{S1}$	0.541	3.950	1.286
k_{S3} (1/h)	4.697	2.775	112.120
k_{S4} (1/h)	6.723	7.167	20.470
k_{S5} (1/h)	20.738	33.643	23.595
k_{S6} (1/h)	0.000	5.716	0.000
k_{S7} (1/h)	58.026	29.412	9.225
K_G (L/mol-h)	0.876	1.342	0.914
K_H (L/mol-h)	2.331	2.257	4.518
K_F (L/mol-h)	0.946	0.643	0.621
K_{FA} (L/mol-h)	0.000	0.571	0.000
K_{OA} (L/mol-h)	2.304	1.415	0.461

Table 5-5. Estimated model parameters at 130 to 190°C for the MCM-41 catalyst.

Temperature (°C)	130	150	170	190
k_{S1} (1/h)	2.039	8.287	5.199	47.113
k_{S2} (1/h)	0.127	4.681	7.408	18.674
$1/K_{S1}$	0.000	0.000	0.000	0.031
k_{S3} (1/h)	10.858	27.385	17.331	150.380
k_{S4} (1/h)	0.000	0.000	8.834	20.695
k_{S5} (1/h)	29.018	20.527	22.181	16.787
k_{S6} (1/h)	0.000	4.648	6.614	0.000
k_{S7} (1/h)	39.004	52.890	35.883	13.880
K_G (L/mol-h)	0.509	0.373	0.801	0.917
K_H (L/mol-h)	0.791	13.262	1.213	3.153
K_F (L/mol-h)	1.034	0.397	1.111	0.760
K_{FA} (L/mol-h)	0.000	0.465	0.661	0.000
K_{OA} (L/mol-h)	1.950	2.545	1.794	0.694

5.5 Effect of Catalyst Pore Size

A major goal of this study is to explore the effect of catalyst properties on the selectivity of the partial dehydration of glucose to organic acids. A catalyst property which has a significant effect on shape-selective reactions is the pore size. Selected kinetic constants at 150°C for the four major reaction processes, including glucose dehydration to HMF, glucose isomerization to fructose, fructose dehydration to HMF, and HMF rehydration to formic acid and 4-oxopentanoic acid, are plotted as a function of mean catalyst pore size in Figure 5-5. The kinetic constants in Figure 5-5 are defined as the forward rate constant per unit of acid activity (k_{Sf}/a_X).

In shape-selective reactions, the size of the reactants and products approach the diameter of the catalyst pore. The ratio of the long axis of a given component to the mean pore diameter of catalyst is defined as λ_i. Values of λ_i for each component are presented in Table 5-6. The long axis values for glucose, fructose, HMF, formic acid, and 4-oxopentanoic acid molecules are obtained from the molecular modeling calculations described in Chapter 3 using values obtained from Table 3-1. The values for λ_i can be used to help discern if certain reactions are shape-selective or non-selective.

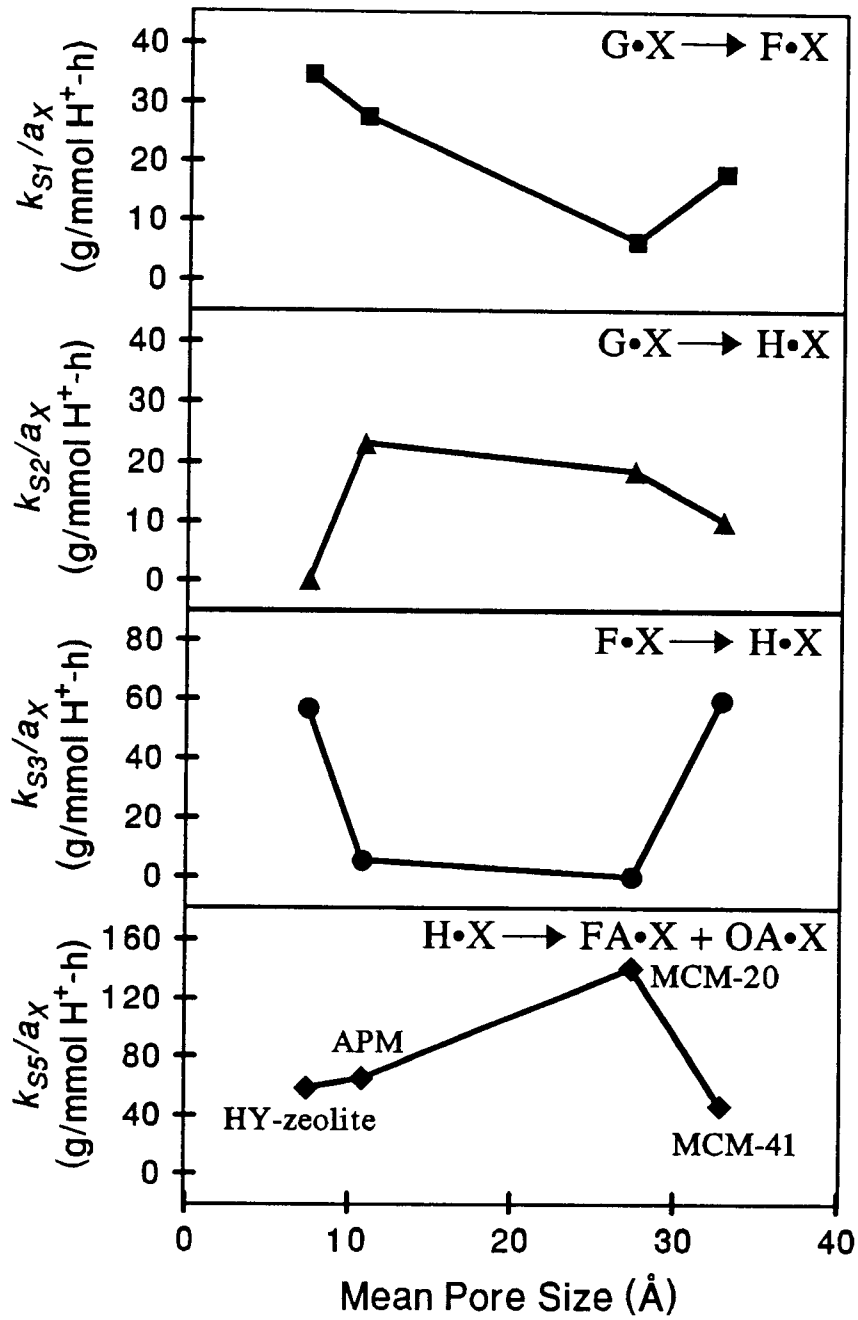

Figure 5-5. Selected kinetic constants (k_{Sj}/a_X) for the four major reaction processes at 150°C vs. mean catalyst pore diameter.

Table 5-6. The ratio of long axis of each component to the mean pore diameter.

Catalyst	$\bar{d}_{pore}$ (Å)	λ_G	λ_F	λ_H	λ_{FA}	λ_{OA}
HY-zeolite	6.8	1.26	1.43	1.36	0.67	1.51
APM	10.8	0.80	0.91	0.86	0.43	0.95
MCM-20	27.4	0.31	0.36	0.34	0.18	0.38
MCM-41	32.8	0.26	0.30	0.28	0.14	0.31

For the HY-zeolite catalysts, the kinetic constants for glucose isomerization to fructose and fructose dehydration to HMF were always higher than the kinetic constant for glucose dehydration to HMF. In comparison, for the APM and MCM-20 catalysts, values of the kinetic constants for glucose isomerization to fructose and glucose dehydration to HMF were comparable to one another for a given catalyst. The kinetic constants for fructose dehydration to HMF were also much smaller than the kinetic constants for glucose dehydration to HMF.

For the APM and MCM-20 catalysts, the pore size is larger than the long axis of the glucose molecule, i.e. λ_G is less than 1. As λ_G and λ_H approach 1, the flux of glucose and HMF molecules are hindered due to the increased collision frequency of molecules with acid sites on the pore wall of the catalyst. The reaction activity of glucose dehydration to HMF increases. As a result, glucose dehydration to HMF dominates over fructose dehydration to HMF.

In the HY-zeolite catalyst, access to intraparticle reaction sites theoretically cannot occur since λ_G, λ_F, and λ_H are all greater than 1. Glucose first isomerizes to fructose and then fructose dehydrates to HMF on the outer surface of the catalyst by non shape-selective reaction processes. Szmant and Chundury (1981) studied the dehydration of fructose and glucose to HMF with a homogeneous acid catalyst and also showed that the dehydration rate of fructose is higher than of glucose. Therefore, we expect that fructose dehydration is preferred over glucose dehydration if the reaction scheme is not shape selective.

For the MCM-41 catalyst, the value for λ_G is less than 0.3. The flux of glucose molecules is not hindered in the pores relative to the APM and MCM-20 catalysts. Consequently the collision frequency of reactant molecules with the acid sites on the MCM-41 catalyst pore wall is relatively low. The reaction activity for glucose is not high enough to promote the direct dehydration of glucose to HMF, and so fructose dehydration to HMF is preferred.

The kinetic constants for partial rehydration of HMF to organic acids increased with increasing catalyst pore size over the range of 10 to 30 Å. The values for λ_H also decreased with increasing the catalyst pore size. This suggests that the pore size of the catalyst should be small enough to increase the collision frequency of HMF molecules with the acid sites on the catalyst pore wall, but large enough to allow the organic acid products, particularly the large 4-oxopentanoic acid molecule, to exit the pores. Since the diffusion of 4-oxopentanoic acid is impeded in small pores, the complete dehydration of 4-oxopentanoic acid to humic solids is also promoted. This process will lower the yield of

4-oxopentanoic acid relative to the faster-diffusing formic acid. This lowered yield is observed experimentally in Figures 5-2 and 5-3.

In summary, as illustrated in Figure 5-5, the dehydration of glucose to HMF and the rehydration of HMF to organic acids are selectively promoted within catalyst pore sizes ranging from 10 to 30 Å. The series reactions of glucose dehydration to HMF and partial rehydration of HMF to organic acids are promoted by shape-selective reaction processes whereas the parallel reactions of glucose isomerization to fructose and fructose dehydration to HMF are minimized.

5.6 Coke Formation

The surface reaction model also predicted the acid-catalyzed decomposition of HMF and organic acids to humic solids (coke). The concentration of coke deposited on the catalyst was expressed as the moles of carbon on the catalyst per unit mass of catalyst. Therefore, coke from HMF, formic acid, and 4-oxopentanoic acid decomposition had carbon contents of 6, 1, and 5 moles of carbon/mole of coke respectively.

In Figures 5-6 and 5-7, the amount of coke from HMF, formic acid, and 4-oxopentanoic acid are predicted as a function of time for HY-zeolite, APM, MCM-20, and MCM-41 catalysts. For HY-zeolite and APM catalysts, the predicted coke formation rapidly increases between 0 to 10 h, and then levels off between 10 to 24 h reaction time. The amount of coke from HMF is the highest and the amount of coke from formic acid is the lowest. For the APM catalyst, the amount of coke from HMF and from 4-oxopentanoic acid are comparable at 24 h reaction time.

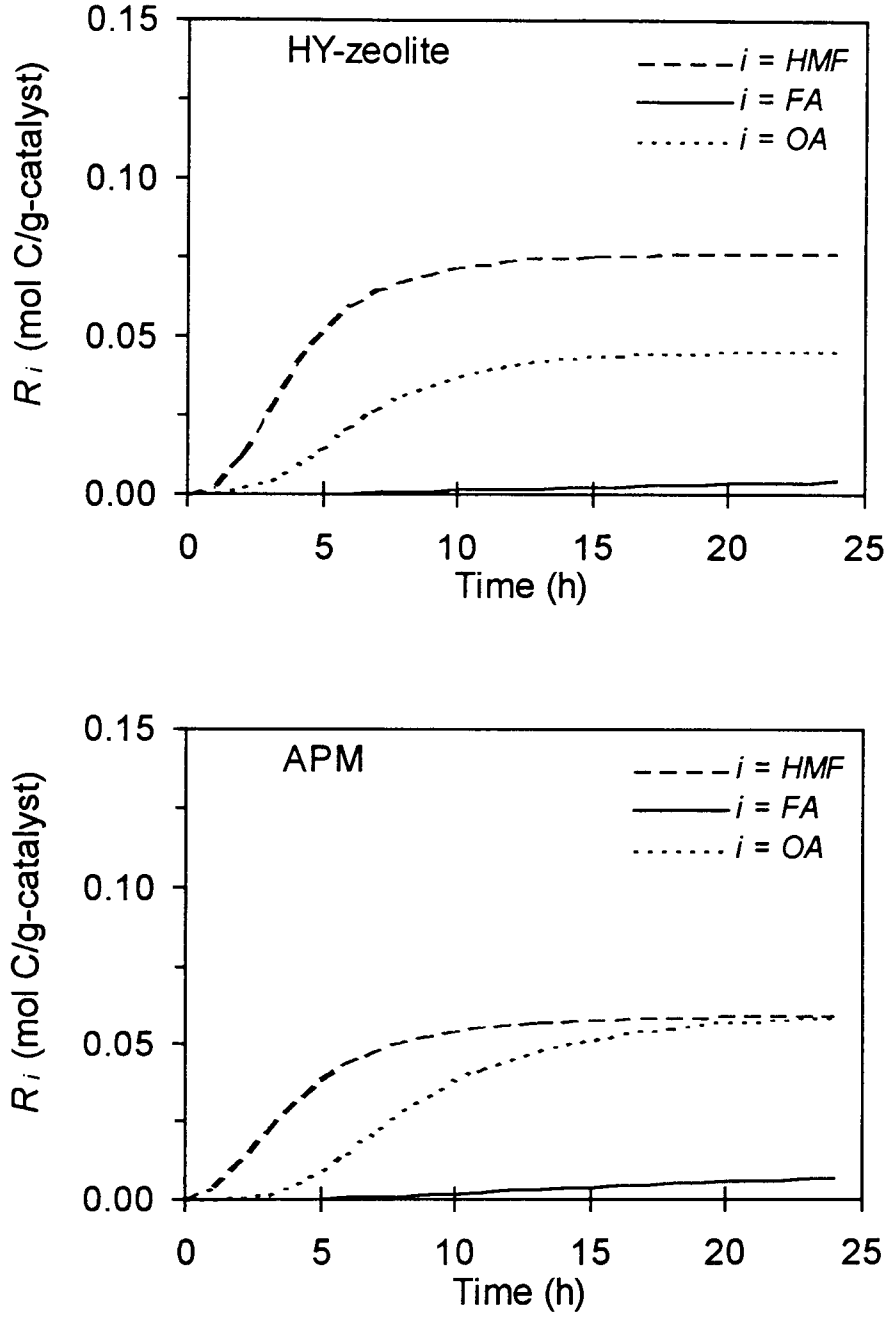

Figure 5-6. Predicted coke formation vs. reaction time at 150°C for HY-zeolite and APM catalysts.

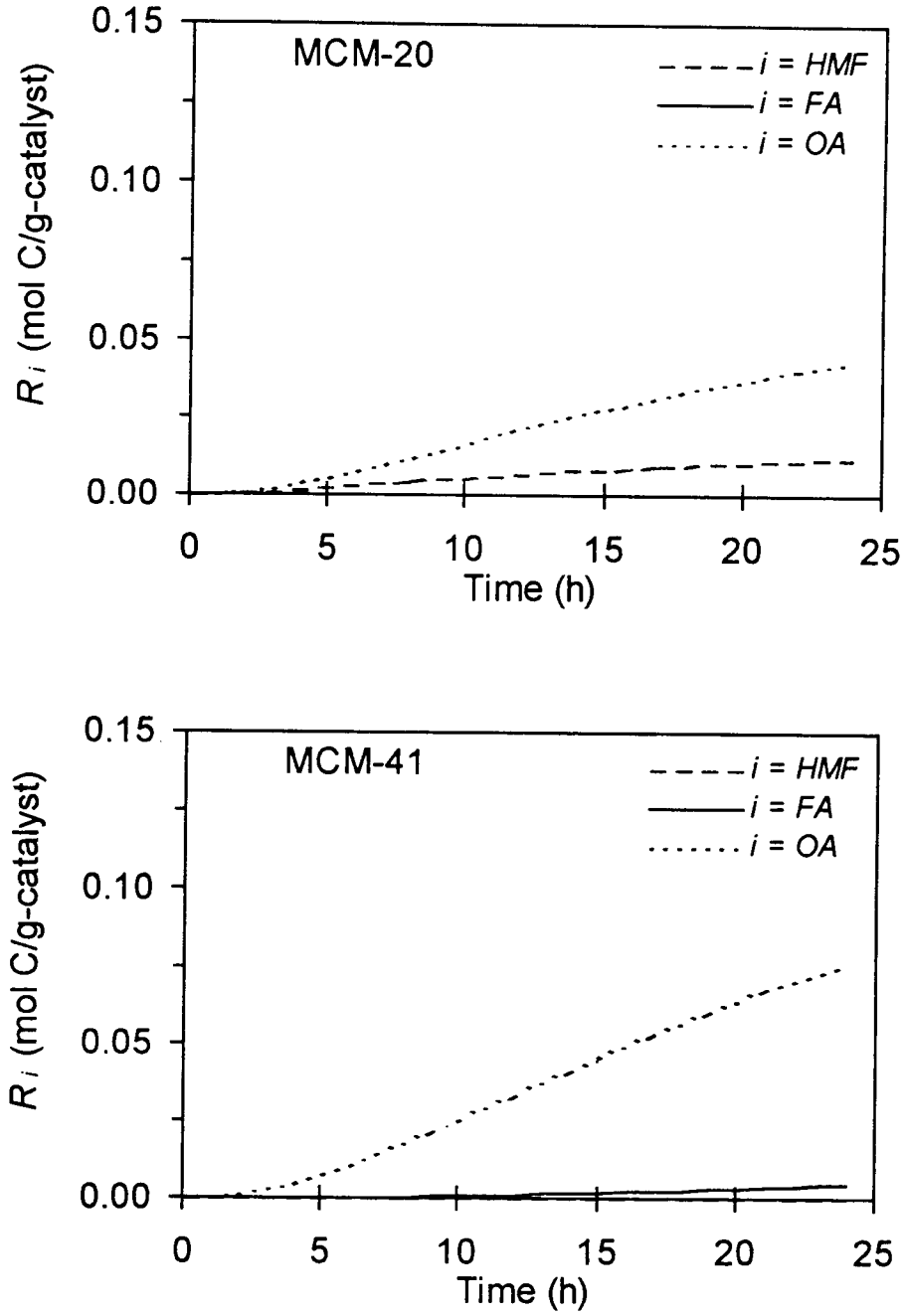

Figure 5-7. Predicted coke formation vs. reaction time at 150°C for MCM-20 and MCM-41 catalysts.

For MCM-20 and MCM-41 catalysts, the predicted coke formation linearly increases with increasing reaction time. The amount of coke from 4-oxopentanoic acid is also the highest. For the MCM-20 catalyst, the model predicted no coke formation from formic acid. For the MCM-41 catalyst, the model predicted no coke formation from HMF. The amounts of coke from HMF and formic acid are the lowest for MCM-20 and MCM-41 respectively.

In summary, these results show different patterns of coke formation depending on the pore size of catalyst. In microporous catalysts, coke formation rapidly increases during the first 10 h and then levels off. In mesoporous catalysts, coke formation linearly increases with reaction time. Coke from HMF rapidly decreases with increasing pore size. However, coke formation from 4-oxopentanoic acid is not strongly dependent on pore size. These results also suggest that coke formation from HMF, formic acid, and 4-oxopentanoic acid are minimized at the catalyst pore sizes ranging from 10 to 30 Å.

The carbon content of the solid residue obtained from the experiment was also estimated to facilitate comparison to model predictions. Before calcination, it was assumed that the solid residue had an empirical formula of CH_2O. After calcination, it was assumed that the coke had 1 mole carbon per mole of coke with an empirical formula of C.

The predicted total coke formation from all decomposition reactions (ΣR_i) after a 24 h reaction time was compared to the total measured coke deposited on the catalyst (Figure 5-8).

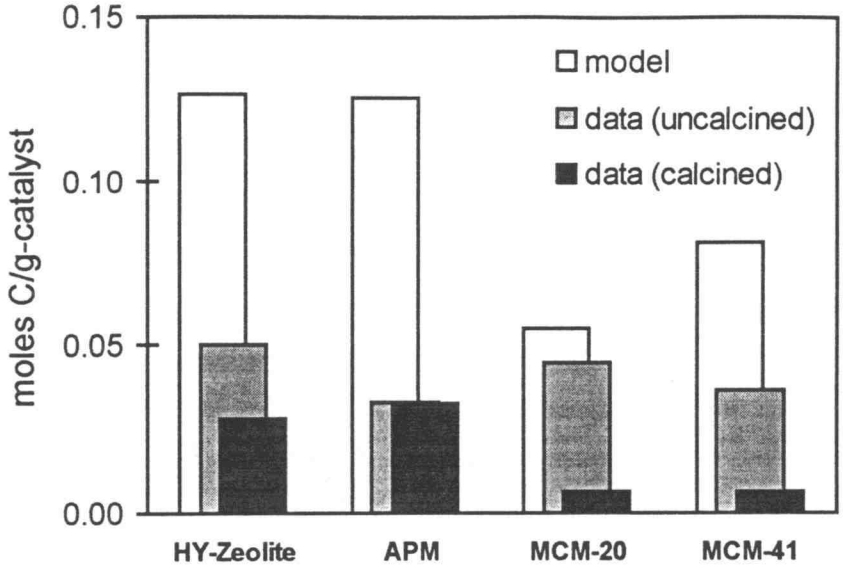

Figure 5-8. Comparison of measured coke formation with predicted coke after 24 h reaction time at 150°C for HY-zeolite, APM, MCM-20, and MCM-41 catalysts.

Coke formation predicted from the model after 24 h reaction time was at least two times greater than the measured coke formation before calcination. Most likely, unknown water-soluble products were produced by the reactions. At least seven water-soluble unknown products were detected by HPLC from the reaction of glucose with HY-zeolite under similar reaction conditions (Lourvanij and Rorrer, 1993). These unknown products could include water-soluble coke precursors such as polymeric HMF. However, unknown products, volatile humic solids, and water-soluble humic solids were all predicted as solid coke by the surface reaction model.

5.7 Catalyst Deactivation

Glucose conversion and product formation data from the reaction of 0.74 M glucose solution with HY-zeolite catalyst powder at 130°C for catalyst loading ranging from 13.3 g/L to 133.3 g/L were considered for analysis of catalyst deactivation by coking. The deactivation of the HY-zeolite catalyst is first characterized by the decrease in acid activity before and after the 24 h reaction. The acid activity before reaction is defined as a_X, whereas the acid activity of the catalyst after 24 h reaction is defined as $a_{X,f}$. The deactivation ratio (θ) of the acid sites on the catalyst surface is defined as

$$\theta = \frac{a_X - a_{X,f}}{a_X} \tag{5-26}$$

Therefore, the total acid site concentration before reaction is given by

$$C_X = C_{cat} \cdot a_X \tag{5-27}$$

and after 24 h reaction is given by

$$C_{X,f} = C_{cat} \cdot a_{X,f} \tag{5-28}$$

The acid activity after 24 h reaction time ($a_{X,f}$) and θ are plotted as a function of C_X (Figure 5-9). The acid activity ($a_{X,f}$) decreased with increasing C_X whereas θ increased with increasing C_X. The deactivation of HY-zeolite catalyst can occur by a solid residue which deposits inside the catalyst pore and blocks acid sites on the pore wall. Measured and predicted coke formation on the catalyst, however, decreased with increasing C_X (Figure 5-10). The sum of predicted surface concentration ($C_{i,X}$) of glucose, HMF, fructose, formic acid, and 4-oxopentanoic acid at 24 h reaction time increased with increasing C_X (Figure 5-11).

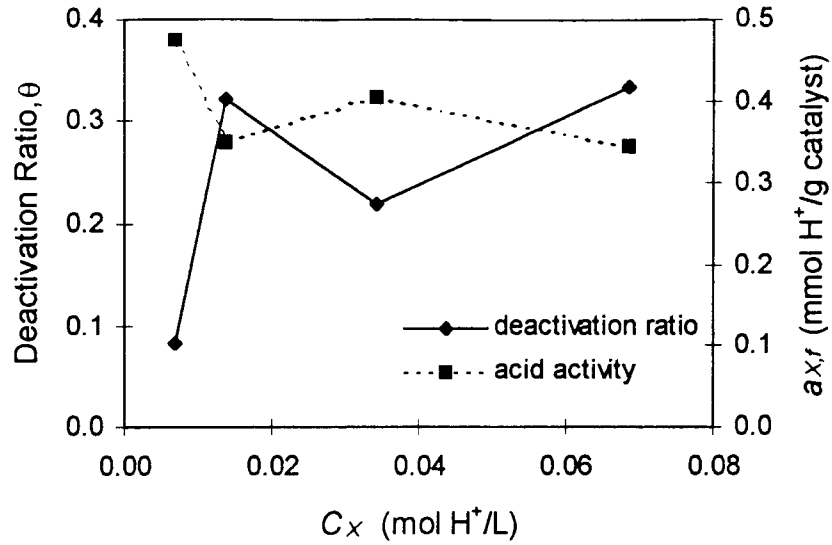

Figure 5-9. Catalyst acid activity ($a_{X,f}$) and deactivation ratio (θ) after 24 h reaction time at 130°C vs. C_X for HY-zeolite.

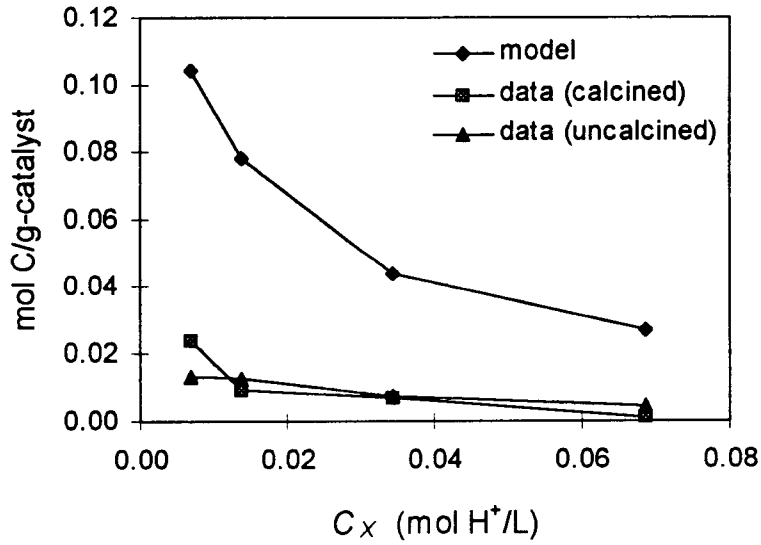

Figure 5-10. Comparison of measured coke formation with predicted coke formation after 24 h reaction time at 130°C vs. C_X for HY-zeolite.

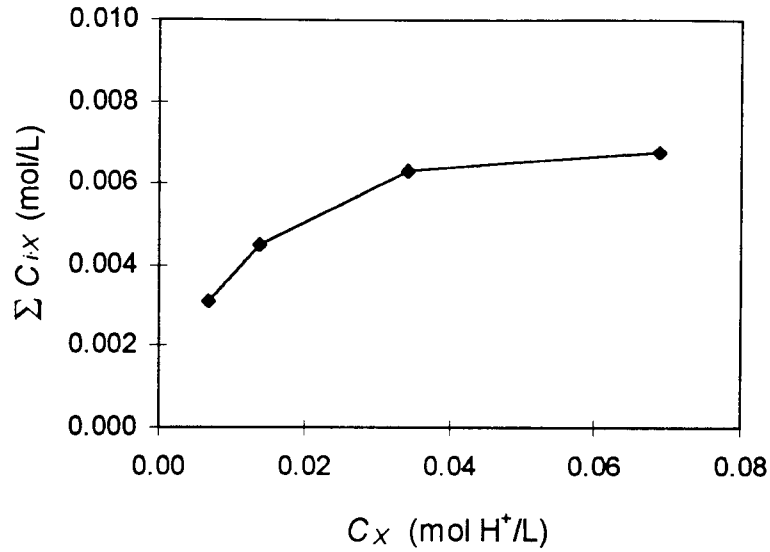

Figure 5-11. Sum of predicted surface concentration (C_{iX}) of five components after 24 h reaction time at 130°C vs. C_X for HY-zeolite.

The above result suggests that the deactivation of the catalyst is due to the blockage of acid sites by glucose, HMF, fructose, formic acid, and 4-oxopentanoic acid adsorbed on the pore wall inside the catalyst pores, rather than by solid residue deposited within the catalyst.

In order to explore the effect of catalyst deactivation on the reaction rates, kinetic constants were estimated based on values for both a_X and a_{Xf}. Then, the reaction activities, determined from the kinetic constants, were analyzed as functions of the total acid site concentration (C_X) and deactivation ratio (θ) of the catalyst. The reaction activities for four reaction processes, including glucose isomerization to fructose, glucose dehydration to HMF, fructose dehydration to HMF, and HMF rehydration to formic acid and 4-oxopentanoic acid, were of particular interest.

The estimated model parameters based on a_X and $a_{X,f}$ are compared in Table 5-7 and 5-8. The kinetic constants (k_{Sj}) at 130°C for the four major reaction processes, glucose isomerization to fructose, glucose dehydration to HMF, fructose dehydration to HMF, and HMF rehydration to formic acid and 4-oxopentanoic acid, based on $a_{X,f}$ are greater than kinetic constants based on a_X. From Figure 5-12, all kinetic constants decreased with increasing C_X. All data suggest that increasing the total acid site concentration in the reaction decreases both the acid activity of HY-zeolite and the reaction rates of four major reaction processes.

The activity ratio (F_{Sj}) of the reaction rate based on a_X to the reaction rate based on $a_{X,f}$ is defined as

$$F_{Sj} = \frac{k_{Sj}(a_X)}{k_{Sj}(a_{X,f})} \tag{5-29}$$

The estimated kinetic constant $k_{Sj}(a_X)$, based on a_X, represents the apparent reaction rate assuming no deactivation of catalyst. The estimated kinetic constant $k_{Sj}(a_{X,f})$, based on $a_{X,f}$, represents the reaction rate determined from the acid activity that remains after the deactivation of the catalyst, which reflects the actual acid activity available for the acid-catalyzed reactions. Calculated values of F_{Sj} are plotted as a function of θ in Figure 5-13 for the four major reaction processes.

The activity ratio for fast reaction with homogeneous blockage of active sites, called anti-selective poisoning by Wheeler (1951), is given by

$$F_{Sj} = \sqrt{1-\theta} \tag{5-30}$$

Predicted values by equation (5-30) are represented by the dashed line in Figure 5-13.

Table 5-7. Estimated model parameters at 130°C for the HY-zeolite catalyst based on a_X.

Catalyst Loading (g/L)	13.33	26.67	66.67	133.33
C_X (mol/L)	0.0069	0.0137	0.0343	0.0687
k_{S1} (1/h)	12.918	6.829	5.898	3.648
k_{S2} (1/h)	0.719	0.535	0.000	0.004
$1/K_{S1}$	0.000	0.000	0.000	0.034
k_{S3} (1/h)	24.458	10.420	7.431	4.409
k_{S4} (1/h)	17.198	28.462	19.551	11.226
k_{S5} (1/h)	79.078	49.858	29.447	12.450
k_{S6} (1/h)	5.136	2.679	2.559	1.539
k_{S7} (1/h)	24.017	13.311	8.261	7.361
K_G (L/mol-h)	0.480	0.627	0.505	0.821
K_H (L/mol-h)	1.268	1.181	0.899	1.837
K_F (L/mol-h)	0.593	0.871	0.769	0.911
K_{FA} (L/mol-h)	0.970	0.267	0.256	0.152
K_{OA} (L/mol-h)	0.992	0.665	0.413	0.294

Table 5-8. Estimated model parameters at 130°C for the HY-zeolite catalyst based on a_{Xf}.

Catalyst Loading (g/L)	13.33	26.67	66.67	133.33
C_{Xf} (mol/L)	0.0063	0.0093	0.0269	0.0460
k_{S1} (1/h)	13.342	8.632	6.743	4.931
k_{S2} (1/h)	0.924	0.729	0.000	0.140
$1/K_{S1}$	0.000	0.000	0.009	0.427
k_{S3} (1/h)	25.052	12.877	8.430	5.451
k_{S4} (1/h)	14.437	20.006	17.743	7.380
k_{S5} (1/h)	81.446	51.419	29.745	12.709
k_{S6} (1/h)	5.647	3.796	3.055	2.280
k_{S7} (1/h)	25.567	16.960	9.554	9.710
K_G (L/mol-h)	0.498	0.765	0.577	0.965
K_H (L/mol-h)	1.392	2.614	1.312	4.875
K_F (L/mol-h)	0.609	1.088	0.882	1.133
K_{FA} (L/mol-h)	1.066	0.380	0.306	0.225
K_{OA} (L/mol-h)	1.056	0.484	0.478	0.388

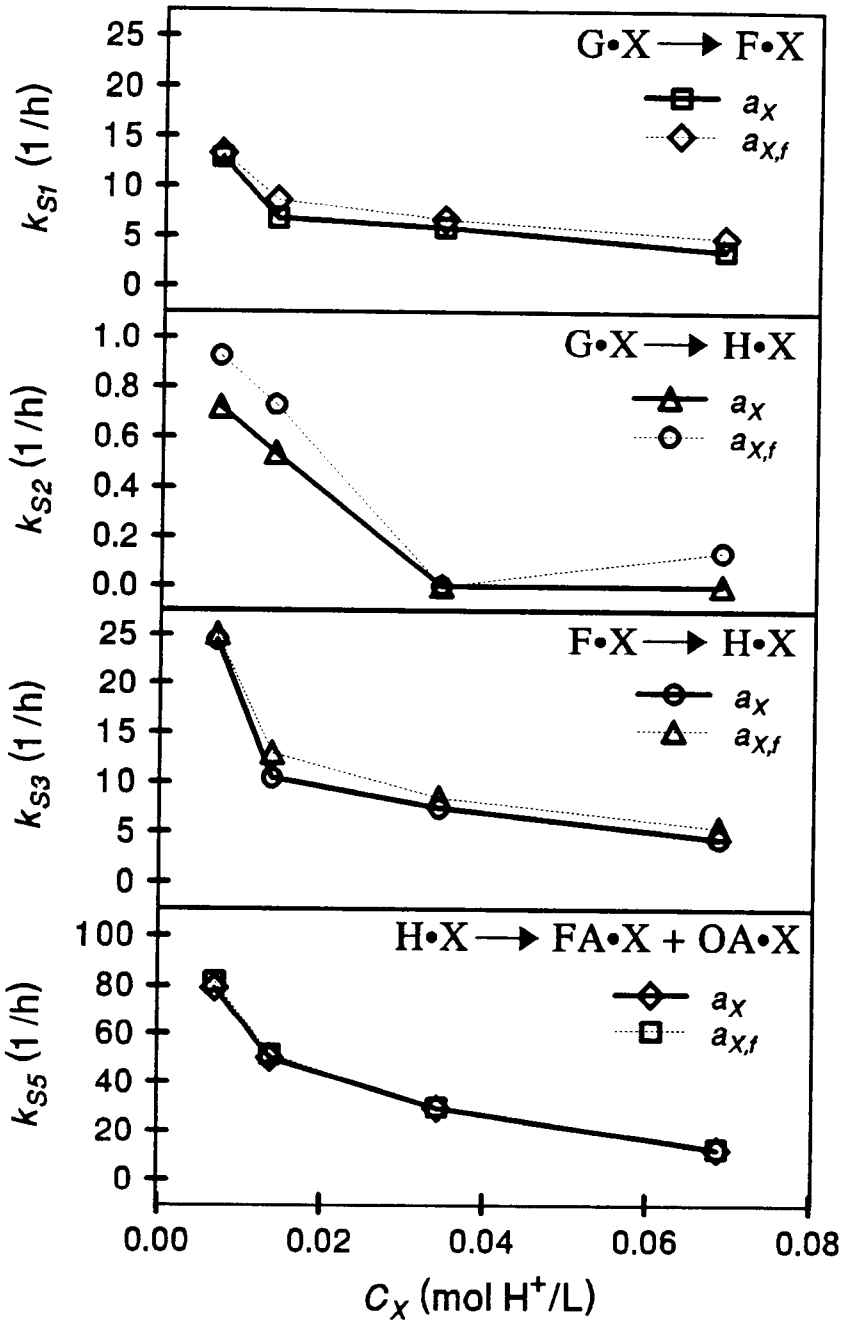

Figure 5-12. Selected kinetic constants (k_{Sj}) for the four major reaction processes at 130°C vs. C_X for HY-zeolite.

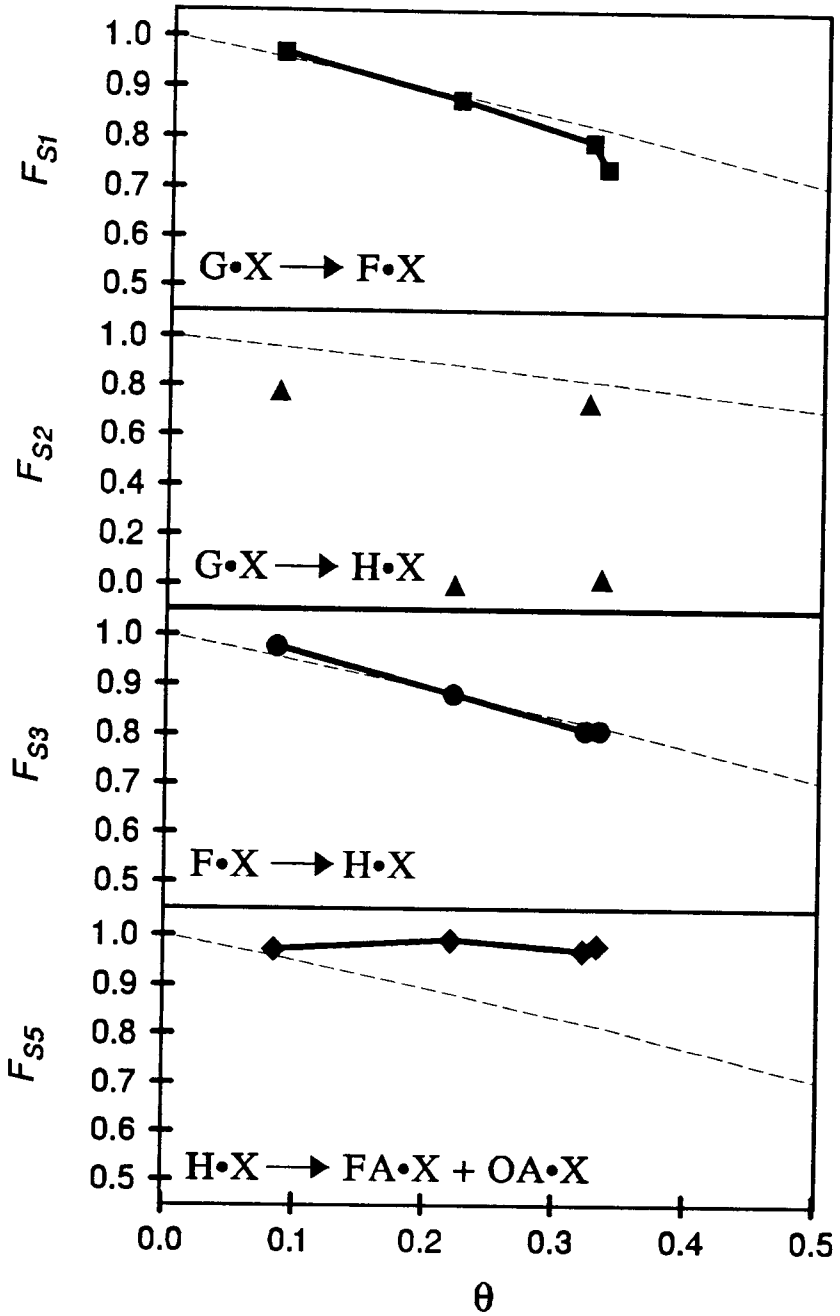

Figure 5-13. Activity ratio (F_{Sj}) for the four major reaction processes at 130°C vs. θ.

From Figure 5-12, the kinetic constants for k_{S2} (glucose dehydration to HMF) are relatively small compared to kinetic constants for the other three major reaction processes. The small value of this kinetic constant significantly affects the sensitivity of model parameter estimations. This result can lead to a scatter in the estimated value of F_{S2} for glucose dehydration to HMF, as shown in Figure 5-13. Furthermore, as described in section 5.5 (Effect of Catalyst Pore Size), Fructose is the preferred substrate over glucose for the dehydration to HMF. Therefore, the analysis will focus on glucose isomerization to fructose, fructose dehydration to HMF, and HMF rehydration to formic acid and 4-oxopentanoic acid.

Estimated values of F_{S1} and F_{S3} for glucose isomerization to fructose and fructose dehydration to HMF decreased with increasing θ, and were well predicted by the equation (5-30). This suggests that the reaction activity of glucose isomerization and fructose dehydration are decreased by the homogeneous blockage of acid sites on the surface of HY-zeolite catalyst.

All values of F_{S5} did not change with θ and were nominally close to 1.0. Therefore, the activity ratio of HMF rehydration to formic acid and 4-oxopentanoic acid is not influenced by the deactivation of the catalyst. Recall from Figure 5-10 that k_{S5} decreased with increasing C_X. It implies that the rate of HMF dehydration to formic acid and 4-oxopentanoic acid does not depend on the acid activity but depends on the total acid site concentration.

Chapter 6

SUMMARY AND CONCLUSIONS

The production of oxygenated hydrocarbons from glucose by catalytic processes is of interest because of the inherent limitations of biological processes. Catalytic processes which use molecular-sieving catalysts can accommodate glucose for direct intraparticle reactions and potentially promote shape-selective reactions as well. The present work focuses on the partial dehydration of glucose to oxygenated hydrocarbons with the solid-acid, molecular-sieving, aluminosilicate catalysts in the micropore to mesopore size range.

The partial dehydration of glucose to hydroxymethylfurfural (HMF) and the subsequent rehydration of HMF to formic acid and 4-oxopentanoic acid in aqueous solution at 130 to 190°C was promoted by microporous pillared clay and mesoporous MCM solid-acid catalysts. Specific catalysts included aluminum-pillared montmorillonite (APM), chromium-pillared montmorillonite (CPM), iron-pillared montmorillonite (FPM), MCM-20, and MCM-41. A reaction temperature of 150°C and greater was required for 100% glucose conversion. The iron-pillared montmorillonite catalyst provided the highest glucose conversion rate, the lowest selectivity of the HMF intermediate reaction product (0.04 mol HMF/mol glucose reacted), and the highest selectivity of formic acid final reaction product (0.6 mol formic acid/mol glucose reacted). The iron-pillared montmorillonite catalyst also possessed the largest micropore volume in the 10 to 50 Å range relative to other pillared montmorillonites. This fraction of the pore size larger than 10 Å allowed the 8.6 Å glucose molecule access to intraparticle acid sites, but still

promoted entrapment of the HMF molecule within the porous matrix, so that the reaction scheme could be selectively directed to the final organic acid products. Despite this improved selectivity, overall yields were lowered by significant coke formation, possibly due to acid-catalyzed degradation of the bulky HMF and 4-oxopentanoic acid molecules within the pores of the catalyst. In this regard, although formic acid and 4-oxopentanoic acid are theoretically produced in stoichiometric amounts, the selectivity of formic acid was much higher than 4-oxopentanoic acid.

A surface reaction model for the partial dehydration of glucose to organic acids by solid-acid, molecular-sieving aluminosilicate catalysts was developed. The model predicted the reaction kinetics of the four major acid-catalyzed reaction processes, including: glucose dehydration to HMF, rehydration and cleavage of HMF to formic acid and 4-oxopentanoic acid, glucose isomerization to fructose, and fructose dehydration to HMF. The model also predicted the rates of coke formation from the complete dehydration of HMF and organic acids.

The surface reaction model provided a framework for understanding the partial dehydration of glucose to organic acids in microporous and mesoporous solid-acid catalysts. Kinetic parameters proposed by the surface reaction model were estimated from glucose conversion and product yield vs. time data at 150°C for HY-zeolite, aluminum-pillared montmorillonite, MCM-20, and MCM-41 aluminosilicate catalysts of 0.5 mmol H^+/g-catalyst nominal solid acid activity under conditions where mass transfer resistances were minimized. The forward rate constants of the four major reaction processes were strongly correlated to the catalyst pore size. Rate constants for the series reactions of

glucose dehydration to HMF and HMF rehydration to organic acids were maximized at pore sizes ranging from 10 to 30 Å, whereas the rate constants for the competing parallel reactions of glucose isomerization to fructose and fructose dehydration to HMF were minimized in this same pore size range. The results suggest that the catalyst pore size has to be large enough to accommodate the 8.6 Å glucose molecule, but small enough to 1) selectively promote the acid-catalyzed dehydration of glucose to HMF, 2) retain the reaction intermediate HMF within the pore, and 3) promote the final rehydration and cleavage of HMF to formic and 4-oxopentanoic acid.

The surface reaction model also predicted coke formation from HMF, formic acid, and 4-oxopentanoic acid. Coke formation within microporous catalysts rapidly increased for the first 10 h of reaction time and then leveled off, whereas coke formation within mesoporous catalysts linearly increased with reaction time. Predicted coke formation from HMF decreased with increasing pore size, implying that HMF molecules avoided a complete dehydration to coke inside the catalysts with larger pores. The total coke formation from HMF and organic acids was also minimized at pore sizes ranging from 10 to 30 Å. However, the reaction model consistently over predicted the measured solid coke formation, suggesting the formation of water-soluble humic solids.

The deactivation of the acid activity for the HY-zeolite catalyst was due to the blockage of acid sites by the product molecules adsorbed on the catalyst pore wall. The forward rate constants of the four major reaction processes were strongly correlated to the total acid site concentration. The reaction activities determined from forward rate constants of the four major reaction processes were strongly correlated to the deactivation

of catalyst. The decrease of reaction activities for glucose isomerization to fructose and fructose dehydration to HMF with the deactivation of HY-zeolite catalyst were well predicted by an anti-selective poisoning process, where the blockage of acid sites was assumed to be homogeneous. The reaction activity of HMF rehydration to organic acids was not influenced by the deactivation of catalyst. The forward rate constant for HMF rehydration to organic acids was, however, influenced by the total acid site concentration.

This study has shown that solid-acid, molecular-sieving catalysts have the potential to promote the selective dehydration of glucose to organic acids, and that the catalyst pore size plays a significant role in determining which reactions are selectively promoted. The results have illustrated the feasibility of using molecular-sieving catalysts to promote shape-selective reactions of large organic molecules for production of oxygenated hydrocarbons.

BIBLIOGRAPHY

Awum, F., Narayan, S., and Ruthven, D. 1988. Measurement of Intracrystalline Diffusivities in NaX Zeolite by Liquid Chromatography. *Industrial & Engineering Chemistry Research* 27: 1510-1515.

Baksh, M.S., Kikkinides, E.S., and Yang, R.T. 1992. Characterization by Physisorption of a New Class of Microporous Adsorbents: Pillared Clays. *Industrial & Engineering Chemistry Research* 31: 2181-2189.

Baugh, K.D., and McCarty, P.L. 1988. Thermochemical Pretreatment of Lignocellulose to Enhance Methane Fermentation: I. Monosaccharide and Furfural Hydrothermal Decomposition and Product Formation Rates. *Biotechnology & Bioengineering* 31: 50-61.

Baugh, K.D., Levy, J.A., and McCarty, P.L. 1988. Thermochemical Pretreatment of Lignocellulose to Enhance Methane Fermentation: II. Evaluation and Application of Pretreatment Model. *Biotechnology & Bioengineering* 31: 62-70.

Beck, J.S., Vartuli, J.C., Roth, W.J., Leonowicz, M.E., Kresge, C.T., Schmitt, K.D., Chu, C.T-W., Olson, D.H., Sheppard, E.W., McCullen, S.B., Higgins, J.B., and Schlenker, J.L. 1992. A New Family of Mesoporous Molecular Sieves Prepared with Liquid Crystal Templates. *Journal of American Chemical Society* 114: 10834- 10843.

Chen, N.Y., Deganan, T.F., and Koenig, L.R. 1986. Liquid Fuel from Carbohydrates. *Chemtech* 16: 506-511.

Constantinides, A. 1987. *Applied Numerical Methods with Personal Computer*. New York: McGraw Hill Inc.

Corma, A., Fornés, V., Navarro, M.T., and Pérez-Pariente, J. 1994. Acidity and Stability of MCM-41 Crystalline Aluminosilicates. *Journal of Catalysis* 148:569-574.

Cussler, E.L. 1984. *Diffusion: Mass Transfer in Fluid Systems*. Cambridge: Cambridge University Press.

Doblin, C., Mathews, J.F., and Turney, T.W. 1991. Hydrocracking and Isomerization of n-Octane and 2,2,4-Trimethylpentane Over a Platinum/Alumina-pillared Clay. *Applied Catalysis* 70: 197-212.

Giannelis, E.P., Rightor, E.G., and Pinnavaia, T.J. 1988. Reactions of Metal-Cluster Carbonyls in Pillared Clay Galleries: Surface Coordination Chemistry and Fischer-Tropsch Catalysis. *Journal of American Chemical Society* 110: 3880-3885.

Haniff, M.I., and Dao, L.H. 1988. Deoxygeneration of Carbohydrates and their Isopropylidene Derivatives over ZSM-5 Zeolite Catalysts. *Applied Catalysis* 39: 33-47.

Horvath, G.E., and Kawazoe, K. 1983. Method for the Calculation of Effective Pore Size Distribution in Molecular Sieve. *Journal of Chemical Engineering Japan* 16: 470-475.

Kung, H.H. 1989. *Transition Metal Oxides: Surface Chemistry and Catalysis (Studies in Surface Science and Catalysis)*. Amsterdam: Elsevier Science Publishers B.V.

Kuster, B.F.M., and Van der Baan, H.S. 1977. The Dehydration of D-Fructose (Formation of 5-Hydroxymethyl-2-furaldehyde and Levulinic Acid): Part II. The Influence of Initial and Catalyst Concentrations on the Dehydration of D-Fructose. *Carbohydrate Research* 54: 165-176.

Kuster, B.F.M. 1977. The Dehydration of D-Fructose (Formation of 5-Hydroxymethyl-2-furaldehyde and Levulinic Acid): Part III. The Influence of Water Concentration on the Dehydration of D-Fructose. *Carbohydrate Research* 54: 177-183.

Levenspiel, O. 1993. *Chemical Reactor Omnibook*. Corvallis: OSU Book Stores Inc.

Lourvanij, K., and Rorrer, G.L. 1993. Reactions of Aqueous Glucose Solutions over Solid-Acid Y-Zeolite Catalysts at 110 to 160°C. *Industrial & Engineering Chemistry Research* 32: 11-19.

Ma, Y.H., Lin, Y.S., and Fleming, H.L. 1988. Adsorption and Diffusion of Polar and Non-Polar Liquids in Aluminas by HPLC. *AIChE Symposium Series* 84: 1-12.

Netrabukkana, R. 1994. *The Diffusion of Glucose and Glucitol in Microporous and Mesoporous Silica-based Catalysts*. M.S. Thesis. Corvallis: Oregon State University.

Petersen, E.E. 1965. *Chemical Reaction Analysis*. New Jersey: Prentice Hall Inc.

Pinnavaia, T.J., Tzou, M-S., and Landau, S.D. 1985. New Chromia Pillared Clay Catalysts. *Journal of American Chemical Society* 107: 4783-4785.

Rightor, E.G., Tzou, M-S., and Pinnavaia, T.J. 1991. Iron Oxide Pillared Clay with Large Gallery Height: Synthesis and Properties. *Journal of Catalysis* 130: 29-40.

Schraufnagel, R.A., and Rase. H.F. 1975. Levulinic Acid from Sucrose Using Acidic Ion-Exchange Resins. *Industrial & Engineering Chemistry Product Research & Development* 14: 40-44.

Smith, J.M. 1981. *Chemical Engineering Kinetics*. 3d ed. New York: McGraw Hill Inc.

Szmant, H.H., and Chundury, D.D. 1981. The Preparation of 5-Hydroxymethyl Furfuraldehyde from High Fructose Corn Syrup and Other Carbohydrates. *Journal of Chemical Technology and Biotechnology* 31: 135-145.

Wheeler, A. 1951. Reactions Rates and Selectivity in Catalyst Pores. In *Advances in Catalysis*, ed. W.G. Frankenburg, E.K. Rideal, and V.I. Komarewsky, 307-309. New York: Academic Press Inc.

APPENDICES

Appendix A

Catalyst Synthesis Procedures

Synthesis of Al-Pillared Montmorillonite

$(Al_{13}O_4(OH)_{24}[Si_{13.09}Al_{4.10}Mg_{0.58}Ca_{0.17}K_{0.03}Ti_{0.01}O_{34.47}Fe_{0.57}]_7)$

Materials

Aluminum chloride, $AlCl_3$

Sodium hydroxide, NaOH

Montmorillonite clay

Pillaring Agent (Aluminum Chlorohydrate) Preparation

1. Hydrolyze $AlCl_3$ with NaOH based on OH/Al molar ratio of 2.5.
2. Age at 50°C for 12 h or until no precipitate is observed.

Pillaring Procedures

1. Prepare 1% wt of montmorillonite in distilled water (1 g in 1 L H_2O).
2. Slowly add pillaring agent (2 L of 1% wt clay slurry to 1 L of 2.1% wt aluminum chlorohydrate, 70 mmol Al/ meq clay).
3. Heat and stir at 70°C for 4 h.
4. Centrifuge and wash until free of Cl-ion (silver nitrate test).
5. Dry wet pillared clay under flowing air in fume hood at ambient temperature.
6. Grind and sieve dry pillared clay if necessary to a particle size < 100 μm.
7. Keep the dry pillared clay in an air-tight container.

Synthesis of Fe-Pillared Montmorillonite

$(Fe(OH)_2[Si_{13.09}Al_{4.10}Mg_{0.58}Ca_{0.17}K_{0.03}Ti_{0.01}O_{34.47}Fe_{0.57}])$

Materials

Ferric chloride, $FeCl_3$

Sodium carbonate, Na_2CO_3

Montmorillonite clay

Pillaring Agent Preparation

1. Hydrolyze 0.2 M $FeCl_3$ with Na_2CO_3 based on 1.5 meq/mol metal (0.15 mol Na_2CO_3 / 0.2 mol $FeCl_3$).
2. Age at 25°C for 24 h. or until no precipitate is observed.
3. Bubble solution with N_2 gas to remove CO_2.

Pillaring Procedures

1. prepare 1% wt of montmorillonite in distilled water (1 g in 1 L H_2O).
2. Slowly add pillaring agent (3.16 g of clay to 1 L of pillaring agent, 70 mmol Fe/ meq clay).
3. Stir at ambient temperature for 4 h.
4. Centrifuge and wash until the pH of liquid fraction is constant (about 10 washings are needed).
5. Dry wet pillared clay under flowing air in fume hood at ambient temperature.
6. Grind and sieve dry pillared clay if necessary to a particle size < 100 μm.
7. Keep the dry pillared clay in an air-tight container.

Synthesis of Cr-Pillared Montmorillonite

$(Cr_2(OH)_2(H_2O)_8[Si_{13.09}Al_{4.10}Mg_{0.58}Ca_{0.17}K_{0.03}Ti_{0.01}O_{34.47}Fe_{0.57}]_4)$

Materials

Chromium Nitrate, $Cr(NO_3)_3$

Sodium carbonate, Na_2CO_3

Montmorillonite clay

Pillaring Agent Preparation

1. Hydrolyze 0.1 M $Cr(NO_3)_3$ with Na_2CO_3 based on 2.0 meq/mol metal (0.1 mol $Cr(NO_3)_3$ / 0.1 mol Na_2CO_3).
2. Age at 95°C for 24 h.

Pillaring Procedures

1. Prepare 1% wt of montmorillonite in distilled water (1 g in 1 L H_2O).
2. Slowly add pillaring agent (1.58 g of clay / 1 L of pillaring agent, 70 mmol Fe/ meq clay).
3. Stir at ambient temperature for 4 h.
4. Centrifuge and wash until the pH of liquid fraction is constant (about 10 washings are needed).
5. Dry wet pillared clay under flowing air in fume hood at ambient temperature.
6. Grind and sieve dry pillared clay if necessary to a particle size < 100 μm.
7. Keep the dry pillared clay in an air-tight container.

Synthesis of Aluminosilicate MCM-41

Materials

HiSil silica

Cetyltrimethylammonium chloride, $C_{16}H_{33}(CH_3)_3NCl$

Amberlite IRA-400(OH) exchange resin

Sodium aluminate (technical grade)

Tetramethylammonium silicate (0.5 TMA/SiO_2, 10 % wt silica)

Procedures

1. Batch exchange 29% wt of aqueous $C_{16}H_{33}(CH_3)_3NCl$ with IRA-400(OH) in a beaker to prepare $C_{16}H_{33}(CH_3)_3NCl/OH$ solution based on 4 meq/g.
2. Add 2.1 g of sodium aluminate, 50 g of tetramethylammonium silicate, and 12.5 g of HiSil silica to 100 g of $C_{16}H_{33}(CH_3)_3NCl/OH$.
3. Stir mixture at 350 rpm in a glass lined 300 mL Parr autoclave at 120°C for 24 h.

4. Recover solid by vacuum filtration. Wash with distilled water.
5. Dry wet catalyst under flowing air in fume hood at ambient temperature.
6. Load about 5 g catalyst into a crucible. Calcine at 540°C for 1 h in flowing N_2 followed by 6 h in flowing air within furnace.
7. Grind and sieve if necessary to a particle size than 100 μm.

Synthesis of Aluminosilicate MCM-20

Materials

HiSil silica

Dodecyltrimethylammonium chloride, $C_{12}H_{25}(CH_3)_3NCl$

Amberlite IRA-400(OH) exchange resin

Sodium aluminate (technical grade)

Tetramethylammonium silicate (0.5 TMA/SiO_2, 10 % wt silica)

Procedures

All procedures are exactly the same as the synthesis of MCM-41 except for the batch exchange of 50% wt aqueous $C_{12}H_{25}(CH_3)_3NCl$ with IRA-400(OH) based on 4 meq/g. To prepare $C_{12}H_{25}(CH_3)_3NCl/OH$ solution, the $C_{12}H_{25}(CH_3)_3NCl/OH$ is substituted for $C_{16}H_{33}(CH_3)_3NCl/OH$ solution in the templating process.

Table A-1. Properties of HY-zeolite catalyst.

Measurement	Mean Pore Diameter $\bar{d}_{pore}$ (Å)	BET Surface Area S (m^2/g)	Acid Activity a_X (mmol H^+/g)	N_2-Analysis File	Ar-Analysis File
# 1	7.0	648.1 ± 3.7	0.52 ± 0.01	Data1.017	Data1.038
# 2	6.6	642.1 ± 6.0	0.52 ± 0.01	--	Data1.029

Table A-2. Properties of unpillared H-montmorillonite catalyst.

Batch	Mean Pore Diameter $\bar{d}_{pore}$ (Å)	BET Surface Area S (m^2/g)	Acid Activity a_X (mmol H^+/g)	N_2-Analysis File	Ar-Analysis File
# 3	17.3	32.8 ± 1.0	0.91 ± 0.02	--	Data1.037
# 4	17.1	49.1 ± 1.0	0.89 ± 0.09	--	Data1.036

Table A-3. Properties of Al-pillared montmorillonite catalyst.

Batch	Mean Pore Diameter $\bar{d}_{pore}$ (Å)	BET Surface Area S (m^2/g)	Acid Activity a_X (mmol H^+/g)	N_2-Analysis File	Ar-Analysis File
# 1	11.4	137.7 ± 0.8	0.52 ± 0.01	Data1.005	Data1.011
# 2	10.2	131.5 ± 2.8	0.52 ± 0.01	--	Data1.049

Table A-4. Properties of Cr-pillared montmorillonite catalyst.

Batch	Mean Pore Diameter $\overline{d}_{pore}$ (Å)	BET Surface Area S (m^2/g)	Acid Activity a_X (mmol H^+/g)	N_2-Analysis File	Ar-Analysis File
# 3	11.7	280.3 ± 3.0	1.00 ± 0.16	Data1.003	Data1.007
# 4	12.2	235.6 ± 2.9	0.86 ± 0.02	--	Data1.031
# 5	12.1	235.2 ± 2.2	0.79 ± 0.02	--	Data1.035

Table A-5. Properties of Fe-pillared montmorillonite catalyst.

Batch	Mean Pore Diameter $\overline{d}_{pore}$ (Å)	BET Surface Area S (m^2/g)	Acid Activity a_X (mmol H^+/g)	N_2-Analysis File	Ar-Analysis File
# 4	15.6	227.2 ± 4.0	0.94 ± 0.08	Data1.004	Data1.006
# 5	14.8	219.8 ± 3.7	0.86 ± 0.03	--	Data1.032
# 6	14.2	239.4 ± 4.2	0.83 ± 0.02	--	Data1.034

Table A-6. Properties of MCM-20 catalyst.

Measurement	Mean Pore Diameter $\overline{d}_{pore}$ (Å)	BET Surface Area S (m^2/g)	Acid Activity a_X (mmol H^+/g)	N_2-Analysis File	Ar-Analysis File
# 1	27.7	548.1 ± 2.4	0.29 ± 0.07	Data1.118	Data1.068
# 2	27.3	535.2 ± 5.1	0.33 ± 0.11	Data1.119	Data1.069

Table A-7. Properties of MCM-41 catalyst.

Batch	Mean Pore Diameter $\overline{d}_{pore}$ (Å)	BET Surface Area S (m^2/g)	Acid Activity a_X (mmol H^+/g)	N_2-Analysis File	Ar-Analysis File
# 1	33.3	655.2 ± 4.0	0.46 ± 0.01	Data1.066	Data1.058
# 2	32.3	863.7 ± 7.5	0.46 ± 0.01	Data1.084	Data1.061

Appendix B

ASAP 2000 Accelerated Surface Area and Porosimetry System Operation Procedures

Start-Up

1. Turn on the power switch at the back of analyzer, start up the computer, open valves and regulators for He, Ar, and N_2 cylinders, turn on the molecular drag pump.
2. Close the gas inlet valves to the ASAP 2000 analyzer.
3. Fill up the cold trap dewar (center dewar on ASAP 2000) with liquid N_2 up to about 3 inches from the dewar mouth.
4. Place the dewar back into position, then slide cold trap stopper into dewar opening.
5. Start the operating program on the computer by executing "RUN20M" file.
6. After the main function menu displays on the monitor, choose "F 8" status/control menu.
7. Choose "F 3" manual control (8.3) from the status/control menu.
8. After the manifold diagram displays, press "F 3" to activate the solenoid valves at positions 1, 2, 4, 5, 6, and 7 on the diagram. This step degasses the system.
9. Observe a pressure gauge of the analysis section on the control panel in front of the analyzer until constant.
10. Shut off the solenoid valves by pressing "F 3" again at all positions on the diagram except at position of 1, 2, and 7.
11. Observe the status on the highlighted part of the computer screen. The status should be idle.
12. Press "ESC" to go back to the main function menu.

Sample Preparation

1. Weigh a clean, oven-dried sample tube with a frit stopper.
2. Weigh dry sample. The analysis requires a minimum surface area about 10 m^2. Therefore, if the estimated surface area of sample is about 150 m^2/g, then the minimum sample mass required is 0.06 g.
3. Load sample into the sample tube. Close the tube with the frit stopper.
4. Weigh the sample and sample tube, then calculate the sample weight before degassing.
5. Remove the plug from one of the degassing port on the analyzer.
6. Put a connector nut, ferrule, and O-ring on the sample tube.
7. Insert the sample tube into the degassing port, tighten the connector nut by hand. Make sure the proper position of ferrule and O-ring (O-ring is between the ferrule and the port).
8. Place the heating mantle to cover the bottom part of sample tube, put the clip on.
9. Set the heating enable switch (red light on). Set the mantle heating temperature and the fast evacuation start point at the control panel.
10. Set a mode selection to auto degas, red light on at "auto" position.
11. On the control panel, press "load", then "left", "right", or both depending on which the degassing port used.
12. Press "begin" to start degassing process.
13. Check the degassing pressure by press "check, then "left" or "right", and "begin".
14. If the pressure read-out is constant, the sample degassing is completed.
15. After the degassing process is completed, press "unload", then "left" or "right", and "begin".
16. After the unloading process is completed (green light on at "ready"), remove the heating mantle.
17. Unscrew the connector nut, remove the sample tube from the degassing port.
18. Put the plug and connector assembly back to the degassing port.

19. Weigh the sample and sample tube, calculate the sample weight after degassing. This value should be lower than the weight before degassing.
20. Sample and sample tube should be placed into the analysis port as soon as possible.

Pre-Analysis

1. Fill up the analysis dewar (right dewar on ASAP 2000) with liquid argon up to about 3 inches from the dewar mouth. Check by the dip stick the level of liquid argon, which should not exceed a hole position on the dip stick.
2. Place the dewar on the elevator. Cover the dewar opening with a foam sheet.
3. Remove a plug from the analysis port on the analyzer.
4. Put the isothermal jacket over the sample tube. For a bulb sample tube, the isothermal jacket is above the bulb. For a straight sample tube, the isothermal jacket is above the sample level retained by tube clip.
5. Insert the sample tube with isothermal jacket into the analysis port, tighten the connector nut by hand, make sure the proper position of ferrule and O-ring (O-ring is between the ferrule and the port).
6. Put the insulated dewar cover around the sample tube between the connector nut and isothermal jacket.
7. Remove the foam-sheet cover.
8. Open the gas inlet valve of argon to the analyzer.

Performing Analysis

1. On the main function menu screen, choose "F 3" sample information menu.
2. Choose "F 3" to add sample information.
3. complete the items on the first screen (3.3, p.1) for sample information

    Sample no.: (automatically provided)

    Sample ID: name of sample up to 40 characters

    Submitter ID: name of person who submits the sample

    Operator ID: name of person who perform analysis

    Report title: (default set to Biochemical Engineering Laboratory)

Sample weight: sample weight after degassing

Type of data: automatically collected

4. After finishing, press "PgDn" to the second screen, add sample-run conditions.
5. Complete the items on the second screen (3.3, p.2) of run condition

   Analysis gas: argon

   Analysis bath temp.: 87.3 K

   Fast evacuation: no

   Preliminary evac. time: 0.5 h

   Leak test: yes

   Measure free space: yes

   Equil. interval: 45 sec

   Crossover pressure: 5.0 mm Hg

   P/P_o tolerance: 5.0 % 5.000 mm Hg

   Leak interval: 120 and 180 sec

   Measure P_o: yes

   P_o interval: 120 min

   Free space evac. time: 0.5 h

   Dose amount: 1.5 cc/g STP

   Min. equil. time: 0 h., Max. equil. time: 8 h
6. After finishing, press "PgDn" to the third screen, add sample pressures.
7. On the pressure screen (3.3, p.3), choose "no" for "use standard pressure tables?". Enter the pressure table no. 4. The pressure table ID is Alumino-Silicate.
8. After finishing, press "PgDn" to the fifth screen, add sample report options.
9. On the report option screen (3.3p5), enter the report option set no. 2. The report ID is Alumino-Silicate.
10. To save all information press "PgDn". After a moment, the screen should go back to the sample information menu.
11. Press "ESC" to go back to the main function menu.
12. Press "F 8" status/control menu and "F 7" zero pressure gauge (8.7).

13. Press "PgDn" to perform zero pressure gauge. After a moment, the screen will go back to the status/control menu.
14. Press "ESC" to go back to the main function menu.
16. Press "F 7" to start run.
17. On the start run screen, enter the unit no. 1 and the sample no., then press "Enter".
18. The information about the sample and analysis will display. Confirm all information.
19. Choose the option for the report after analysis and the report destination.
20. Press "PgDn" to start performing analysis, the main function menu will display.
21. Lower the safety shield as far as possible.
23. Press "F 8" status/control menu and "F 4" to monitor the analysis. The run status/control screen (8.4) will display.

Post-Analysis

1. Wait until the status on the highlighted part of computer screen is idle.
2. Raise the safety shield. Cover the dewar with the foam sheet.
3. Remove the insulated dewar cover, unscrew the connector nut, and remove the sample tube from the analysis port.
4. Put the plug and connector assembly back to the analysis port.
5. Remove the isothermal jacket from the sample tube.
6. Clean the sample tube using the provided cleaning brush. The sample can be kept or discarded.
7. Rinse the sample tube with distilled water and acetone.
8. Dry and keep the sample tube in the oven at 60°C.

Shut Down

1. Close the gas inlet valves to the ASAP 2000 analyzer.
2. Turn off the molecular drag pump switch.

3. Exit the operating program by press "F 9" utility menu and "F 10" exit to DOS. Choose "no" at the prompt, then press "PgDn" to exit the program to the DOS prompt.
4. Turn off computer and monitor.
5. Turn off the main power switch of the analyzer system, lower the safety shield, and lift the control panel to the up-position.

ASAP 2000 Analysis Conditions

Analysis gas: argon

Molecular cross section: 0.142 nm^2

Non-ideality correction factor: 0.000066

Density conversion factor (D_ρ): 0.00128

Horvath-Kawazoe diameter of molecule (*DA*): 2.95 Å

Horvath-Kawazoe diameter of maximum interaction energy: 2.53 Å

Diameter of sample atom; based on Zeolite (*DS*): 3.04 Å

Diameter of sample maximum interaction energy: 2.917 Å

Interaction parameter; based on Zeolite and argon at 87.3 K (*IP*): 3.19×10^{-43} ergs-cm^4

Thermal transpiration correction molecular hard sphere diameter: 3.625 Å

Bath temperature (*T*): 87.3 K (liquid argon)

Degassing temperature: 110°C for 12 h.

Fast evacuation start pressure: 750 μm Hg

Analysis vacuum set point for gas switching: 25 μm Hg

Controlling program: ASAP 2000M v 2.03

Appendix C

Horvath-Kawazoe Calculation

For each collected-absolute equilibrium pressure (p) data point, values of d_{pore} are chosen in an iterative manner and the following equation (C-1) is solved for the absolute equilibrium pressure (p). The value of d_{pore} is determined when the calculated absolute pressure is within 0.1% of the collected absolute pressure. An absolute pressure lower limit is determined such that d_{pore} in the following equation is never equal to zero. All pressure points less than this limit are discarded.

$$\ln\left(\frac{p}{p_o}\right) = \frac{K}{RT} \times \frac{IP \times 10^{32} J.\text{Å}^4 / J.cm^4}{\delta^4\left(d_{pore} - D\right)} \times \left[\frac{\delta^4}{3\left(d_{pore} - \frac{D}{2}\right)^3} - \frac{\delta^{10}}{9\left(d_{pore} - \frac{D}{2}\right)^9} - \frac{\delta^4}{3\left(\frac{D}{2}\right)^3} + \frac{\delta^{10}}{9\left(\frac{D}{2}\right)^9}\right] \quad \text{(C-1)}$$

where:

K Avogadro's number, 6.023×10^{23} molecules/mol

R gas constant, 8.314×10^{7} ergs/mol-K

T analysis bath temperature, K

δ gas-solid nuclear separation at zero interaction energy, Å

$$\delta = (ZS + ZA)/2 \quad \text{(C-2)}$$

where

ZS sample equilibrium diameter at zero interaction energy, Å

ZA gas equilibrium diameter at zero interaction energy, Å

D sum of gas molecule and sample molecule diameters, Å

$$D = DA + DS \quad \text{(C-3)}$$

where

DA diameter of gas molecule, Å

DS diameter of sample molecule, Å

d_{pore} pore diameter (nucleus to nucleus), Å

p equilibrium pressure, mm Hg

p_o saturated pressure, mm Hg

IP interaction parameter, 10^{-43} ergs-cm^4

Based on the previous calculations, the following terms can be estimated

1. Adjusted Pore Diameter ($d_{pore,A}$), Å

$$d_{pore,A,l} = d_{pore,l} - DS \tag{C-4}$$

2. Cumulative Pore Volume (V_{CUM}), cm^3/g

$$V_{CUM,l} = V_l D_\rho \tag{C-5}$$

where:

V_l measured volume of gas at point "l" designated for Horvath-Kawazoe calculation, cm^3

D_ρ density conversion factor, cm^3 liquid/cm^3 STP

3. $d(V)/d(d_{pore})$ Pore Volume, cm^3/g-Å

$$\frac{d(V)}{d\left(d_{pore}\right)} = \frac{V_{CUM,l} - V_{CUM,l-1}}{d_{pore,A,l} - d_{pore,A,l-1}} \tag{C-6}$$

Appendix D

HP 5890 Series II Gas Chromatography Operating Procedures

Start-Up

1. Turn on the power switch of the HP 5890 series II Gas Chromatography (GC) unit. Start up HP Vectra 486/33N computer.
2. Open the gas cylinder valves, regulator, and final regulator located at the auxiliary flow panel on the left side on the GC unit. Set the carrier regulator to 60 psi.
3. Prepare the bubble flow meter; add soap or leak detecting liquid if necessary.
4. Press "FLOW" and "B" on the control panel of the GC unit to monitor flow rate for channel B.
5. Open the total flow valve for channel B (split). Increase the flow rate of carrier gas to the desired value by observing the display in the control panel.
6. Place the rubber tube of the bubble flow meter over the split/splitless purge outlet.
7. Press "TIME" on the control panel three times until the stopwatch displays.
8. Measure total flow rate using the bubble flow meter and stopwatch on control panel (flowrate = volume/elapsed time).
9. Adjust the total flow rate to the desired value. Repeat the measurement in step 8.
10. Disconnect the rubber tube. Put in the flame ionization detector adapter to the end of rubber tube.
11. Place the other end of the adapter into the flame ionization detector (FID) outlet on the top of GC unit.
12. Measure the flow rate through the column using the bubble flow meter and stopwatch.
13. Adjust the column head pressure valve to obtain the desired flow rate through the column.
14. Open the auxiliary gas valve (AUX) for detector B to fully opening.

15. Adjust the flow rate of auxiliary gas by tuning the screw in the middle of valve knob using the screw driver. Measure the flow rate using the bubble flow meter and stopwatch.
16. Open the hydrogen valve to fully opening.
17. Adjust the flow rate of hydrogen by tuning the final stage regulator located at the auxiliary flow panel. Measure the flow rate using the bubble flow meter and stopwatch.
18. Open the air valve to fully opening and adjust the flow rate similar to the adjusting flow rate of hydrogen.
19. Remove the bubble flow meter.
20. Start the FID by pressing the FID ignitor until hearing a "pop" sound.
21. On the control panel, press "FLOW" and "A" to monitor the flow rate of column in channel A.
22. To prevent the column coating from thermally deteriorating, continuously flow the carrier gas through the column by opening the carrier flow valve until the pressure gauge read-out is about 2-4 psi.
23. Open the reference gas valve (REF) for the thermal conductivity detector (TCD) about half way to prevent burn-out of the filament in the TCD.
24. Execute the Windows operating system, then execute "hp chem" in "hp chemstation" work group.
25. On the control screen, choose "Load" in "Method" menu.
26. Choose an appropriate system controlling file.
27. After loading the controlling file, the GC unit should start warming up, and the set-up information should display.
28. In "Instruments" menu, confirm the "temperature program", "enable detector", "signal", "channel of data acquisition", and "analysis run time".
29. In "Data Analysis" menu, choose "Edit Calibration Table", and confirm the calibration data for the analysis.
30. In "Data Analysis" menu, choose "Edit Calibration Setting". Confirm the amount of internal standard (ISTD) and unit of the amount.

31. Wait until the run status window is green and shows the "Ready" message.
32. Clean and rinse the 10 μL syringe with HPLC grade water.

Pre-Analysis

1. Prepare the standard solution with internal standard.
2. In "Run Control" menu, choose "Sample Info". Change file directory, file name, add other information as necessary. This first analysis checks the system operation.
3. Load the standard solution into the syringe to a desired amount. Look for bubbles. Reload if any bubbles are trapped inside the syringe.
4. Insert the syringe needle all the way into the rear injector port, inject the sample, press "ENTER" on the control panel, and remove the syringe.
5. Observe that the run status window is blue and displays "Run in Progress" message. The chromatogram window should display the red vertical line indicating the starting point of data acquisition.
6. Flush the syringe with HPLC grade water.
7. Adjust the attenuation (Attn) as Y-axis and time (Time) as X-axis of the chromatogram window as necessary.
8. At the end of sample analysis run time, the Integration Result Window will display. Scroll up and down as desired; close window.
9. To print the results, in "Data Analysis" menu, choose "Specify Report", click on the item "Printer" and choose "Combined Chromatogram and Report on Same Page (Printer Only)". Click "OK" to exit this menu.
10. Confirm the result of the standard solution analysis with the calibration data in "Data Analysis" menu, especially the retention time.
11. Adjust the retention time if necessary, then save the new calibration data.

Performing Analysis

1. Prepare the sample solution with internal standard.
2. In the "Run Control" menu, choose "Sample Info", change file name, and add other information as necessary.
3. Load the sample solution into the syringe to a desired amount. Look for bubbles. Reload if any bubbles are trapped inside.
4. Insert the syringe needle all the way into the rear injector port, inject the sample, press "ENTER" on the control panel, and remove the syringe.
5. Observe the run status window is blue and displays "Run in Progress" message. The chromatogram window should display a red vertical line indicating the starting point of data acquisition.
6. Flush the syringe with HPLC grade water.
7. Adjust the attenuation (Attn) as Y-axis and time (Time) as X-axis of chromatogram window as necessary.
8. At the end of sample analysis run time, the Integration Result Window will display. Scroll up and down as desired; close window.
9. To print the result, in "Data Analysis" menu, choose "Specify Report", turn on the item "Printer" and choose "Combined Chromatogram and Report on Same Page (Printer Only)". Click "OK" to exit this menu.
10. To disable the result printing after each sample run, turn off the item specified in step 9.
11. Repeat step 2 to 8 until a series of sample analyses are completed.

Data Analysis

The following procedures are for the chromatogram data analysis in case of the data is not automatically integrated after each sample run.

1. In "Data Analysis" menu, choose "Main Screen"
2. On the main screen window, choose "Files", then "Load Data Files" to load the chromatogram data files.
3. After the chromatogram displays, choose "Integrate" in "Integration" menu.

4. The integration base line, integration start and end markers, and retention time will display on the chromatogram.
5. To enlarge any section of chromatogram, in "Graphics" menu, choose "Zoom In".
6. After the cursor changes from an arrow to a "+", move the cursor to the point where the top-left corner of the block will be enlarged. Press and hold the left button on the mouse.
7. Move the mouse while holding the left button to the right bottom corner of the enlarged block. The shaded block should display the section of the enlarged chromatogram.
8. After releasing the mouse button, the chromatogram window will display the selection at a larger scale.
9. To manually integrate chromatogram, choose "Manual Integration" in "Integration" menu, then choose "Draw Base Line".
10. After the cursor changes from an arrow to a "+", move cursor to the starting point of integration, press and hold the left mouse button, move cursor to the end point of integration, the base line will follow the cursor to this end point.
11. Press the left mouse button twice to perform the integration.
12. The integration base line, integration start and end markers, integrated peak area, and retention time will display on the chromatogram.
13. To print report, follow the step 9 in the "Performing Analysis" section.
14. To return to the control screen (top level), choose "Return to Top" in "Files" menu.

Shut Down

1. In "Instruments" menu, choose "Temperature".
2. Turn off the detector and injector heaters in the zone temperature window, then decrease the initial temperature set point of the oven program to 25°C.
3. In "Instruments" menu, choose "Detector", then turn off the TCD and FID detectors.

4. Shut off the REF valve of TCD detector, shut off air, hydrogen, and auxiliary gas of FID detector.
5. Decrease the total flow rate for channel B (split) to about 1.5 times of the analysis flow rate through column. Observe the flow rate on the control panel display by pressing "FLOW" and "B".
6. Wait until the oven temperature is equal to ambient temperature or the set point temperature of 25°C.
7. Shut off the carrier flow valve for channel A.
8. In "Method" menu, choose "Load" and "END.MTH" method file, which is the shut down set-up file.
9. In "Run Control" menu, choose "Exit" to leave the Chemstation program.
10. Quit Windows. Shut off the computer.
11. Allow the carrier gas to flow through the column at least 12 h. Shut off the total flow valve if no analyses will be performed within 24 h.
12. Turn off the GC unit.

HP 5890 series II Analytical Conditions

Column: HP-FFAP (10 m x 0.53 mm ID x 1.0 μm coating) capillary column

Carrier gas: helium (He)

Detector: flame ionization detector (FID)

Total flow rate: 200 mL/min

Column flow rate: 10 mL/min

Split ratio: 20:1

Septum purge flow rate: 4-5 mL/min

Auxiliary gas: nitrogen

Column + auxiliary gas flow rate: 30 mL/min

Column + auxiliary gas + hydrogen flow rate: 60 mL/min

Column + auxiliary gas + hydrogen + air flow rate: 400 mL/min

Injector temperature: 220°C

Detector temperature: 240°C

Oven temperature program: initial at 90°C for 5.4 min
linear increase at 25°C/min to 180°C
final at 180°C for 6 min

Total analysis time: 15 min

Controlling program: HP 3365 series II Chemstation

Appendix E

GC Calibration

Analysis Parameters

Column: HP-FFAP (10 m x 0.53 mm ID x 1.0 μm coating) capillary column

Carrier gas: helium (He)

Detector: flame ionization detector (FID)

Total flow rate: 200 mL/min

Column flow rate: 10 mL/min

Split ratio: 20:1

Auxiliary gas: nitrogen

Injector temperature: 220°C

Detector temperature: 240°C

Oven temperature program: initial at 90°C for 5.4 min
linear increase at 25°C/min to 180°C
final at 180°C for 6 min

Sample volume: 2 μL

Internal standard: butyric acid, 3.393 mg/mL = 0.0068 mg/2 μL

Peak window: ± 5% of calibrated retention time

Table E-1. GC calibration data of 4-oxopentanoic acid.

Concentration $C_{C,OA}$ (mg/mL)	Sample Amount $m_{C,OA}$ (mg)	Peak Area $A_{C,OA}$ (counts-sec)	Amount Ratio $m_{C,OA}/m_S$ (mg OA/mg BA)	Area Ratio $A_{C,OA}/A_S$ (area OA/area BA)
0.677	0.0014	153020.29	0.200	0.146
0.846	0.0017	205601.80	0.250	0.173
1.128	0.0023	247498.68	0.333	0.229
1.692	0.0034	335714.29	0.499	0.361
3.383	0.0068	688623.36	0.998	0.720

Response factor of 4-oxopentanoic acid ($R_{F,OA}$)

$R_{F,OA}$ = 0.718 ± 0.005 area ratio/amount ratio, r^2 = 0.999 (1s, n = 10)

Table E-2. GC calibration data of HMF.

Concentration $C_{C,H}$ (mg/mL)	Sample Amount $m_{C,H}$ (mg)	Peak Area $A_{C,H}$ (counts-sec)	Amount Ratio $m_{C,H}/m_S$ (mg HMF/mg BA	Area Ratio $A_{C,H}/A_S$ (area HMF/area BA)
0.339	0.0007	82085.31	0.100	0.078
0.424	0.0008	123627.78	0.125	0.104
0.565	0.0011	141694.57	0.167	0.131
0.843	0.0017	184203.91	0.249	0.198
1.695	0.0034	363433.64	0.500	0.380

Response factor of HMF ($R_{F,HMF}$)

$R_{F,HMF}$ = 0.772 ± 0.009 area ratio/amount ratio, r^2 = 0.998 (1s, n = 10)

Appendix F

Reaction Analysis Data

Reaction Run # 20 Analysis

Materials

(D)-Glucose weight: 20.00 g

Distilled water weight: 150.05 g

Catalyst: H-Y zeolite

Catalyst weight: 10.0021 g

Internal standard: Butyric Acid, 18.150 mg
myo-Inositol, 90.072 mg

Process Parameters

Reaction temperature: 130°C

Mixing speed: 300 rpm

Total reaction time: 24 h

Pressure: 30-60 psi

Table F-1. Reaction run # 20.

Time (h)	Glucose (mol/L)	HMF (mol/L)	Fructose (mol/L)	Formic Acid (mol/L)	4-Oxopentanoic Acid (mol/L)
0.0	0.7461	0.0000	0.0000	0.0000	0.0000
1.0	0.6104	0.0028	0.0914	0.0000	0.0000
2.0	0.6327	0.0031	0.1076	0.0007	0.0000
3.0	0.5768	0.0057	0.1393	0.0157	0.0134
4.0	0.5156	0.0099	0.1671	0.0238	0.0157
5.0	0.4489	0.0146	0.1830	0.0368	0.0201
6.0	0.3977	0.0175	0.1897	0.0475	0.0262
7.0	0.3487	0.0211	0.1893	0.0643	0.0360
8.0	0.3111	0.0282	0.1845	0.0931	0.0621
9.0	0.2661	0.0291	0.1654	0.1037	0.0663
10.0	0.2494	0.0349	0.1665	0.1251	0.0652
12.0	0.2264	0.0364	0.1535	0.1486	0.0870
14.0	0.1892	0.0394	0.1357	0.1737	0.0986
16.0	0.1577	0.0406	0.1155	0.1851	0.0977
24.0	0.1255	0.0459	0.0926	0.2176	0.1057

Reaction Run # 24 Analysis

Materials

(D)-Glucose weight: 20.00 g

Distilled water weight: 150.23 g

Catalyst: H-Y zeolite

Catalyst weight: 10.0115 g

Internal standard: Butyric Acid, 18.15 mg

myo-Inositol, 90.072 mg

Process Parameters

Reaction temperature: 120°C

Mixing speed: 300 rpm

Total reaction time: 24 h

Pressure: 30-60 psi

Table F-2. Reaction run # 24.

Time (h)	Glucose (mol/L)	HMF (mol/L)	Fructose (mol/L)	Formic Acid (mol/L)	4-Oxopentanoic Acid (mol/L)
0.0	0.7489	0.0000	0.0000	0.0000	0.0000
1.0	0.7001	0.0011	0.0380	0.0009	0.0000
2.0	0.6867	0.0011	0.0542	0.0013	0.0000
3.0	0.6570	0.0018	0.0786	0.0016	0.0004
4.0	0.6257	0.0031	0.1030	0.0065	0.0054
5.0	0.5816	0.0050	0.1293	0.0041	0.0020
6.0	0.5417	0.0073	0.1507	0.0133	0.0050
7.0	0.5143	0.0094	0.1623	0.0223	0.0128
8.0	0.4857	0.0112	0.1725	0.0319	0.0151
9.0	0.4532	0.0143	0.1797	0.0336	0.0280
10.0	0.4297	0.0140	0.1838	0.0387	0.0219
12.0	0.3839	0.0174	0.1745	0.0556	0.0335
14.0	0.3818	0.0180	0.1762	0.0560	0.0359
16.0	0.3676	0.0204	0.1809	0.0691	0.0363
24.0	0.2811	0.0319	0.1608	0.1328	0.0705

Reaction Run # 25 Analysis

Materials

(D)-Glucose weight: 20.00 g

Distilled water: 150.27 g

Catalyst: H-Y-zeolite

Catalyst weight: 10.0085 g

Internal standard: Butyric Acid, 18.15 mg

myo-Inositol, 90.072 mg

Reaction Parameters

Reaction temperature: 110°C

Mixing speed: 300 rpm

Total reaction time: 24 h

Pressure: 30-60 psi

Table F-3. Reaction run # 25.

Time (h)	Glucose (mol/L)	HMF (mol/L)	Fructose (mol/L)	Formic Acid (mol/L)	4-Oxopentanoic Acid (mol/L)
0.0	0.7478	0.0000	0.0000	0.0000	0.0000
1.0	0.7249	0.0007	0.0211	0.0006	0.0000
2.0	0.7190	0.0006	0.0199	0.0005	0.0000
3.0	0.7010	0.0006	0.0429	0.0031	0.0000
4.0	0.6841	0.0008	0.0564	0.0021	0.0000
5.0	0.6663	0.0011	0.0690	0.0022	0.0013
6.0	0.6474	0.0016	0.0828	0.0035	0.0017
7.0	0.6343	0.0021	0.0963	0.0034	0.0019
8.0	0.6078	0.0028	0.1068	0.0117	0.0031
9.0	0.5922	0.0035	0.1161	0.0122	0.0034
10.0	0.5749	0.0042	0.1247	0.0106	0.0038
12.0	0.5570	0.0052	0.1398	0.0153	0.0101
14.0	0.5293	0.0062	0.1493	0.0213	0.0114
16.0	0.5153	0.0077	0.1571	0.0152	0.0060
24.0	0.4946	0.0093	0.1675	0.0265	0.0175

Reaction Run # 26 Analysis

Materials

(D)-Glucose weight: 20.00 g

Distilled water weight: 150.37 g

Catalyst: H-Y zeolite

Catalyst weight: 2.0100 g

Internal standard: Butyric Acid, 18.150 mg

myo-Inositol, 90.072 mg

Reaction Parameters

Reaction temperature: 130°C

Mixing speed: 300 rpm

Total reaction time: 24 h

Pressure 30-60 psi

Table F-4. Reaction run # 26.

Time (h)	Glucose (mol/L)	HMF (mol/L)	Fructose (mol/L)	Formic Acid (mol/L)	4-Oxopentanoic Acid (mol/L)
0.0	0.7487	0.0000	0.0000	0.0000	0.0000
1.0	0.7235	0.0010	0.0284	0.0008	0.0009
2.0	0.7202	0.0013	0.0330	0.0006	0.0007
3.0	0.6924	0.0026	0.0544	0.0024	0.0009
4.0	0.6534	0.0048	0.0777	0.0059	0.0018
5.0	0.6229	0.0072	0.0957	0.0115	0.0087
6.0	0.5865	0.0100	0.1122	0.0250	0.0110
7.0	0.5468	0.0135	0.1273	0.0267	0.0154
8.0	0.5233	0.0161	0.1394	0.0340	0.0202
9.0	0.4857	0.0193	0.1474	0.0464	0.0256
10.0	0.4602	0.0223	0.1570	0.0541	0.0313
12.0	0.4127	0.0264	0.1634	0.0718	0.0400
14.0	0.3753	0.0293	0.1682	0.0860	0.0481
16.0	0.3272	0.0326	0.1657	0.1087	0.0547
24.0	0.2502	0.0505	0.1469	0.1695	0.0852

Reaction Run # 28 Analysis

Materials

(D)-Glucose weight: 20.00 g

Distilled water weight: 150.43 g

Catalyst: H-Y zeolite

Catalyst weight: 4.0008 g

Internal standard: Butyric Acid, 18.075 mg
myo-Inositol, 90.072 mg

Reaction Parameters

Reaction temperature: 130°C

Mixing speed: 300 rpm

Total reaction time: 24 h

Pressure 30-60 psi

Table F-5. Reaction run # 28.

Time (h)	Glucose (mol/L)	HMF (mol/L)	Fructose (mol/L)	Formic Acid (mol/L)	4-Oxopentanoic Acid (mol/L)
0.0	0.7555	0.0000	0.0000	0.0000	0.0000
1.0	0.6854	0.0013	0.0478	0.0007	0.0000
2.0	0.6868	0.0016	0.0535	0.0016	0.0000
3.0	0.6478	0.0041	0.0914	0.0035	0.0014
4.0	0.6022	0.0067	0.1143	0.0133	0.0107
5.0	0.5651	0.0102	0.1364	0.0200	0.0144
6.0	0.5202	0.0139	0.1507	0.0173	0.0218
7.0	0.4752	0.0173	0.1621	0.0409	0.0226
8.0	0.4432	0.0206	0.1727	0.0564	0.0270
9.0	0.4133	0.0231	0.1788	0.0639	0.0356
10.0	0.3762	0.0267	0.1777	0.0795	0.0446
12.0	0.3337	0.0268	0.1683	0.0901	0.0000
14.0	0.2942	0.0283	0.1626	0.1014	0.0582
16.0	0.2654	0.0324	0.1586	0.1324	0.0000
24.0	0.2067	0.0456	0.1274	0.1966	0.0857

Reaction Run # 33 Analysis

Materials

(D)-Glucose weight: 20.00 g

Distilled water weight: 150.04 g

Catalyst: H-Y zeolite

Catalyst weight: 20.0116 g

Internal standard: Butyric Acid, 18.075 mg

myo-Inositol, 90.072 mg

Reaction Parameters

Reaction temperature: 130°C

Mixing speed: 300 rpm

Total reaction time: 24 h

Pressure: 30-60 psi

Table F-6. Reaction run # 33.

Time (h)	Glucose (mol/L)	HMF (mol/L)	Fructose (mol/L)	Formic Acid (mol/L)	4-Oxopentanoic Acid (mol/L)
0.0	0.7441	0.0000	0.0000	0.0000	0.0000
1.0	0.5508	0.0042	0.1388	0.0088	0.0000
2.0	0.5469	0.0048	0.1463	0.0052	0.0010
3.0	0.4298	0.0110	0.1862	0.0253	0.0138
4.0	0.3620	0.0165	0.2042	0.0509	0.0225
5.0	0.3140	0.0204	0.2002	0.0634	0.0342
6.0	0.2652	0.0202	0.1859	0.0809	0.0388
7.0	0.2206	0.0223	0.1669	0.0994	0.0463
8.0	0.1885	0.0251	0.1489	0.1207	0.0505
9.0	0.1672	0.0311	0.1274	0.1511	0.0728
10.0	0.1494	0.0249	0.1212	0.1354	0.0601
12.0	0.1291	0.0267	0.1050	0.1558	0.0000
14.0	0.1124	0.0323	0.0873	0.2068	0.0772
16.0	0.0890	0.0309	0.0684	0.1912	0.0777
24.0	0.0604	0.0309	0.0496	0.2085	0.0997

Reaction Run # 43 Analysis

Materials

(D)-Glucose weight: 20.07 g

Distilled water weight: 150.00 g

Catalyst: H-Y zeolite

Catalyst weight: 10.0075 g

Internal standard: Butyric Acid, 18.052 mg
myo-Inositol, 89.944 mg

Reaction Parameters

Reaction temperature: 160°C

Mixing speed: 300 rpm

Total reaction time: 24 h

Pressure 30-120 psi

Table F-7. Reaction run # 43.

Time (h)	Glucose (mol/L)	HMF (mol/L)	Fructose (mol/L)	Formic Acid (mol/L)	4-Oxopentanoic Acid (mol/L)
0.0	0.7476	0.0000	0.0000	0.0000	0.0000
1.0	0.4383	0.0228	0.1074	0.0652	0.0264
2.0	0.2386	0.0517	0.1646	0.0974	0.0466
3.0	0.1240	0.0585	0.1007	0.2154	0.0801
4.0	0.0564	0.0554	0.0508	0.2321	0.1211
5.0	0.0237	0.0467	0.0150	0.2009	0.1164
6.0	0.0095	0.0374	0.0065	0.1946	0.1208
7.0	0.0020	0.0214	0.0000	0.1816	0.1279
8.0	0.0000	0.0174	0.0000	0.1815	0.1363
9.0	0.0000	0.0134	0.0000	0.1824	0.1803
10.0	0.0000	0.0118	0.0000	0.1818	0.1445
12.0	0.0000	0.0061	0.0000	0.1573	0.1455
14.0	0.0000	0.0033	0.0000	0.1567	0.1420
16.0	0.0000	0.0013	0.0000	0.1405	0.1031
24.0	0.0000	0.0005	0.0000	0.1778	0.1069

Reaction Run # 60 Analysis

Materials

(D)-Glucose weight: 20.07 g

Distilled water weight: 150.92 g

Catalyst: Al-pillared montmorillonite # 1

Catalyst weight: 5.0091 g

Internal standard: Butyric Acid, 18.038 mg

myo-Inositol, 75.000 mg

Reaction Parameters

Reaction temperature: 150°C

Mixing speed: 400 rpm

Total reaction time: 24 h

Pressure: 30-60 psi

Table F-8. Reaction run # 60.

Time (h)	Glucose (mol/L)	HMF (mol/L)	Fructose (mol/L)	Formic Acid (mol/L)	4-Oxopentanoic Acid (mol/L)
0.0	0.7407	0.0000	0.0000	0.0000	0.0000
1.0	0.3734	0.0290	0.1054	0.0000	0.0078
2.0	0.2773	0.0327	0.1116	0.0000	0.0090
3.0	0.1905	0.0622	0.0876	0.1382	0.0079
4.0	0.1427	0.0680	0.0703	0.1909	0.0126
5.0	0.1200	0.0881	0.0428	0.2424	0.0219
6.0	0.1026	0.0804	0.0072	0.2328	0.0232
7.0	0.0933	0.0845	0.0000	0.2404	0.0317
8.0	0.0861	0.0740	0.0000	0.2415	0.0362
9.0	0.0801	0.0625	0.0000	0.2407	0.0368
10.0	0.0748	0.0547	0.0000	0.2440	0.0393
12.0	0.0705	0.0436	0.0000	0.2090	0.0412
14.0	0.0663	0.0351	0.0000	0.2411	0.0505
16.0	0.0621	0.0285	0.0000	0.2279	0.0607
24.0	0.0566	0.0038	0.0000	0.2126	0.0645

Reaction Run # 63 Analysis

Materials

(D)-Glucose weight: 20.01 g

Distilled water weight: 150.03 g

Catalyst: H-montmorillonite # 2

Catalyst weight: 5.0119 g

Internal standard: Butyric Acid, 18.006 mg

myo-Inositol, 75.000 mg

Reaction Parameters

Reaction temperature: 150°C

Mixing speed: 400 rpm

Total reaction time: 24 h

Pressure: 30-60 psi

Table F-9. Reaction run # 63.

Time (h)	Glucose (mol/L)	HMF (mol/L)	Fructose (mol/L)	Formic Acid (mol/L)	4-Oxopentanoic Acid (mol/L)
0.0	0.7335	0.0000	0.0000	0.0000	0.0000
1.0	0.5741	0.0228	0.0661	0.0151	0.0000
2.0	0.5793	0.0257	0.0893	0.0234	0.0000
3.0	0.5153	0.0397	0.1045	0.0687	0.0034
4.0	0.4532	0.0599	0.1057	0.1051	0.0055
5.0	0.4358	0.0712	0.1054	0.1337	0.0085
6.0	0.4025	0.0895	0.0979	0.1892	0.0103
7.0	0.3814	0.0955	0.0915	0.1963	0.0144
8.0	0.3635	0.1096	0.0865	0.2057	0.0179
9.0	0.3472	0.1154	0.0800	0.2025	0.0210
10.0	0.3294	0.1175	0.0742	0.2105	0.0250
12.0	0.3062	0.1214	0.0659	0.1954	0.0287
14.0	0.2766	0.1220	0.0565	0.1959	0.0339
16.0	0.2538	0.1319	0.0487	0.2173	0.0399
24.0	0.2121	0.1200	0.0360	0.2155	0.0453

Reaction Run # 64 Analysis

Materials

(D)-Glucose weight: 20.01 g

Distilled water weight: 150.18 g

Catalyst: Cr-pillared montmorillonite # 3

Catalyst weight: 5.0040 g

Internal standard: Butyric Acid, 18.006 mg

myo-Inositol, 75.000 mg

Reaction Parameters

Reaction temperature: 150°C

Mixing speed: 400 rpm

Total reaction time: 24 h

Pressure: 30-60 psi

Table F-10. Reaction run # 64.

Time (h)	Glucose (mol/L)	HMF (mol/L)	Fructose (mol/L)	Formic Acid (mol/L)	4-Oxopentanoic Acid (mol/L)
0.0	0.7555	0.0000	0.0000	0.0000	0.0000
1.0	0.3579	0.0656	0.1384	0.1312	0.0129
2.0	0.3208	0.0654	0.1359	0.1222	0.0132
3.0	0.2541	0.0827	0.1170	0.1583	0.0184
4.0	0.2063	0.0964	0.0962	0.1859	0.0220
5.0	0.1554	0.1275	0.0629	0.2073	0.0429
6.0	0.1441	0.1340	0.0352	0.2152	0.0511
7.0	0.1327	0.1206	0.0094	0.2291	0.0604
8.0	0.1252	0.0916	0.0044	0.2316	0.0588
9.0	0.1189	0.0999	0.0031	0.2294	0.1014
10.0	0.1132	0.0816	0.0000	0.2290	0.0941
12.0	0.1095	0.0798	0.0000	0.2439	0.1023
14.0	0.1051	0.0604	0.0000	0.2360	0.0996
16.0	0.0988	0.0484	0.0000	0.2324	0.1070
24.0	0.0862	0.0318	0.0000	0.2324	0.1144

Reaction Run # 65 Analysis

Materials

(D)-Glucose weight: 20.00 g

Distilled water weight: 150.10 g

Catalyst: Fe-pillared montmorillonite # 4

Catalyst weight: 5.0076 g

Internal standard: Butyric Acid, 18.006 mg
myo-Inositol, 75.000 mg

Reaction Parameters

Reaction temperature: 150°C

Mixing speed: 400 rpm

Total reaction time: 24 h

Pressure: 30-60 psi

Table F-11. Reaction run # 65.

Time (h)	Glucose (mol/L)	HMF (mol/L)	Fructose (mol/L)	Formic Acid (mol/L)	4-Oxopentanoic Acid (mol/L)
0.0	0.7587	0.0000	0.0000	0.0000	0.0000
1.0	0.3472	0.0207	0.1585	0.1099	0.0040
2.0	0.3064	0.0200	0.1478	0.1201	0.0095
3.0	0.1881	0.0201	0.1157	0.1925	0.0097
4.0	0.1145	0.0238	0.0799	0.2259	0.0077
5.0	0.0705	0.0202	0.0403	0.4236	0.0088
6.0	0.0459	0.0148	0.0226	0.4127	0.0089
7.0	0.0340	0.0105	0.0000	0.3847	0.0080
8.0	0.0252	0.0100	0.0000	0.3292	0.0080
9.0	0.0195	0.0088	0.0000	0.3077	0.0080
10.0	0.0145	0.0064	0.0000	0.2946	0.0080
12.0	0.0000	0.0051	0.0000	0.3016	0.0094
14.0	0.0000	0.0019	0.0000	0.2791	0.0077
16.0	0.0000	0.0002	0.0000	0.2624	0.0071
24.0	0.0000	0.0002	0.0000	0.2305	0.0085

Reaction Run # 67 Analysis

Material

(D)-Glucose weight: 20.01 g

Distilled water weight: 150.06 g

Catalyst: Cr-pillared montmorillonite # 4

Catalyst weight: 5.0027 g

Internal standard: Butyric Acid, 18.006 mg

myo-Inositol, 75.000 mg

Reaction Parameters

Reaction temperature: 170°C

Mixing speed: 400 rpm

Total reaction time: 24 h

Pressure: 30-60 psi

Table F-12. Reaction run # 67.

Time (h)	Glucose (mol/L)	HMF (mol/L)	Fructose (mol/L)	Formic Acid (mol/L)	4-Oxopentanoic Acid (mol/L)
0.0	0.7403	0.0000	0.0000	0.0000	0.0000
1.0	0.2845	0.0837	0.0967	0.1883	0.0145
2.0	0.1629	0.1192	0.0724	0.2051	0.0274
3.0	0.1016	0.1263	0.0289	0.1898	0.0537
4.0	0.0696	0.0923	0.0163	0.1963	0.0757
5.0	0.0511	0.0604	0.0000	0.1988	0.0915
6.0	0.0429	0.0420	0.0000	0.2045	0.1087
7.0	0.0363	0.0244	0.0000	0.1860	0.1016
8.0	0.0321	0.0153	0.0000	0.1802	0.1277
9.0	0.0266	0.0130	0.0000	0.1801	0.1234
10.0	0.0233	0.0108	0.0000	0.1796	0.1312
12.0	0.0205	0.0069	0.0000	0.1766	0.1384
14.0	0.0174	0.0052	0.0000	0.1677	0.1331
16.0	0.0125	0.0000	0.0000	0.1582	0.1239
24.0	0.0000	0.0000	0.0000	0.1538	0.1372

Reaction Run # 68 Analysis

Materials

(D)-Glucose weight: 20.01 g

Distilled water weight: 150.05 g

Catalyst: Fe-pillared montmorillonite # 5

Catalyst weight: 5.0108 g

Internal standard: Butyric Acid, 18.006 mg
myo-Inositol, 75.000 mg

Reaction Parameters

Reaction temperature: 170°C

Mixing speed: 400 rpm

Total reaction time: 24 h

Pressure: 30-60 psi

Table F-13. Reaction run # 68.

Time (h)	Glucose (mol/L)	HMF (mol/L)	Fructose (mol/L)	Formic Acid (mol/L)	4-Oxopentanoic Acid (mol/L)
0.0	0.7295	0.0000	0.0000	0.0000	0.0000
1.0	0.0991	0.0196	0.0347	0.1353	0.0109
2.0	0.0312	0.0115	0.0086	0.3289	0.0164
3.0	0.0156	0.0058	0.0057	0.2854	0.0166
4.0	0.0000	0.0032	0.0027	0.2263	0.0165
5.0	0.0000	0.0007	0.0028	0.2040	0.0179
6.0	0.0000	0.0001	0.0036	0.2174	0.0222
7.0	0.0000	0.0000	0.0000	0.2008	0.0235
8.0	0.0000	0.0000	0.0000	0.2341	0.0185
9.0	0.0000	0.0000	0.0000	0.1851	0.0180
10.0	0.0000	0.0000	0.0000	0.1890	0.0198
12.0	0.0000	0.0000	0.0000	0.1851	0.0240
14.0	0.0000	0.0000	0.0000	0.1705	0.0233
16.0	0.0000	0.0000	0.0000	0.1625	0.0212
24.0	0.0000	0.0000	0.0000	0.1541	0.0213

Reaction Run # 69 Analysis

Materials

(D)-Glucose weight: 20.02 g

Distilled water weight: 150.4 g

Catalyst: H-montmorillonite # 3

Catalyst weight: 5.0083 g

Internal standard: Butyric Acid, 18.034 mg

myo-Inositol, 75.000 mg

Reaction Parameters

Reaction temperature: 170°C

Mixing speed: 400 rpm

Total reaction time: 24 h

Pressure: 30-60 psi

Table F-14. Reaction run # 69.

Time (h)	Glucose (mol/L)	HMF (mol/L)	Fructose (mol/L)	Formic Acid (mol/L)	4-Oxopentanoic Acid (mol/L)
0.0	0.7364	0.0000	.0000	0.0000	0.0000
1.0	0.5321	0.0562	0.0805	0.0796	0.0062
2.0	0.4483	0.0733	0.0912	0.1232	0.0064
3.0	0.3692	0.1159	0.0796	0.2182	0.0149
4.0	0.2967	0.1330	0.0621	0.2460	0.0246
5.0	0.2397	0.1447	0.0426	0.2333	0.0378
6.0	0.1942	0.1456	0.0298	0.2053	0.0524
7.0	0.1628	0.1372	0.0217	0.2110	0.0653
8.0	0.1272	0.1174	0.0174	0.2080	0.0696
9.0	0.1062	0.1024	0.0134	0.2373	0.0784
10.0	0.0894	0.0932	0.0101	0.1997	0.0925
12.0	0.0563	0.0690	0.0066	0.1566	0.0902
14.0	0.0412	0.0497	0.0042	0.1554	0.0929
16.0	0.0252	0.0367	0.0025	0.1540	0.0944
24.0	0.0132	0.0155	0.0000	0.1191	0.0678

Reaction Run # 71 Analysis

Materials

(D)-Glucose weight: 20.00 g

Distilled water weight: 150.08 g

Catalyst: Cr-pillared montmorillonite # 5

Catalyst weight: 5.0038 g

Internal standard: Butyric Acid, 18.034 mg

myo-Inositol, 75.000 mg

Reaction Parameters

Reaction temperature: 130°C

Mixing speed: 400 rpm

Total reaction time: 24 h

Pressure: 30-60 psi

Table F-15. Reaction run # 71.

Time (h)	Glucose (mol/L)	HMF (mol/L)	Fructose (mol/L)	Formic Acid (mol/L)	4-Oxopentanoic Acid (mol/L)
0	0.7131	0.0000	0.0000	0.0000	0.0000
1	0.5569	0.0160	0.1091	0.0000	0.0070
2	0.5148	0.0163	0.1153	0.0400	0.0051
3	0.4795	0.0261	0.1271	0.0416	0.0028
4	0.4391	0.0300	0.1347	0.0569	0.0045
5	0.4119	0.0408	0.1356	0.0675	0.0048
6	0.3835	0.0465	0.1370	0.0756	0.0042
7	0.3424	0.0557	0.1344	0.1043	0.0055
8	0.3193	0.0582	0.1314	0.1030	0.0073
9	0.3127	0.0650	0.1295	0.1157	0.0082
10	0.2987	0.0687	0.1315	0.1213	0.0069
12	0.2798	0.0686	0.1267	0.1297	0.0072
14	0.2614	0.0785	0.1185	0.1381	0.0076
16	0.2313	0.0879	0.1075	0.1607	0.0092
24	0.2078	0.0882	0.0932	0.1668	0.0101

Reaction Run # 72 Analysis

Materials

(D)-Glucose weight: 20.01 g

Distilled water weight: 150.31 g

Catalyst: H-montmorillonite # 5

Catalyst weight: 5.0076 g

Internal standard: Butyric Acid, 18.034 mg

myo-Inositol, 75.000 mg

Reaction Parameters

Reaction temperature: 130°C

Mixing speed: 400 rpm

Total reaction time: 24 h

Pressure: 30-60 psi

Table F-16. Reaction run # 72.

Time (h)	Glucose (mol/L)	HMF (mol/L)	Fructose (mol/L)	Formic Acid (mol/L)	4-Oxopentanoic Acid (mol/L)
0.0	0.7349	0.0000	0.0000	0.0000	0.0000
1.0	0.7038	0.0130	0.0330	0.0000	0.0075
2.0	0.7138	0.0153	0.0276	0.0000	0.0056
3.0	0.6733	0.0152	0.0390	0.0000	0.0031
4.0	0.6562	0.0172	0.0550	0.0000	0.0028
5.0	0.6300	0.0182	0.0678	0.0000	0.0031
6.0	0.6085	0.0184	0.0796	0.0000	0.0033
7.0	0.6105	0.0229	0.0924	0.0000	0.0025
8.0	0.5702	0.0241	0.0947	0.0000	0.0038
9.0	0.5550	0.0279	0.1004	0.0000	0.0034
10.0	0.5493	0.0317	0.1060	0.0000	0.0039
12.0	0.5349	0.0359	0.1080	0.0000	0.0047
14.0	0.5088	0.0377	0.1131	0.0527	0.0046
16.0	0.4895	0.0461	0.1135	0.0804	0.0058
24.0	0.4703	0.0498	0.1094	0.1067	0.0065

Reaction Run # 73 Analysis

Materials

(D)-Glucose weight: 20.01 g

Distilled water weight: 150.18 g

Catalyst: Fe-pillared montmorillonite # 6

Catalyst weight: 5.0020 g

Internal standard: Butyric Acid, 18.034 mg
myo-Inositol, 75.000 mg

Reaction Parameters

Reaction temperature: 130°C

Mixing speed: 400 rpm

Total reaction time: 24 h

Pressure: 30-60 psi

Table F-17. Reaction run # 73.

Time (h)	Glucose (mol/L)	HMF (mol/L)	Fructose (mol/L)	Formic Acid (mol/L)	4-Oxopentanoic Acid (mol/L)
0.0	0.7212	0.0000	0.0000	0.0000	0.0000
1.0	0.5897	0.0128	0.0952	0.0520	0.0081
2.0	0.5600	0.0150	0.0961	0.0640	0.0090
3.0	0.4784	0.0167	0.1333	0.0528	0.0093
4.0	0.4068	0.0182	0.1474	0.0684	0.0094
5.0	0.3290	0.0198	0.1554	0.0973	0.0106
6.0	0.2899	0.0182	0.1529	0.1110	0.0109
7.0	0.2612	0.0207	0.1437	0.1200	0.0123
8.0	0.2231	0.0218	0.1305	0.1366	0.0131
9.0	0.2016	0.0195	0.1210	0.1509	0.0141
10.0	0.1830	0.0180	0.1093	0.1615	0.0173
12.0	0.1675	0.0178	0.0986	0.1756	0.0226
14.0	0.1423	0.0193	0.0851	0.1806	0.0288
16.0	0.1222	0.0150	0.0704	0.1857	0.0308
24.0	0.0972	0.0131	0.0510	0.3625	0.0235

Reaction Run # 76 Analysis

Materials

(D)-Glucose weight: 20.01 g

Distilled water weight: 150.16g

Catalyst: H-Y zeolite

Catalyst weight: 5.0073 g

Internal standard: Butyric Acid, 18.990 mg
myo-Inositol, 75.000 mg

Reaction Parameters

Reaction temperature: 150°C

Mixing speed: 400 rpm

Total reaction time: 24 h

Pressure: 30-60 psi

Table F-18. Reaction run # 76.

Time (h)	Glucose (mol/L)	HMF (mol/L)	Fructose (mol/L)	Formic Acid (mol/L)	4-Oxopentanoic Acid (mol/L)
0.0	0.7325	0.0000	0.0000	0.0000	0.0000
1.0	0.4872	0.0190	0.1611	0.0217	0.0000
2.0	0.4263	0.0246	0.1559	0.0728	0.0000
3.0	0.3221	0.0419	0.1627	0.1071	0.0000
4.0	0.2201	0.0585	0.1413	0.1918	0.0071
5.0	0.1533	0.0724	0.1055	0.2314	0.0110
6.0	0.1036	0.0718	0.0733	0.2579	0.0117
7.0	0.0680	0.0680	0.0484	0.2217	0.0140
8.0	0.0673	0.0624	0.0449	0.1975	0.0175
9.0	0.0296	0.0542	0.0184	0.2077	0.0186
10.0	0.0253	0.0465	0.0130	0.1701	0.0194
12.0	0.0158	0.0338	0.0072	0.1628	0.0214
14.0	0.0153	0.0291	0.0046	0.1705	0.0221
16.0	0.0096	0.0190	0.0010	0.1584	0.0229
24.0	0.0077	0.0127	0.0000	0.1659	0.0254

Reaction Run # 77 Analysis

Materials

(D)-Glucose weight: 20.00 g

Distilled water weight: 150.45 g

Catalyst: Al-pillared montmorillonite # 2

Catalyst weight: 5.0035 g

Internal standard: Butyric Acid, 18.990 mg

myo-Inositol, 75.000 mg

Reaction Parameters

Reaction temperature: 170°C

Mixing speed: 400 rpm

Total reaction time: 24 h

Pressure: 30-60 psi

Table F-19. Reaction run # 77.

Time (h)	Glucose (mol/L)	HMF (mol/L)	Fructose (mol/L)	Formic Acid (mol/L)	4-Oxopentanoic Acid (mol/L)
0.0	0.7344	0.0000	0.0000	0.0000	0.0000
1.0	0.2532	0.1014	0.1128	0.1911	0.0253
2.0	0.1668	0.0925	0.0900	0.2515	0.0343
3.0	0.0648	0.0878	0.0372	0.2247	0.0402
4.0	0.0311	0.0546	0.0135	0.1960	0.0482
5.0	0.0149	0.0410	0.0027	0.1749	0.0681
6.0	0.0114	0.0204	0.0022	0.1941	0.0809
7.0	0.0000	0.0103	0.0013	0.1935	0.0799
8.0	0.0000	0.0071	0.0020	0.1712	0.0814
9.0	0.0000	0.0021	0.0000	0.1775	0.0757
10.0	0.0000	0.0014	0.0000	0.1697	0.0823
12.0	0.0000	0.0000	0.0000	0.1842	0.0848
14.0	0.0000	0.0000	0.0000	0.1785	0.0872
16.0	0.0000	0.0000	0.0000	0.1505	0.0887
24.0	0.0000	0.0000	0.0000	0.1510	0.0863

Reaction Run # 78 Analysis

Materials

(D)-Glucose weight: 20.01 g

Distilled water weight: 150.03 g

Catalyst: Al-pillared montmorillonite # 2

Catalyst weight: 5.0062 g

Internal standard: Butyric Acid, 18.990 mg
myo-Inositol, 75.000 mg

Reaction Parameters

Reaction temperature: 130°C

Mixing speed: 400 rpm

Total reaction time: 24 h

Pressure: 30-60 psi

Table F-20. Reaction run # 78.

Time (h)	Glucose (mol/L)	HMF (mol/L)	Fructose (mol/L)	Formic Acid (mol/L)	4-Oxopentanoic Acid (mol/L)
0.0	0.7399	0.0000	0.0000	0.0000	0.0000
1.0	0.6585	0.0124	0.0558	0.0023	0.0000
2.0	0.6470	0.0148	0.0554	0.0068	0.0024
3.0	0.6151	0.0172	0.0820	0.0093	0.0034
4.0	0.5699	0.0188	0.1057	0.0200	0.0043
5.0	0.5187	0.0227	0.1263	0.0367	0.0038
6.0	0.4521	0.0302	0.1438	0.0510	0.0036
7.0	0.4021	0.0387	0.1588	0.0788	0.0041
8.0	0.3790	0.0423	0.1653	0.0872	0.0042
9.0	0.3509	0.0449	0.1626	0.1113	0.0046
10.0	0.3203	0.0490	0.1639	0.1376	0.0048
12.0	0.2958	0.0525	0.1545	0.1688	0.0058
14.0	0.2531	0.0585	0.1441	0.1781	0.0070
16.0	0.2220	0.0611	0.1352	0.2075	0.0080
24.0	0.1693	0.0628	0.1071	0.2109	0.0098

Reaction Run # 80 Analysis

Materials

(D)-Glucose weight: 20.00 g

Distilled water weight: 150.01 g

Catalyst: H-Y zeolite

Catalyst weight: 5.0183 g

Internal standard: Butyric Acid: 18.090 mg

myo-Inositol: 75.000 mg

Reaction Parameters

Reaction temperature: 150°C

Mixing speed: 400 rpm

Total reaction time: 24 h

Pressure: 30-60 psi

Table F-21. Reaction run # 80.

Time (h)	Glucose (mol/L)	HMF (mol/L)	Fructose (mol/L)	Formic Acid (mol/L)	4-Oxopentanoic Acid (mol/L)
0.0	0.7525	0.0000	0.0000	0.0000	0.0000
1.0	0.5121	0.0240	0.1624	0.0132	0.0076
2.0	0.4594	0.0266	0.1512	0.0440	0.0064
3.0	0.3076	0.0418	0.1571	0.1048	0.0042
4.0	0.1914	0.0540	0.1225	0.1805	0.0025
5.0	0.1179	0.0635	0.0843	0.2399	0.0015
6.0	0.0872	0.0596	0.0674	0.2387	0.0013
7.0	0.0573	0.0594	0.0391	0.2473	0.0007
8.0	0.0423	0.0487	0.0256	0.2342	0.0006
9.0	0.0346	0.0452	0.0175	0.2378	0.0004
10.0	0.0259	0.0404	0.0112	0.2190	0.0003
12.0	0.0207	0.0309	0.0073	0.2217	0.0003
14.0	0.0153	0.0213	0.0000	0.1589	0.0000
16.0	0.0000	0.0149	0.0000	0.1971	0.0000
24.0	0.0000	0.0053	0.0000	0.1293	0.0000

Reaction Run # 82 Analysis

Materials

(D)-Glucose weight: 20.01 g

Distilled water weight: 150.05 g

Catalyst: Fe-pillared montmorillonite # 8

Catalyst weight: 5.0017 g

Internal standard: Butyric Acid, 18.090 mg

myo-Inositol, 75.000 mg

Reaction Parameters

Reaction temperature: 130°C

Mixing speed: 400 rpm

Total reaction time: 24 h

Pressure: 30-60 psi

Table F-22. Reaction run # 82.

Time (h)	Glucose (mol/L)	HMF (mol/L)	Fructose (mol/L)	Formic Acid (mol/L)	4-Oxopentanoic Acid (mol/L)
0.0	0.7252	0.0000	0.0000	0.0000	0.0000
1.0	0.6541	0.0080	0.0782	0.0330	0.0035
2.0	0.6363	0.0088	0.0803	0.0416	0.0037
3.0	0.5602	0.0099	0.0961	0.0738	0.0030
4.0	0.5108	0.0090	0.1279	0.0550	0.0047
5.0	0.4279	0.0117	0.1451	0.0657	0.0041
6.0	0.3523	0.0111	0.1570	0.0866	0.0041
7.0	0.3133	0.0126	0.1606	0.1012	0.0042
8.0	0.2990	0.0199	0.1547	0.1060	0.0056
9.0	0.2537	0.0124	0.1415	0.1148	0.0054
10.0	0.2301	0.0134	0.1339	0.1326	0.0063
12.0	0.1853	0.0152	0.1100	0.1256	0.0065
14.0	0.1521	0.0156	0.0893	0.1386	0.0073
16.0	0.1323	0.0157	0.0841	0.2691	0.0070
24.0	0.1077	0.0158	0.0590	0.2371	0.0030

Reaction Run # 86 Analysis

Materials

(D)-Glucose weight: 20.00 g

Distilled water weight: 150.07 g

Catalyst: MCM-41 # 1

Catalyst weight: 5.0088 g

Internal standard: Butyric Acid, 18.390 mg

Manitol, 30.000 mg

Reaction Parameters

Reaction temperature: 150°C

Mixing speed: 400 rpm

Total reaction time: 24 h

Pressure: 30-60 psi

Table F-23. Reaction run # 86.

Time (h)	Glucose (mol/L)	HMF (mol/L)	Fructose (mol/L)	Formic Acid (mol/L)	4-Oxopentanoic Acid (mol/L)
0.0	0.7802	0.0000	0.0000	0.0000	0.0000
1.0	0.7539	0.0112	0.0299	0.0000	0.0000
2.0	0.7109	0.0188	0.0568	0.0064	0.0023
3.0	0.6455	0.0240	0.0579	0.0080	0.0038
4.0	0.6004	0.0420	0.0814	0.0864	0.0033
5.0	0.5454	0.0528	0.0947	0.1162	0.0039
6.0	0.5089	0.0708	0.1049	0.1642	0.0042
7.0	0.4406	0.0878	0.1066	0.1874	0.0049
8.0	0.3843	0.1032	0.1029	0.2559	0.0068
9.0	0.3536	0.1071	0.1108	0.2654	0.0079
10.0	0.3073	0.1179	0.0949	0.2863	0.0098
12.0	0.2736	0.1217	0.0940	0.2761	0.0121
14.0	0.2147	0.1213	0.0807	0.2723	0.0156
16.0	0.1619	0.1279	0.0619	0.2928	0.0223
24.0	0.0616	0.0947	0.0231	0.2459	0.0387

Reaction Run # 87 Analysis

Materials

(D)-Glucose weight: 20.01 g

Distilled water weight: 150.09 g

Catalyst: MCM-41 # 1

Catalyst weight: 5.0024 g

Internal standard: Butyric Acid, 18.390 mg

Manitol, 30.000 mg

Reaction Parameters

Reaction temperature: 150°C

Mixing speed: 400 rpm

Total reaction time: 24 h

Pressure: 30-60 psi

Table F-24. Reaction run # 87.

Time (h)	Glucose (mol/L)	HMF (mol/L)	Fructose (mol/L)	Formic Acid (mol/L)	4-Oxopentanoic Acid (mol/L)
0.0	0.7864	0.0000	0.0000	0.0000	0.0000
1.0	0.7529	0.0019	0.0173	0.0000	0.0000
2.0	0.7231	0.0214	0.0249	0.0069	0.0034
3.0	0.6678	0.0282	0.0477	0.0222	0.0029
4.0	0.5944	0.0398	0.0666	0.0353	0.0033
5.0	0.5324	0.0563	0.0800	0.0955	0.0033
6.0	0.4704	0.0725	0.0915	0.1432	0.0034
7.0	0.4410	0.0894	0.0973	0.1801	0.0039
8.0	0.3601	0.1018	0.0906	0.2186	0.0059
9.0	0.3288	0.1121	0.0917	0.2261	0.0067
10.0	0.2970	0.1216	0.0904	0.2639	0.0090
12.0	0.2500	0.1202	0.0874	0.2040	0.0110
14.0	0.1958	0.1354	0.0777	0.2541	0.0159
16.0	0.1535	0.1356	0.0669	0.2615	0.0224
24.0	0.0833	0.1239	0.0507	0.2844	0.0316

Reaction Run # 88 Analysis

Materials

(D)-Glucose weight: 16.00 g

Distilled water weight: 120.04 g

Catalyst: MCM-41 # 1

Catalyst weight: 4.0045 g

Internal standard: Butyric Acid, 18.390 mg

Manitol, 30.000 mg

Reaction Parameters

Reaction temperature: 170°C

Mixing speed: 400 rpm

Total reaction time: 24 h

Pressure: 30-60 psi

Table F-25. Reaction run # 88.

Time (h)	Glucose (mol/L)	HMF (mol/L)	Fructose (mol/L)	Formic Acid (mol/L)	4-Oxopentanoic Acid (mol/L)
0.0	0.7414	0.0000	0.0000	0.0000	0.0000
1.0	0.5373	0.0273	0.0454	0.0117	0.0063
2.0	0.5553	0.0437	0.0670	0.0211	0.0043
3.0	0.3912	0.0689	0.0775	0.1222	0.0049
4.0	0.2011	0.0696	0.0585	0.1399	0.0069
5.0	0.1882	0.1564	0.0804	0.2731	0.0217
6.0	0.1239	0.1136	0.0576	0.2115	0.0245
7.0	0.0868	0.1328	0.0463	0.2378	0.0305
8.0	0.0707	0.1159	0.0299	0.2317	0.0309
9.0	0.0500	0.1052	0.0216	0.2186	0.0445
10.0	0.0184	0.0857	0.0107	0.2239	0.0494
12.0	0.0081	0.0573	0.0059	0.1896	0.0559
14.0	0.0027	0.0324	0.0022	0.1746	0.0549
16.0	0.0000	0.0130	0.0000	0.1641	0.0431
24.0	0.0000	0.0018	0.0000	0.1173	0.0391

Reaction Run # 89 Analysis

Materials

(D)-Glucose weight: 20.02 g

Distilled water weight: 150.01 g

Catalyst: MCM-41 # 2

Catalyst weight: 5.0062 g

Internal standard: Butyric Acid, 19.548 mg

Manitol, 60.038 mg

Reaction Parameters

Reaction temperature: 190°C

Mixing speed: 400 rpm

Total reaction time: 24 h

Pressure: 30-60 psi

Table F-26. Reaction run # 89.

Time (h)	Glucose (mol/L)	HMF (mol/L)	Fructose (mol/L)	Formic Acid (mol/L)	4-Oxopentanoic Acid (mol/L)
0.0	0.7537	0.0000	0.0000	0.0000	0.0000
1.0	0.2265	0.1163	0.0932	0.2508	0.0163
2.0	0.1511	0.1419	0.0719	0.2875	0.0316
3.0	0.0561	0.1395	0.0154	0.2478	0.0365
4.0	0.0222	0.0869	0.0053	0.2143	0.0535
5.0	0.0050	0.0464	0.0000	0.1918	0.0628
6.0	0.0036	0.0256	0.0000	0.1843	0.0705
7.0	0.0000	0.0126	0.0000	0.1653	0.0776
8.0	0.0000	0.0050	0.0000	0.1639	0.0723
9.0	0.0000	0.0001	0.0000	0.1301	0.0476
10.0	0.0000	0.0001	0.0000	0.0854	0.0459
12.0	0.0000	0.0000	0.0000	0.1120	0.0455
14.0	0.0000	0.0000	0.0000	0.1110	0.0373
16.0	0.0000	0.0000	0.0000	0.1021	0.0315
24.0	0.0000	0.0000	0.0000	0.0935	0.0342

Reaction Run # 91 Analysis

Materials

(D)-Glucose weight: 16.0081 g

Distilled water weight: 120.12 g

Catalyst: MCM-41 # 2

Catalyst weight: 4.0052 g

Internal standard: Butyric Acid, 19.548 mg

Manitol, 60.038 mg

Reaction Parameters

Reaction temperature: 130°C

Mixing speed: 400 rpm

Total reaction time: 24 h

Pressure: 30-60 psi

Table F-27. Reaction run # 91.

Time (h)	Glucose (mol/L)	HMF (mol/L)	Fructose (mol/L)	Formic Acid (mol/L)	4-Oxopentanoic Acid (mol/L)
0.0	0.7539	0.0000	0.0000	0.0000	0.0000
1.0	0.7530	0.0054	0.0000	0.0000	0.0000
2.0	0.7482	0.0041	0.0000	0.0000	0.0000
3.0	0.7459	0.0084	0.0088	0.0000	0.0000
4.0	0.7394	0.0100	0.0153	0.0000	0.0000
5.0	0.7181	0.0146	0.0262	0.0000	0.0000
6.0	0.6910	0.0190	0.0290	0.0000	0.0000
7.0	0.6698	0.0227	0.0371	0.0054	0.0000
8.0	0.6410	0.0236	0.0399	0.0122	0.0000
9.0	0.6354	0.0308	0.0512	0.0239	0.0000
10.0	0.6313	0.0241	0.0399	0.0330	0.0000
12.0	0.6231	0.0383	0.0608	0.0372	0.0000
14.0	0.5997	0.0378	0.0635	0.0767	0.0000
16.0	0.5982	0.0417	0.0597	0.0647	0.0082
24.0	0.4702	0.0738	0.0869	0.1863	0.0077

Reaction Run # 92 Analysis

Materials

(D)-Glucose weight: 20.01 g

Distilled water weight: 150.26 g

Catalyst: MCM-20 # 2

Catalyst weight: 5.0045 g

Internal standard: Butyric Acid, 18.003 mg

Manitol, 60.078 mg

Reaction Parameters

Reaction temperature: 150°C

Mixing speed: 400 rpm

Total reaction time: 24 h

Pressure: 30-60 psi

Table F-28. Reaction run # 92.

Time (h)	Glucose (mol/L)	HMF (mol/L)	Fructose (mol/L)	Formic Acid (mol/L)	4-Oxopentanoic Acid (mol/L)
0.0	0.7416	0.0000	0.0000	0.0000	0.0000
1.0	0.7059	0.0095	0.0069	0.0000	0.0053
2.0	0.6828	0.0111	0.0176	0.0107	0.0066
3.0	0.6722	0.0176	0.0323	0.0172	0.0059
4.0	0.6420	0.0260	0.0397	0.0292	0.0103
5.0	0.6045	0.0385	0.0454	0.0619	0.0075
6.0	0.5763	0.0446	0.0528	0.0977	0.0071
7.0	0.5390	0.0487	0.0597	0.1199	0.0053
8.0	0.5066	0.0640	0.0629	0.1364	0.0054
9.0	0.4695	0.0704	0.0663	0.1501	0.0096
10.0	0.4479	0.0846	0.0737	0.1744	0.0070
12.0	0.4182	0.0847	0.0792	0.1982	0.0070
14.0	0.3824	0.1010	0.0836	0.2090	0.0097
16.0	0.3262	0.1256	0.0837	0.1573	0.0131
24.0	0.2645	0.1406	0.0749	0.1837	0.0185

Table F-29. Summary of acid activity and coke deposit data after 24 h reaction time for each batch reaction study.

Reaction Run #	Acid Activity After 24 h Reaction Time a_{Xf} (mmol H^+/g)	Coke Deposit Before Calcination (g coke/g-catalyst)	Coke Deposit Before Calcination (g coke/g-catalyst)
20	0.39 ± 0.02	0.220	0.083
24	0.40 ± 0.02	0.023	0.015
25	0.42 ± 0.01	0.005	0.004
26	0.47 ± 0.01	0.714	0.157
28	0.35 ± 0.03	0.286	0.151
33	0.34 ± 0.00	0.045	0.052
43	0.39 ± 0.05	0.264	0.104
60	0.48 ± 0.00	0.991	0.394
63	0.49 ± 0.00	1.286	0.245
64	0.56 ± 0.00	0.714	0.336
65	0.64 ± 0.06	0.467	0.357
67	0.63 ± 0.01	0.832	0.471
68	0.67 ± 0.03	0.447	0.436
69	0.67 ± 0.04	1.087	0.217
71	0.53 ± 0.06	0.138	0.099
72	0.32 ± 0.00	0.240	0.085
73	0.58 ± 0.00	0.248	0.180
76	0.37 ± 0.02	1.510	0.339
77	0.44 ± 0.01	0.948	0.336
78	0.51 ± 0.03	0.242	0.065
80	0.42 ± 0.01	1.091	0.330
82	0.57 ± 0.01	0.264	0.162
86	0.33 ± 0.00	1.103	0.077
87	0.34 ± 0.02	1.038	0.072
88	0.16 ± 0.00	1.378	0.060
89	0.16 ± 0.00	1.374	0.055
91	0.44 ± 0.01	0.212	0.088
92	0.28 ± 0.01	1.349	0.073

Appendix G

Numerical Method for Non-Linear Regression

Surface Reaction Model

The rate equations are

$$\frac{dC_{T,G}}{dt} = \frac{dC_{G\cdot X}}{dt} = -k_{S2}K_G C_X C_G - k_{S1}(K_G C_X C_G - \frac{K_F C_X}{K_{S1}} C_F)$$

$$= g_1(t, \mathbf{C}, \mathbf{k}) \qquad \text{(G-1)}$$

$$\frac{dC_{T,H}}{dt} = \frac{dC_{H\cdot X}}{dt} = k_{S2}K_G C_X C_G + k_{S3}K_F C_X C_F - k_{S4}K_H C_X C_H - \frac{k_{S5}}{C_X} K_H C_X C_H C_{v,X}$$

$$= g_2(t, \mathbf{C}, \mathbf{k}) \qquad \text{(G-2)}$$

$$\frac{dC_{T,F}}{dt} = \frac{dC_{F\cdot X}}{dt} = -k_{S3}K_F C_X C_F + k_{S1}(K_G C_X C_G - \frac{K_F C_X}{K_{S1}} C_F)$$

$$= g_3(t, \mathbf{C}, \mathbf{k}) \qquad \text{(G-3)}$$

$$\frac{dC_{T,FA}}{dt} = \frac{dC_{FA\cdot X}}{dt} = \frac{k_{S5}}{C_X} K_H C_X C_H C_{v,X} - k_{S6}K_{FA} C_X C_{FA}$$

$$= g_4(t, \mathbf{C}, \mathbf{k}) \qquad \text{(G-4)}$$

$$\frac{dC_{T,OA}}{dt} = \frac{dC_{OA\cdot X}}{dt} = \frac{k_{S5}}{C_X} K_H C_X C_H C_{v,X} - k_{S7}K_{OA} C_X C_{OA}$$

$$= g_5(t, \mathbf{C}, \mathbf{k}) \qquad \text{(G-5)}$$

$$\frac{dC_{R,H}}{dt} = g_{R,1}(t, \mathbf{C}, \mathbf{k}) = k_{S4}K_H C_X C_H \qquad \text{(G-6)}$$

$$\frac{dC_{R,FA}}{dt} = g_{R,2}(t, \mathbf{C}, \mathbf{k}) = k_{S6}K_{FA} C_X C_{FA} \qquad \text{(G-7)}$$

$$\frac{dC_{R,OA}}{dt} = g_{R,3}(t, \mathbf{C}, \mathbf{k}) = k_{S7}K_{OA} C_X C_{OA} \qquad \text{(G-8)}$$

where

$$\mathbf{C} = C_G, C_H, C_F, C_{FA}, C_{OA}, C_X, C_{v,X}$$

$$\mathbf{k} = k_{S1}, k_{S2}, 1/K_{S1}, k_{S3}, k_{S4}, k_{S5}/C_X, k_{S6}, k_{S7}, K_G, K_H, K_F, K_{FA}, K_{OA}$$

The surface concentrations are defined by

$$C_{i\cdot X} = C_{T,i} - C_i \tag{G-9}$$

$$C_{G\cdot X} = K_G C_X C_G \tag{G-10}$$

$$C_{H\cdot X} = K_H C_X C_H \tag{G-11}$$

$$C_{F\cdot X} = K_F C_X C_F \tag{G-12}$$

$$C_{FA\cdot X} = K_{FA} C_X C_{FA} \tag{G-13}$$

$$C_{OA\cdot X} = K_{OA} C_X C_{OA} \tag{G-14}$$

$$C_X = \sum_i C_{i\cdot X} + C_{v,X} = C_{G\cdot X} + C_{H\cdot X} + C_{F\cdot X} + C_{FA\cdot X} + C_{OA\cdot X} + C_{v,X} \tag{G-15}$$

The total acid site concentration (C_X) is obtained by experiment from

$$C_X = C_{cat}\, a_X \tag{G-16}$$

The initial conditions at $t = 0$ are

$$C_{G,0} = C_{T,G,0} \tag{G-17}$$

$$C_{H,0} = C_{F,0} = C_{FA,0} = C_{OA,0} = 0 \tag{G-18}$$

$$C_{T,H,0} = C_{T,F,0} = C_{T,FA,0} = C_{T,OA,0} = 0 \tag{G-19}$$

$$C_{R,H,0} = C_{R,FA,0} = C_{R,OA,0} \tag{G-20}$$

The rate equations for glucose, fructose, HMF, formic acid, and 4-oxopentanoic acid (equations G-1 to G-5) are used in a non-linear regression method to estimate the rate constants (k_{Sj}) and adsorption equilibrium constants (K_i). The rate equations (equations G-6 to G-8) are used to predict the coke formation.

Non-Linear Regression Analysis

The rate equations G-1 to G-5 are first numerically solved by the 4th order Runge-Kutta method for ordinary differential equation (ODE), given the initial conditions (equations G-17 to G-20). The details and modification of this numerical method will be described later in the Numerical Solution of ODEs.

The solution can be expressed as a function of time and rate constants as

$$C_G = f_1(t, \mathbf{k}) \tag{G-21}$$

$$C_H = f_2(t, \boldsymbol{k}) \tag{G-22}$$

$$C_F = f_3(t, \boldsymbol{k}) \tag{G-23}$$

$$C_{FA} = f_4(t, \boldsymbol{k}) \tag{G-24}$$

$$C_{OA} = f_5(t, \boldsymbol{k}) \tag{G-25}$$

For a multiple regression, the weighted sum of squared residuals (*SSR*) is given by

$$SSR = \sum_{i=1}^{h}\sum_{l=1}^{n_i} w_i (C^*_{i,l} - C_{i,l})^T (C^*_{i,l} - C_{i,l}) \tag{G-26}$$

where w_i = weighting factor corresponding to the "i" component

$C^*_{i,l}$ = experimental data of the "i" component at "l" point

$C_{i,l}$ = calculated values of the "i" component from equations G-21 to G-25

h = total number of component = 5

n_i = total point of experimental data of the "i" component

The weighting factor (w_i) is determined because the variance (σ^2_i) of all distributions are not equal for multiple regression. Therefore, the individual sum of squares must be multiplied by a weighting factor which is proportional to $1/\sigma^2_i$ in order to form an unbiased weighted sum of squared residuals. The equation for evaluating the weighting factor is given by

$$w_i = \frac{1/\sigma_i^2}{\frac{1}{\sum_{i=1}^{h} n_i}\left[\sum_{i=1}^{h}\sum_{l=1}^{n_i} 1/\sigma_i^2\right]} \tag{G-27}$$

where σ^2_i is the variance for each vector of the "i" component

The non-linear function C_i can be converted to linear function by a Taylor series expansion around an estimated value of the parameter vector $\boldsymbol{k}$ by

$$C_{i,l}(t, \boldsymbol{k} + \Delta\boldsymbol{k}) = C_{i,l}(t, \boldsymbol{k}) + \frac{\partial C_{i,l}}{d\boldsymbol{k}}\Delta\boldsymbol{k} \tag{G-28}$$

The problem is transformed from $\boldsymbol{k}$ estimation to $\Delta\boldsymbol{k}$ estimation. Equation G-26 is transformed to

$$SSR = \sum_{i=1}^{h}\sum_{l=1}^{n_i} w_i (C_{i,l}^* - C_{i,l} - A_i \Delta k)^T (C_{i,l}^* - C_{i,l} - A_i \Delta k) \tag{G-29}$$

where A_i is the Jacobian matrix of partial derivatives of $C_{i,l}$ with respect to k evaluated at all "l" where the experimental data are available. The Jacobian matrix is defined by

$$A_i = \begin{bmatrix} \frac{\partial C_{i,1}}{\partial k_{S2}} & \cdots & \frac{\partial C_{i,1}}{\partial K_{OA}} \\ \downarrow & \downarrow & \downarrow \\ \frac{\partial C_{i,n_i}}{\partial k_{S2}} & \cdots & \frac{\partial C_{1,n_i}}{\partial K_{OA}} \end{bmatrix} \tag{G-30}$$

The details of constructing the Jacobian matrix for the differential equations will be described later in the Jacobian Matrix section.

According to the Marquardt method, after taking the partial derivative of Φ with respect to k and setting it equal to zero, the vector of Δk can be obtained by

$$\Delta k = \left[\sum_{i=1}^{h} w_i A_i^T A_i + \alpha I\right]^{-1} \left[\sum_{i=1}^{h}\sum_{l=1}^{n_i} w_i A_i^T (C_{i,l}^* - C_{i,l})\right] \tag{G-31}$$

The value of α in a αI diagonal matrix is chosen at each iteration so that the corrected parameter vector will result in a lower sum of squared residual in the next iteration. Therefore the method of choosing α must give a small value of α when the Gauss-Newton method will converge efficiently, and a large value of α when the Steepest-Descent method is necessary.

The correcting vector Δk is applied to the estimated k to obtain a new estimated of the rate constant vector as

$$k_{new} = k_{previous} + \Delta k \tag{G-32}$$

When new vector for k is applied to the rate equations, then the solution of rate equations, the sum of squared residuals, and the k adjustment is estimated iteratively until the Δk does not change and the sum of squared residuals is minimized.

Jacobian Matrix

The rate equations of the surface reaction model consist of differential equations. Therefore variational equations must be developed in order to construct the Jacobian

matrix. Each variational equation is obtained by taking the partial derivative of g_i with respect to $\boldsymbol{k}$. After rearranging, the variational equation is

$$\frac{d}{dt}\left(\frac{\partial C_i}{\partial \boldsymbol{k}}\right) = \frac{\partial g_i}{\partial \boldsymbol{k}} - \frac{\partial g_i}{\partial C_i}\frac{\partial C_i}{\partial \boldsymbol{k}} \tag{G-33}$$

The integration of the variational equation will provide the profiles of elements required to construct the Jacobian matrix.

The variational equations of glucose (G) are

$$\frac{d}{dt}\left(\frac{\partial C_G}{\partial k_{S2}}\right) = g_6 = -k_{S2}K_G C_X \frac{\partial C_G}{\partial k_{S2}} - k_{S1}K_G C_X \frac{\partial C_G}{\partial k_{S2}} + \frac{k_{S1}K_F C_X}{K_{S1}}\frac{\partial C_F}{\partial k_{S2}} - K_G C_X C_G \tag{G-34}$$

$$\frac{d}{dt}\left(\frac{\partial C_G}{\partial k_{S1}}\right) = g_7 = -k_{S2}K_G C_X \frac{\partial C_G}{\partial k_{S1}} - k_{S1}K_G C_X \frac{\partial C_G}{\partial k_{S1}} + \frac{k_{S1}K_F C_X}{K_{S1}}\frac{\partial C_F}{\partial k_{S1}} - K_G C_X C_G + \frac{K_F C_X}{K_{S1}} C_F \tag{G-35}$$

$$\frac{d}{dt}\left(\frac{\partial C_G}{\partial (1/K_{S1})}\right) = g_8 = -k_{S2}K_G C_X \frac{\partial C_G}{\partial (1/K_{S1})} - k_{S1}K_G C_X \frac{\partial C_G}{\partial (1/K_{S1})} + \frac{k_{S1}K_F C_X}{K_{S1}}\frac{\partial C_F}{\partial (1/K_{S1})} - k_{S1}K_F C_X C_F \tag{G-36}$$

$$\frac{d}{dt}\left(\frac{\partial C_G}{\partial k_{S3}}\right) = g_9 = -k_{S2}K_G C_X \frac{\partial C_G}{\partial k_{S3}} - k_{S1}K_G C_X \frac{\partial C_G}{\partial k_{S3}} + \frac{k_{S1}K_F C_X}{K_{S1}}\frac{\partial C_F}{\partial k_{S3}} \tag{G-37}$$

$$\frac{d}{dt}\left(\frac{\partial C_G}{\partial k_{S4}}\right) = g_{10} = -k_{S2}K_G C_X \frac{\partial C_G}{\partial k_{S4}} - k_{S1}K_G C_X \frac{\partial C_G}{\partial k_{S4}} + \frac{k_{S1}K_F C_X}{K_{S1}}\frac{\partial C_F}{\partial k_{S4}} \tag{G-38}$$

$$\frac{d}{dt}\left(\frac{\partial C_G}{\partial (k_{S5}/C_X)}\right) = g_{11} = -k_{S2}K_G C_X \frac{\partial C_G}{\partial (k_{S5}/C_X)} - k_{S1}K_G C_X \frac{\partial C_G}{\partial (k_{S5}/C_X)} + \frac{k_{S1}K_F C_X}{K_{S1}}\frac{\partial C_F}{\partial (k_{S5}/C_X)} \tag{G-39}$$

$$\frac{d}{dt}\left(\frac{\partial C_G}{\partial k_{S6}}\right) = g_{12} = -k_{S2}K_G C_X \frac{\partial C_G}{\partial k_{S6}} - k_{S1}K_G C_X \frac{\partial C_G}{\partial k_{S6}} + \frac{k_{S1}K_F C_X}{K_{S1}}\frac{\partial C_F}{\partial k_{S6}} \tag{G-40}$$

$$\frac{d}{dt}\left(\frac{\partial C_G}{\partial k_{S7}}\right) = g_{13} = -k_{S2}K_G C_X \frac{\partial C_G}{\partial k_{S7}} - k_{S1}K_G C_X \frac{\partial C_G}{\partial k_{S7}} + \frac{k_{S1}K_F C_X}{K_{S1}} \frac{\partial C_F}{\partial k_{S7}} \tag{G-41}$$

$$\frac{d}{dt}\left(\frac{\partial C_G}{\partial K_G}\right) = g_{14} = -k_{S2}K_G C_X \frac{\partial C_G}{\partial K_G} - k_{S1}K_G C_X \frac{\partial C_G}{\partial K_G} + \frac{k_{S1}K_F C_X}{K_{S1}} \frac{\partial C_F}{\partial K_G} - k_{S2}C_X C_G - k_{S1}C_X C_g \tag{G-42}$$

$$\frac{d}{dt}\left(\frac{\partial C_G}{\partial K_H}\right) = g_{15} = -k_{S2}K_G C_X \frac{\partial C_G}{\partial K_H} - k_{S1}K_G C_X \frac{\partial C_G}{\partial K_H} + \frac{k_{S1}K_F C_X}{K_{S1}} \frac{\partial C_F}{\partial K_H} \tag{G-43}$$

$$\frac{d}{dt}\left(\frac{\partial C_G}{\partial K_F}\right) = g_{16} = -k_{S2}K_G C_X \frac{\partial C_G}{\partial K_F} - k_{S1}K_G C_X \frac{\partial C_G}{\partial K_F} + \frac{k_{S1}K_F C_X}{K_{S1}} \frac{\partial C_F}{\partial K_F} + \frac{k_{S1}C_X}{K_{S1}} C_F \tag{G-44}$$

$$\frac{d}{dt}\left(\frac{\partial C_G}{\partial K_{FA}}\right) = g_{17} = -k_{S2}K_G C_X \frac{\partial C_G}{\partial K_{FA}} - k_{S1}K_G C_X \frac{\partial C_G}{\partial K_{FA}} + \frac{k_{S1}K_F C_X}{K_{S1}} \frac{\partial C_F}{\partial K_{FA}} \tag{G-45}$$

$$\frac{d}{dt}\left(\frac{\partial C_G}{\partial K_{OA}}\right) = g_{18} = -k_{S2}K_G C_X \frac{\partial C_G}{\partial K_{OA}} - k_{S1}K_G C_X \frac{\partial C_G}{\partial K_{OA}} + \frac{k_{S1}K_F C_X}{K_{S1}} \frac{\partial C_F}{\partial K_{OA}} \tag{G-46}$$

The variational equations of HMF (H) are

$$\frac{d}{dt}\left(\frac{\partial C_H}{\partial k_{S2}}\right) = g_{19} = k_{S2}K_G C_X \frac{\partial C_G}{\partial k_{S2}} + k_{S3}K_F C_X \frac{\partial C_F}{\partial k_{S2}} - k_{S4}K_H C_X \frac{\partial C_H}{\partial k_{S2}} - \frac{k_{S5}K_H C_X}{C_X} \frac{\partial C_H}{\partial k_{S2}} C_{v,X} + K_G C_X C_G \tag{G-47}$$

$$\frac{d}{dt}\left(\frac{\partial C_H}{\partial k_{S1}}\right) = g_{20} = k_{S2}K_G C_X \frac{\partial C_G}{\partial k_{S1}} + k_{S3}K_F C_X \frac{\partial C_F}{\partial k_{S1}} - k_{S4}K_H C_X \frac{\partial C_H}{\partial k_{S1}} - \frac{k_{S5}K_H C_X}{C_X} \frac{\partial C_H}{\partial k_{S1}} C_{v,X} \tag{G-48}$$

$$\frac{d}{dt}\left(\frac{\partial C_H}{\partial (1/K_{S1})}\right) = g_{21} = k_{S2}K_G C_X \frac{\partial C_G}{\partial (1/K_{S1})} + k_{S3}K_F C_X \frac{\partial C_F}{\partial (1/K_{S1})} - k_{S4}K_H C_X \frac{\partial C_H}{\partial (1/K_{S1})} - \frac{k_{S5}K_H C_X}{C_X} \frac{\partial C_H}{\partial (1/K_{S1})} C_{v,X} \tag{G-49}$$

$$\frac{d}{dt}\left(\frac{\partial C_H}{\partial k_{S3}}\right) = g_{22} = k_{S2}K_G C_X \frac{\partial C_G}{\partial k_{S3}} + k_{S3}K_F C_X \frac{\partial C_F}{\partial k_{S3}} - k_{S4}K_H C_X \frac{\partial C_H}{\partial k_{S3}} - \frac{k_{S5}K_H C_X}{C_X}\frac{\partial C_H}{\partial k_{S3}} C_{v,X} + K_F C_X C_F \tag{G-50}$$

$$\frac{d}{dt}\left(\frac{\partial C_H}{\partial k_{S4}}\right) = g_{23} = k_{S2}K_G C_X \frac{\partial C_G}{\partial k_{S4}} + k_{S3}K_F C_X \frac{\partial C_F}{\partial k_{S4}} - k_{S4}K_H C_X \frac{\partial C_H}{\partial k_{S4}} - \frac{k_{S5}K_H C_X}{C_X}\frac{\partial C_H}{\partial k_{S4}} C_{v,X} - K_H C_X C_H \tag{G-51}$$

$$\frac{d}{dt}\left(\frac{\partial C_H}{\partial (k_{S5}/C_X)}\right) = g_{24} = k_{S2}K_G C_X \frac{\partial C_G}{\partial (k_{S5}/C_X)} + k_{S3}K_F C_X \frac{\partial C_F}{\partial (k_{S5}/C_X)} - k_{S4}K_H C_X \frac{\partial C_H}{\partial (k_{S5}/C_X)} - \frac{k_{S5}K_H C_X}{C_X}\frac{\partial C_H}{\partial (k_{S5}/C_X)} C_{v,X} - K_H C_X C_H C_{v,X} \tag{G-52}$$

$$\frac{d}{dt}\left(\frac{\partial C_H}{\partial k_{S6}}\right) = g_{25} = k_{S2}K_G C_X \frac{\partial C_G}{\partial k_{S6}} + k_{S3}K_F C_X \frac{\partial C_F}{\partial k_{S6}} - k_{S4}K_H C_X \frac{\partial C_H}{\partial k_{S6}} - \frac{k_{S5}K_H C_X}{C_X}\frac{\partial C_H}{\partial k_{S6}} C_{v,X} \tag{G-53}$$

$$\frac{d}{dt}\left(\frac{\partial C_H}{\partial k_{S7}}\right) = g_{26} = k_{S2}K_G C_X \frac{\partial C_G}{\partial k_{S7}} + k_{S3}K_F C_X \frac{\partial C_F}{\partial k_{S7}} - k_{S4}K_H C_X \frac{\partial C_H}{\partial k_{S7}} - \frac{k_{S5}K_H C_X}{C_X}\frac{\partial C_H}{\partial k_{S7}} C_{v,X} \tag{G-54}$$

$$\frac{d}{dt}\left(\frac{\partial C_H}{\partial K_G}\right) = g_{27} = k_{S2}K_G C_X \frac{\partial C_G}{\partial K_G} + k_{S3}K_F C_X \frac{\partial C_F}{\partial K_G} - k_{S4}K_H C_X \frac{\partial C_H}{\partial K_G} - \frac{k_{S5}K_H C_X}{C_X}\frac{\partial C_H}{\partial K_G} C_{v,X} + k_{S2}C_X C_G \tag{G-55}$$

$$\frac{d}{dt}\left(\frac{\partial C_H}{\partial K_H}\right) = g_{28} = k_{S2}K_G C_X \frac{\partial C_G}{\partial K_H} + k_{S3}K_F C_X \frac{\partial C_F}{\partial K_H} - k_{S4}K_H C_X \frac{\partial C_H}{\partial K_H} - \frac{k_{S5}K_H C_X}{C_X}\frac{\partial C_H}{\partial K_H} C_{v,X} - k_{S4}C_X C_H - \frac{k_{S5}}{C_X} C_X C_H C_{v,X} \tag{G-56}$$

$$\frac{d}{dt}\left(\frac{\partial C_H}{\partial K_F}\right) = g_{29} = k_{S2}K_G C_X \frac{\partial C_G}{\partial K_F} + k_{S3}K_F C_X \frac{\partial C_F}{\partial K_F} - k_{S4}K_H C_X \frac{\partial C_H}{\partial K_F} - \frac{k_{S5}K_H C_X}{C_X}\frac{\partial C_H}{\partial K_F} C_{v,X} + k_{S3}C_X C_F \tag{G-57}$$

$$\frac{d}{dt}\left(\frac{\partial C_H}{\partial K_{FA}}\right) = g_{30} = k_{S2}K_G C_X \frac{\partial C_G}{\partial K_{FA}} + k_{S3}K_F C_X \frac{\partial C_F}{\partial K_{FA}} - k_{S4}K_H C_X \frac{\partial C_H}{\partial K_{FA}} - \frac{k_{S5}K_H C_X}{C_X}\frac{\partial C_H}{\partial K_{FA}} C_{v,X} \tag{G-58}$$

$$\frac{d}{dt}\left(\frac{\partial C_H}{\partial K_{OA}}\right) = g_{31} = k_{S2}K_G C_X \frac{\partial C_G}{\partial K_{OA}} + k_{S3}K_F C_X \frac{\partial C_F}{\partial K_{OA}} - k_{S4}K_H C_X \frac{\partial C_H}{\partial K_{OA}} - \frac{k_{S5}K_H C_X}{C_X}\frac{\partial C_H}{\partial K_{OA}} C_{v,X} \tag{G-59}$$

The variational equations of fructose (F) are

$$\frac{d}{dt}\left(\frac{\partial C_F}{\partial k_{S2}}\right) = g_{32} = -k_{S3}K_F C_X \frac{\partial C_F}{\partial k_{S2}} + k_{S1}K_G C_X \frac{\partial C_G}{\partial k_{S2}} - \frac{k_{S1}K_F C_X}{K_{S1}}\frac{\partial C_F}{\partial k_{S2}} \tag{G-60}$$

$$\frac{d}{dt}\left(\frac{\partial C_F}{\partial k_{S1}}\right) = g_{33} = -k_{S3}K_F C_X \frac{\partial C_F}{\partial k_{S1}} + k_{S1}K_G C_X \frac{\partial C_G}{\partial k_{S1}} - \frac{k_{S1}K_F C_X}{K_{S1}}\frac{\partial C_F}{\partial k_{S1}} + K_G C_X C_G - \frac{K_F C_X}{K_{S1}} C_F \tag{G-61}$$

$$\frac{d}{dt}\left(\frac{\partial C_F}{\partial (1/K_{S1})}\right) = g_{34} = -k_{S3}K_F C_X \frac{\partial C_F}{\partial (1/K_{S1})} + k_{S1}K_G C_X \frac{\partial C_G}{\partial (1/K_{S1})} - \frac{k_{S1}K_F C_X}{K_{S1}}\frac{\partial C_F}{\partial (1/K_{S1})} - k_{S1}K_F C_X C_F \tag{G-62}$$

$$\frac{d}{dt}\left(\frac{\partial C_F}{\partial k_{S3}}\right) = g_{35} = -k_{S3}K_F C_X \frac{\partial C_F}{\partial k_{S3}} + k_{S1}K_G C_X \frac{\partial C_G}{\partial k_{S3}} - \frac{k_{S1}K_F C_X}{K_{S1}}\frac{\partial C_F}{\partial k_{S3}} - K_F C_X C_F \tag{G-63}$$

$$\frac{d}{dt}\left(\frac{\partial C_F}{\partial k_{S4}}\right) = g_{36} = -k_{S3}K_F C_X \frac{\partial C_F}{\partial k_{S4}} + k_{S1}K_G C_X \frac{\partial C_G}{\partial k_{S4}} - \frac{k_{S1}K_F C_X}{K_{S1}}\frac{\partial C_F}{\partial k_{S4}} \tag{G-64}$$

$$\frac{d}{dt}\left(\frac{\partial C_F}{\partial(k_{S5}/C_X)}\right) = g_{37} = -k_{S3}K_F C_X \frac{\partial C_F}{\partial(k_{S5}/C_X)} + k_{S1}K_G C_X \frac{\partial C_G}{\partial(k_{S5}/C_X)} - \frac{k_{S1}K_F C_X}{K_{S1}} \frac{\partial C_F}{\partial(k_{S5}/C_X)} \tag{G-65}$$

$$\frac{d}{dt}\left(\frac{\partial C_F}{\partial k_{S6}}\right) = g_{38} = -k_{S3}K_F C_X \frac{\partial C_F}{\partial k_{S6}} + k_{S1}K_G C_X \frac{\partial C_G}{\partial k_{S6}} - \frac{k_{S1}K_F C_X}{K_{S1}} \frac{\partial C_F}{\partial k_{S6}} \tag{G-66}$$

$$\frac{d}{dt}\left(\frac{\partial C_F}{\partial k_{S7}}\right) = g_{39} = -k_{S3}K_F C_X \frac{\partial C_F}{\partial k_{S7}} + k_{S1}K_G C_X \frac{\partial C_G}{\partial k_{S7}} - \frac{k_{S1}K_F C_X}{K_{S1}} \frac{\partial C_F}{\partial k_{S7}} \tag{G-67}$$

$$\frac{d}{dt}\left(\frac{\partial C_F}{\partial K_G}\right) = g_{40} = -k_{S3}K_F C_X \frac{\partial C_F}{\partial K_G} + k_{S1}K_G C_X \frac{\partial C_G}{\partial K_G} - \frac{k_{S1}K_F C_X}{K_{S1}} \frac{\partial C_F}{\partial K_G} + k_{S1}C_X C_G \tag{G-68}$$

$$\frac{d}{dt}\left(\frac{\partial C_F}{\partial K_H}\right) = g_{41} = -k_{S3}K_F C_X \frac{\partial C_F}{\partial K_H} + k_{S1}K_G C_X \frac{\partial C_G}{\partial K_H} - \frac{k_{S1}K_F C_X}{K_{S1}} \frac{\partial C_F}{\partial K_H} \tag{G-69}$$

$$\frac{d}{dt}\left(\frac{\partial C_F}{\partial K_F}\right) = g_{42} = -k_{S3}K_F C_X \frac{\partial C_F}{\partial K_F} + k_{S1}K_G C_X \frac{\partial C_G}{\partial K_F} - \frac{k_{S1}K_F C_X}{K_{S1}} \frac{\partial C_F}{\partial K_F} - k_{S1}C_X C_F - \frac{k_{S1}C_X}{K_{S1}} C_F \tag{G-70}$$

$$\frac{d}{dt}\left(\frac{\partial C_F}{\partial K_{FA}}\right) = g_{43} = -k_{S3}K_F C_X \frac{\partial C_F}{\partial K_{FA}} + k_{S1}K_G C_X \frac{\partial C_G}{\partial K_{FA}} - \frac{k_{S1}K_F C_X}{K_{S1}} \frac{\partial C_F}{\partial K_{FA}} \tag{G-71}$$

$$\frac{d}{dt}\left(\frac{\partial C_F}{\partial K_{OA}}\right) = g_{44} = -k_{S3}K_F C_X \frac{\partial C_F}{\partial K_{OA}} + k_{S1}K_G C_X \frac{\partial C_G}{\partial K_{OA}} - \frac{k_{S1}K_F C_X}{K_{S1}} \frac{\partial C_F}{\partial K_{OA}} \tag{G-72}$$

The variational equations of formic acid (FA) are

$$\frac{d}{dt}\left(\frac{\partial C_{FA}}{\partial k_{S2}}\right) = g_{45} = \frac{k_{S5}K_h C_X}{C_X} \frac{\partial C_H}{\partial k_{S2}} C_{v,X} - k_{S6}K_{FA}C_X \frac{\partial C_{FA}}{\partial k_{S2}} \tag{G-73}$$

$$\frac{d}{dt}\left(\frac{\partial C_{FA}}{\partial k_{S1}}\right) = g_{46} = \frac{k_{S5}K_h C_X}{C_X} \frac{\partial C_H}{\partial k_{S1}} C_{v,X} - k_{S6}K_{FA}C_X \frac{\partial C_{FA}}{\partial k_{S1}} \tag{G-74}$$

$$\frac{d}{dt}\left(\frac{\partial C_{FA}}{\partial(1/K_{S1})}\right) = g_{47} = \frac{k_{S5}K_h C_X}{C_X} \frac{\partial C_H}{\partial(1/K_{S1})} C_{v,X} - k_{S6}K_{FA}C_X \frac{\partial C_{FA}}{\partial(1/K_{S1})} \tag{G-75}$$

$$\frac{d}{dt}\left(\frac{\partial C_{FA}}{\partial k_{S3}}\right) = g_{48} = \frac{k_{S5}K_hC_X}{C_X}\frac{\partial C_H}{\partial k_{S3}}C_{v,X} - k_{S6}K_{FA}C_X\frac{\partial C_{FA}}{\partial k_{S3}} \tag{G-76}$$

$$\frac{d}{dt}\left(\frac{\partial C_{FA}}{\partial k_{S4}}\right) = g_{49} = \frac{k_{S5}K_hC_X}{C_X}\frac{\partial C_H}{\partial k_{S4}}C_{v,X} - k_{S6}K_{FA}C_X\frac{\partial C_{FA}}{\partial k_{S4}} \tag{G-77}$$

$$\frac{d}{dt}\left(\frac{\partial C_{FA}}{\partial (k_{S5}/C_X)}\right) = g_{50} = \frac{k_{S5}K_hC_X}{C_X}\frac{\partial C_H}{\partial (k_{S5}/C_X)}C_{v,X} - k_{S6}K_{FA}C_X\frac{\partial C_{FA}}{\partial (k_{S5}/C_X)} + K_HC_XC_HC_{v,X} \tag{G-78}$$

$$\frac{d}{dt}\left(\frac{\partial C_{FA}}{\partial k_{S6}}\right) = g_{51} = \frac{k_{S5}K_hC_X}{C_X}\frac{\partial C_H}{\partial k_{S6}}C_{v,X} - k_{S6}K_{FA}C_X\frac{\partial C_{FA}}{\partial k_{S6}} - K_{FA}C_XC_{FA} \tag{G-79}$$

$$\frac{d}{dt}\left(\frac{\partial C_{FA}}{\partial k_{S7}}\right) = g_{52} = \frac{k_{S5}K_hC_X}{C_X}\frac{\partial C_H}{\partial k_{S7}}C_{v,X} - k_{S6}K_{FA}C_X\frac{\partial C_{FA}}{\partial k_{S7}} \tag{G-80}$$

$$\frac{d}{dt}\left(\frac{\partial C_{FA}}{\partial K_G}\right) = g_{53} = \frac{k_{S5}K_hC_X}{C_X}\frac{\partial C_H}{\partial K_G}C_{v,X} - k_{S6}K_{FA}C_X\frac{\partial C_{FA}}{\partial K_G} \tag{G-81}$$

$$\frac{d}{dt}\left(\frac{\partial C_{FA}}{\partial K_H}\right) = g_{54} = \frac{k_{S5}K_hC_X}{C_X}\frac{\partial C_H}{\partial K_H}C_{v,X} - k_{S6}K_{FA}C_X\frac{\partial C_{FA}}{\partial K_H} + \frac{k_{S5}C_X}{C_X}C_HC_{v,X} \tag{G-82}$$

$$\frac{d}{dt}\left(\frac{\partial C_{FA}}{\partial K_F}\right) = g_{55} = \frac{k_{S5}K_hC_X}{C_X}\frac{\partial C_H}{\partial K_F}C_{v,X} - k_{S6}K_{FA}C_X\frac{\partial C_{FA}}{\partial K_F} \tag{G-83}$$

$$\frac{d}{dt}\left(\frac{\partial C_{FA}}{\partial K_{FA}}\right) = g_{56} = \frac{k_{S5}K_hC_X}{C_X}\frac{\partial C_H}{\partial K_{FA}}C_{v,X} - k_{S6}K_{FA}C_X\frac{\partial C_{FA}}{\partial K_{FA}} - k_{S6}C_XC_{FA} \tag{G-84}$$

$$\frac{d}{dt}\left(\frac{\partial C_{FA}}{\partial K_{OA}}\right) = g_{57} = \frac{k_{S5}K_hC_X}{C_X}\frac{\partial C_H}{\partial K_{OA}}C_{v,X} - k_{S6}K_{FA}C_X\frac{\partial C_{FA}}{\partial K_{OA}} \tag{G-85}$$

The variational equations of 4-oxopentanoic acid (OA) are

$$\frac{d}{dt}\left(\frac{\partial C_{OA}}{\partial k_{S2}}\right) = g_{58} = \frac{k_{S5}K_hC_X}{C_X}\frac{\partial C_H}{\partial k_{S2}}C_{v,X} - k_{S7}K_{OA}C_X\frac{\partial C_{OA}}{\partial k_{S2}} \tag{G-86}$$

$$\frac{d}{dt}\left(\frac{\partial C_{OA}}{\partial k_{S1}}\right) = g_{59} = \frac{k_{S5}K_hC_X}{C_X}\frac{\partial C_H}{\partial k_{S1}}C_{v,X} - k_{S7}K_{OA}C_X\frac{\partial C_{OA}}{\partial k_{S1}} \tag{G-87}$$

$$\frac{d}{dt}\left(\frac{\partial C_{OA}}{\partial (1/K_{S1})}\right) = g_{60} = \frac{k_{S5}K_hC_X}{C_X}\frac{\partial C_H}{\partial (1/K_{S1})}C_{v,X} - k_{S7}K_{OA}C_X\frac{\partial C_{OA}}{\partial (1/K_{S1})} \tag{G-88}$$

$$\frac{d}{dt}\left(\frac{\partial C_{OA}}{\partial k_{S3}}\right) = g_{61} = \frac{k_{S5}K_hC_X}{C_X}\frac{\partial C_H}{\partial k_{S3}}C_{v,X} - k_{S7}K_{OA}C_X\frac{\partial C_{OA}}{\partial k_{S3}} \tag{G-89}$$

$$\frac{d}{dt}\left(\frac{\partial C_{OA}}{\partial k_{S4}}\right) = g_{62} = \frac{k_{S5}K_hC_X}{C_X}\frac{\partial C_H}{\partial k_{S4}}C_{v,X} - k_{S7}K_{OA}C_X\frac{\partial C_{OA}}{\partial k_{S4}} \tag{G-90}$$

$$\frac{d}{dt}\left(\frac{\partial C_{OA}}{\partial (k_{S5}/C_X)}\right) = g_{63} = \frac{k_{S5}K_hC_X}{C_X}\frac{\partial C_H}{\partial (k_{S5}/C_X)}C_{v,X} - k_{S7}K_{OA}C_X\frac{\partial C_{OA}}{\partial (k_{S5}/C_X)} + K_HC_XC_HC_{v,X} \tag{G-91}$$

$$\frac{d}{dt}\left(\frac{\partial C_{OA}}{\partial k_{S6}}\right) = g_{64} = \frac{k_{S5}K_hC_X}{C_X}\frac{\partial C_H}{\partial k_{S6}}C_{v,X} - k_{S7}K_{OA}C_X\frac{\partial C_{OA}}{\partial k_{S6}} \tag{G-92}$$

$$\frac{d}{dt}\left(\frac{\partial C_{OA}}{\partial k_{S7}}\right) = g_{65} = \frac{k_{S5}K_hC_X}{C_X}\frac{\partial C_H}{\partial k_{S7}}C_{v,X} - k_{S7}K_{FA}C_X\frac{\partial C_{OA}}{\partial k_{S7}} - K_{OA}C_XC_{OA} \tag{G-93}$$

$$\frac{d}{dt}\left(\frac{\partial C_{OA}}{\partial K_G}\right) = g_{66} = \frac{k_{S5}K_hC_X}{C_X}\frac{\partial C_H}{\partial K_G}C_{v,X} - k_{S7}K_{OA}C_X\frac{\partial C_{OA}}{\partial K_G} \tag{G-94}$$

$$\frac{d}{dt}\left(\frac{\partial C_{OA}}{\partial K_H}\right) = g_{67} = \frac{k_{S5}K_hC_X}{C_X}\frac{\partial C_H}{\partial K_H}C_{v,X} - k_{S7}K_{OA}C_X\frac{\partial C_{OA}}{\partial K_H} + \frac{k_{S5}C_X}{C_X}C_HC_{v,X} \tag{G-95}$$

$$\frac{d}{dt}\left(\frac{\partial C_{OA}}{\partial K_F}\right) = g_{68} = \frac{k_{S5}K_hC_X}{C_X}\frac{\partial C_H}{\partial K_F}C_{v,X} - k_{S7}K_{OA}C_X\frac{\partial C_{OA}}{\partial K_F} \tag{G-96}$$

$$\frac{d}{dt}\left(\frac{\partial C_{OA}}{\partial K_{FA}}\right) = g_{69} = \frac{k_{S5}K_hC_X}{C_X}\frac{\partial C_H}{\partial K_{FA}}C_{v,X} - k_{S7}K_{OA}C_X\frac{\partial C_{OA}}{\partial K_{FA}} \tag{G-97}$$

$$\frac{d}{dt}\left(\frac{\partial C_{OA}}{\partial K_{OA}}\right) = g_{70} = \frac{k_{S5}K_hC_X}{C_X}\frac{\partial C_H}{\partial K_{OA}}C_{v,X} - k_{S7}K_{OA}C_X\frac{\partial C_{OA}}{\partial K_{OA}} - k_{S7}C_XC_{OA} \tag{G-98}$$

At $t = 0$, all $\partial C_i/\partial \boldsymbol{k} = 0$.

The variational equations (equations G-34 to G-98) of all components with respect to all rate constants and adsorption equilibrium constants are integrated simultaneously by the 4th order Runge-Kutta method. The integrated results are the profiles of $\partial C_G/\partial \boldsymbol{k}$, $\partial C_H/\partial \boldsymbol{k}$, $\partial C_F/\partial \boldsymbol{k}$, $\partial C_{FA}/\partial \boldsymbol{k}$, and $\partial C_{OA}/\partial \boldsymbol{k}$ which are needed to construct the Jacobian matrix of $\boldsymbol{A_G}$, $\boldsymbol{A_H}$, $\boldsymbol{A_F}$, $\boldsymbol{A_{FA}}$, and $\boldsymbol{A_{OA}}$.

The Jacobian matrix ($\boldsymbol{A_i}$) constructed with the elements of $\partial C_i/\partial \boldsymbol{k}$ profiles are described below. The Jacobian matrix of glucose ($\boldsymbol{A_G}$) is

$$A_G = \begin{bmatrix} \frac{\partial C_{G,1}}{\partial k_{S2}} & \frac{\partial C_{G,1}}{\partial k_{S1}} & \cdots & \frac{\partial C_{G,1}}{\partial K_{OA}} \\ \frac{\partial C_{G,2}}{\partial k_{S2}} & \frac{\partial C_{G,2}}{\partial k_{S1}} & \cdots & \frac{\partial C_{G,2}}{\partial K_{OA}} \\ \downarrow & \downarrow & \downarrow & \downarrow \\ \frac{\partial C_{G,n_G}}{\partial k_{S2}} & \frac{\partial C_{G,n_g}}{\partial k_{S1}} & \cdots & \frac{\partial C_{G,n_G}}{\partial K_{OA}} \end{bmatrix} \tag{G-99}$$

The Jacobian matrix of HMF (A_H) is

$$A_H = \begin{bmatrix} \frac{\partial C_{H,1}}{\partial k_{S2}} & \frac{\partial C_{H,1}}{\partial k_{S1}} & \cdots & \frac{\partial C_{H,1}}{\partial K_{OA}} \\ \frac{\partial C_{H,2}}{\partial k_{S2}} & \frac{\partial C_{H,2}}{\partial k_{S1}} & \cdots & \frac{\partial C_{H,2}}{\partial K_{OA}} \\ \downarrow & \downarrow & \downarrow & \downarrow \\ \frac{\partial C_{H,n_H}}{\partial k_{S2}} & \frac{\partial C_{H,n_H}}{\partial k_{S1}} & \cdots & \frac{\partial C_{H,n_H}}{\partial K_{OA}} \end{bmatrix} \tag{G-100}$$

The Jacobian matrix of fructose (A_F) is

$$A_F = \begin{bmatrix} \frac{\partial C_{F,1}}{\partial k_{S2}} & \frac{\partial C_{F,1}}{\partial k_{S1}} & \cdots & \frac{\partial C_{F,1}}{\partial K_{OA}} \\ \frac{\partial C_{F,2}}{\partial k_{S2}} & \frac{\partial C_{F,2}}{\partial k_{S1}} & \cdots & \frac{\partial C_{F,2}}{\partial K_{OA}} \\ \downarrow & \downarrow & \downarrow & \downarrow \\ \frac{\partial C_{F,n_F}}{\partial k_{S2}} & \frac{\partial C_{F,n_F}}{\partial k_{S1}} & \cdots & \frac{\partial C_{F,n_F}}{\partial K_{OA}} \end{bmatrix} \tag{G-101}$$

The Jacobian matrix of formic acid (A_{FA}) is

$$A_{FA} = \begin{bmatrix} \frac{\partial C_{FA,1}}{\partial k_{S2}} & \frac{\partial C_{FA,1}}{\partial k_{S1}} & \cdots & \frac{\partial C_{FA,1}}{\partial K_{OA}} \\ \frac{\partial C_{FA,2}}{\partial k_{S2}} & \frac{\partial C_{FA,2}}{\partial k_{S1}} & \cdots & \frac{\partial C_{FA,2}}{\partial K_{OA}} \\ \downarrow & \downarrow & \downarrow & \downarrow \\ \frac{\partial C_{FA,n_{FA}}}{\partial k_{S2}} & \frac{\partial C_{FA,n_{FA}}}{\partial k_{S1}} & \cdots & \frac{\partial C_{FA,n_{FA}}}{\partial K_{OA}} \end{bmatrix} \tag{G-102}$$

The Jacobian matrix of 4-oxpentanoic acid (A_{OA}) is

$$A_{OA} = \begin{bmatrix} \frac{\partial C_{OA,1}}{\partial k_{S2}} & \frac{\partial C_{OA,1}}{\partial k_{S1}} & \cdots & \frac{\partial C_{OA,1}}{\partial K_{OA}} \\ \frac{\partial C_{OA,2}}{\partial k_{S2}} & \frac{\partial C_{OA,2}}{\partial k_{S1}} & \cdots & \frac{\partial C_{OA,2}}{\partial K_{OA}} \\ \downarrow & \downarrow & \downarrow & \downarrow \\ \frac{\partial C_{OA,n_{OA}}}{\partial k_{S2}} & \frac{\partial C_{OA,n_{OA}}}{\partial k_{S1}} & \cdots & \frac{\partial C_{OA,n_{OA}}}{\partial K_{OA}} \end{bmatrix} \quad \text{(G-103)}$$

The Jacobian matrices of A_G, A_H, A_F, A_{FA}, and A_{OA} are used to calculate the correcting factor (Δk) in the equation G-31 according to the Marquardt method.

Numerical Solution of ODEs

The 4th order Runge-Kutta method is applied to the numerical integration of the model rate equations and variational equations. In each step of integration, the surface concentration of each components and the vacant acid site concentration are first calculated by

$$C_{G\cdot X,t} = K_G C_X C_{G,t} \quad \text{(G-104)}$$

$$C_{H\cdot X,t} = K_H C_X C_{H,t} \quad \text{(G-105)}$$

$$C_{F\cdot X,t} = K_F C_X C_{F,t} \quad \text{(G-106)}$$

$$C_{FA\cdot X,t} = K_{FA} C_X C_{FA,t} \quad \text{(G-107)}$$

$$C_{OA\cdot X,t} = K_{OA} C_X C_{OA,t} \quad \text{(G-108)}$$

and

$$C_{v,X,t} = C_X - C_{G\cdot X,t} - C_{H\cdot X,t} - C_{F\cdot X,t} - C_{FA\cdot X,t} - C_{OA\cdot X,t} \quad \text{(G-109)}$$

The values of K_i are estimated from the Marquardt method as described in the previous section. These values of $C_{i\cdot X,t}$ and $C_{v,X,t}$ are used in the integration process to obtain the values of C_i and $\partial C_i/\partial k$ for the next step. For example, the 4th order Runge-Kutta formula of the glucose rate equation is expressed as

$$C_{G\cdot X,t+\Delta t} = C_{G\cdot X,t} + 1/6(m_{1,G} + m_{2,G} + m_{3,G} + m_{4,G}) \quad \text{(G-110)}$$

$$C_{T,G,t+\Delta t} = C_{T,G,t} + 1/6(m_{1,G} + m_{2,G} + m_{3,G} + m_{4,G}) \quad \text{(G-111)}$$

where

$$m_{1,G} = \Delta t\, g_1(t, C_{G,t}, C_{H,t}, C_{F,t}, C_{FA,t}, C_{OA,t}, C_{v,X,t}, C_X) \quad \text{(G-112)}$$

$$m_{2,G} = \Delta t\, g_1(t + \Delta t/2, C_{G,t} + m_{1,G}/2, C_{H,t} + m_{1,H}/2, C_{F,t} + m_{1,F}/2, C_{FA,t} + m_{1,FA}/2, C_{OA,t} + m_{1,OA}/2, C_{v,X,t}, C_X) \quad \text{(G-113)}$$

$$m_{3,G} = \Delta t\, g_1(t + \Delta t/2, C_{G,t} + m_{2,G}/2, C_{H,t} + m_{2,H}/2, C_{F,t} + m_{2,F}/2, C_{FA,t} + m_{2,FA}/2, C_{OA,t} + m_{2,OA}/2, C_{v,X,t}, C_X) \quad \text{(G-114)}$$

$$m_{4,G} = \Delta t\, g_1(t + \Delta t, C_{G,t} + m_{3,G}, C_{H,t} + m_{3,H}, C_{F,t} + m_{3,F}, C_{FA,t} + m_{3,FA}, C_{OA,t} + m_{3,OA}, C_{v,X,t}, C_X) \quad \text{(G-115)}$$

The 4th order Runge-Kutta formulas for HMF, fructose, formic acid, and 4-oxopentanoic acid concentrations can be derived in similar manner.

The 4th order Runge-Kutta formula for the variational equation of glucose ($\partial C_G/\partial k_{S2}$) is expressed as

$$\left.\frac{\partial C_G}{\partial k_{S2}}\right|_{t+\Delta t} = \left.\frac{\partial C_G}{\partial k_{S2}}\right|_t + 1/6(m'_{1,G} + m'_{2,G} + m'_{3,G} + m'_{4,G}) \quad \text{(G-116)}$$

where

$$m'_{1,G} = \Delta t\, g_6(t, \left.\frac{\partial C_G}{\partial k_{S2}}\right|_t, \left.\frac{\partial C_H}{\partial k_{S2}}\right|_t, \left.\frac{\partial C_F}{\partial k_{S2}}\right|_t, \left.\frac{\partial C_{FA}}{\partial k_{S2}}\right|_t, \left.\frac{\partial C_{OA}}{\partial k_{S2}}\right|_t, C_{G,t}, C_{H,t}, C_{F,t}, C_{FA,t}, C_{OA,t}, C_{v,X,t}, C_X) \quad \text{(G-117)}$$

$$m'_{2,G} = \Delta t\, g_6(t + \Delta t/2, \left.\frac{\partial C_G}{\partial k_{S2}}\right|_t + m'_{1,G}/2, \left.\frac{\partial C_H}{\partial k_{S2}}\right|_t + m'_{1,H}/2, \left.\frac{\partial C_F}{\partial k_{S2}}\right|_t + m'_{1,F}/2, \left.\frac{\partial C_{FA}}{\partial k_{S2}}\right|_t + m'_{1,FA}/2, \left.\frac{\partial C_{OA}}{\partial k_{S2}}\right|_t + m'_{1,OA}/2, C_{G,t} + m'_{1,G}/2, C_{H,t} + m'_{1,H}/2, C_{F,t} + m'_{1,F}/2, C_{FA,t} + m'_{1,FA}/2, C_{OA,t} + m'_{1,OA}/2, C_{v,X,t}, C_X) \quad \text{(G-118)}$$

$$m'_{3,G} = \Delta t\, g_6(t + \Delta t/2, \left.\frac{\partial C_G}{\partial k_{S2}}\right|_t + m'_{2,G}/2, \left.\frac{\partial C_H}{\partial k_{S2}}\right|_t + m'_{2,H}/2, \left.\frac{\partial C_F}{\partial k_{S2}}\right|_t + m'_{2,F}/2, \left.\frac{\partial C_{FA}}{\partial k_{S2}}\right|_t + m'_{2,FA}/2, \left.\frac{\partial C_{OA}}{\partial k_{S2}}\right|_t + m'_{2,OA}/2, C_{G,t} + m'_{2,G}/2, C_{H,t} + m'_{2,H}/2, C_{F,t} + m'_{2,F}/2, C_{FA,t} + m'_{2,FA}/2, C_{OA,t} + m'_{2,OA}/2, C_{v,X,t}, C_X) \quad \text{(G-119)}$$

$$m'_{4,G} = \Delta t\, g_6(t + \Delta t, \left.\frac{\partial C_G}{\partial k_{S2}}\right|_t + m'_{3,G}, \left.\frac{\partial C_H}{\partial k_{S2}}\right|_t + m'_{3,H}, \left.\frac{\partial C_F}{\partial k_{S2}}\right|_t + m'_{3,F},$$

$$\left.\frac{\partial C_{FA}}{\partial k_{S2}}\right|_t + m'_{3,FA}, \left.\frac{\partial C_{OA}}{\partial k_{S2}}\right|_t + m'_{3,OA}, C_{G,t} + m_{3,G}, C_{H,t} + m_{3,H}, C_{F,t}$$

$$+ m_{3,F}, C_{FA,t} + m_{3,FA}, C_{OA,t} + m_{3,OA}, C_{v,X,t}, C_X) \qquad \text{(G-120)}$$

Total coke formation (the sum of $C_{R,H}$, $C_{R,FA}$, and $C_{R,OA}$) is also predicted from the rate equations G-6 to G-8 using the 4th order Runge-Kutta method. The example of the example of 4th order Runge-Kutta formula of $C_{R,H}$ is given by

$$C_{R,H,t+\Delta t} = C_{R,H,t} + 1/6(m_{1,R,H} + m_{2,R,H} + m_{3,R,H} + m_{4,R,H}) \qquad \text{(G-121)}$$

where

$$m_{1,R,H} = \Delta t\, g_{R,1}(t, C_{G,t}, C_{H,t}, C_{F,t}, C_{FA,t}, C_{OA,t}, C_{v,X,t}, C_X) \qquad \text{(G-122)}$$

$$m_{2,R,G} = \Delta t\, g_{R,1}(t + \Delta t/2, C_{G,t} + m_{1,R,G}/2, C_{H,t} + m_{1,R,H}/2, C_{F,t} + m_{1,R,F}/2,$$

$$C_{FA,t} + m_{1,R,FA}/2, C_{OA,t} + m_{1,R,OA}/2, C_{v,X,t}, C_X) \qquad \text{(G-123)}$$

$$m_{3,R,G} = \Delta t\, g_{R,1}(t + \Delta t/2, C_{G,t} + m_{2,R,G}/2, C_{H,t} + m_{2,R,H}/2, C_{F,t} + m_{2,R,F}/2,$$

$$C_{FA,t} + m_{2,R,FA}/2, C_{OA,t} + m_{2,R,OA}/2, C_{v,X,t}, C_X) \qquad \text{(G-124)}$$

$$m_{4,R,G} = \Delta t\, g_{R,1}(t + \Delta t, C_{G,t} + m_{3,R,G}, C_{H,t} + m_{3,R,H}, C_{F,t} + m_{3,R,F},$$

$$C_{FA,t} + m_{3,R,FA}, C_{OA,t} + m_{3,R,OA}, C_{v,X,t}, C_X) \qquad \text{(G-125)}$$

After the integration, the liquid phase concentration of 5 components are calculated by

$$C_{G,t+\Delta t} = C_{T,G,t+\Delta t} - C_{G\cdot X,t+\Delta t} \qquad \text{(G-126)}$$

$$C_{H,t+\Delta t} = C_{T,H,t+\Delta t} - C_{H\cdot X,t+\Delta t} \qquad \text{(G-127)}$$

$$C_{F,t+\Delta t} = C_{T,F,t+\Delta t} - C_{F\cdot X,t+\Delta t} \qquad \text{(G-128)}$$

$$C_{FA,t+\Delta t} = C_{T,FA,t+\Delta t} - C_{FA\cdot X,t+\Delta t} \qquad \text{(G-129)}$$

$$C_{OA,t+\Delta t} = C_{T,OA,t+\Delta t} - C_{OA\cdot X,t+\Delta t} \qquad \text{(G-130)}$$

These liquid phase concentrations are used in the calculation of surface concentrations and the vacant acid site concentration in the next step by equations G-104 to G-109.

The integration described above are iteratively repeated until the calculation at the final reaction time (t_f) obtained. The liquid phase concentration of each component ($C_{i,l}$)

will be compared with the experimental data ($C^*_{i,l}$) at the same reaction time according to the non-linear regression analysis using Marquardt method. The profiles of $\partial C_G/\partial \boldsymbol{k}$, $\partial C_H/\partial \boldsymbol{k}$, $\partial C_F/\partial \boldsymbol{k}$, $\partial C_{FA}/\partial \boldsymbol{k}$, and $\partial C_{OA}/\partial \boldsymbol{k}$ will also be used in the Jacobian matrix of $\boldsymbol{A_G}$, $\boldsymbol{A_H}$, $\boldsymbol{A_F}$, $\boldsymbol{A_{FA}}$, and $\boldsymbol{A_{OA}}$ (equations G-99 to G-103) required by the Marquardt method.

Method of Calculation

The Non-Linear Regression program (NLR) has been developed by Constantinides (1987) to fit mathematical models to multiresponse data in order to determine a number of unknown parameters. The Marquardt algorithm, which utilizes an interpolation technique to combine the Gauss-Newton and steepest-descent methods, is used in this program. The integration subroutine and the input subroutine have been modified to perform the calculation of surface concentration and liquid phase concentration as described previously.

Program Requirement

The entire program is written in the FORTRAN source code which is complied and run under the DOS/Windows operating system. The NLR program is responsible for calling upon the subroutines as needed. The NLR program is menu driven for data input and adjustment. All data are in the files with extension *.DAT. The rate equations and variational equations are the subroutine EQU in the file RATE_EQ1.FOR. The rate equations for surface concentration of all five components and coke, and adsorption equilibrium equations are the subroutine EQUD and EQUI respectively in the file EQUD.FOR. When the new model is used, the model subroutines in both source code files need to be complied and linked to the NLR program.

Program Input

The model and variational equations in subroutine EQU must strictly be in the form of

$$G(i) = f[X, Y(1), Y(2), ..., Y(n), B(1), B(2), ..., CK, CV] \qquad \text{(G-131)}$$

For example, the rate equation of glucose, g_1 (equation G-1) will be

G(1) = -B(1)B(9)CKY(1) - B(2)(B(9)CKY(1) - B(3)B(11)CKY(3)) (G-132)

and the variational of glucose with respect to k_{S2}, g_6 (equation G-34) will be

G(6) = -B(1)B(9)CKY(6) - B(2)B(9)CKY(6) + B(2)B(3)B(11)CKY(32)
- B(9)CKY(1) (G-133)

where

G( ) = derivative of dC_i/dt or $d/dt(\partial C_i/\partial k_j)$

X = time (t)

Y(i) = liquid phase concentration (C_i) or $\partial C_i/\partial k_j$

f[ ] = function to be integrated (g_i)

B( ) = parameter to be determined (k_j and K_i)

CK = acid site concentration (C_X)

CV = vacant acid site concentration ($C_{v,X}$)

The rate equations of all five components and coke formation in subroutine EQUD must be in the form of

GS(i) = f[X, Y(1), Y(2), ..., Y(n), B(1), B(2), ..., CK, CV] (G-134)

and the adsorption equilibrium equations in subroutine EQUI must be in the form of

YS(i) = YB(i)B(j)CVK (G-135)

where

GS( ) = derivative of dC_i/dt

YS( ) = surface concentration ($C_{i,X}$)

YB( ) = liquid phase concentration (C_i)

CVK = acid site concentration (C_X)

The completed lists and descriptions of all variables used in the model equation subroutines are provided in Table G-1 and G-2. The completed source code of the model equation subroutines are also provided in the Equation Subroutine section.

The following items need to be completed before performing the non-linear regression:

1. Total number of dependent variables: number of components
2. Number of variables being fitted to data: number of components being fitted
3. Total number of parameters being estimated: total number of k_j and K_i

4. Number of differential equations (model and variational)
5. Initial value of independent variable: initial reaction time
6. Final value of independent variable: final reaction time
7. Number of integration steps
8. Number of locations of the independent variable at which experimental points can exist: number of points for presenting integration result
9. Number of integration steps per experimental point: number of integration steps/number of locations
10. Maximum number of experimental points for any location: number of repeated experiment for each component at each reaction time
11. Number of rate equations of bulk components and coke formation
12. The effect of coke-blocked sites: program can account for the acid sites decreased by coke blocking, the ratio of blocking must be provided.
13. Coke formation as surface reaction: program can account the coke formation as the surface reaction resulting in the decreased vacant site concentration.
14. Active site concentration: total acid site concentration
15. Maximum number of iterations for NLR search
16. NONEG: 0 = allow negative parameters, 1 = set negative parameters to zero
17. NORMAL: 0 = regular sum of square, 1 = normalized sum of square
18. Normalize the increment of parameters: yes or no
19. Marquardt constants: SIGZR, ALFA, and BETA
20. NLR convergence constant: *CONV* and *EPS*
21. Initial conditions of model rate equations and variational equations
22. Initial guess values of estimated parameters k_j and K_i

All of the above items are stored in the ASCII file with extension *.CON which can be adjusted independently.

According to the Marquardt method, SIGZR is the initial value of α in equation (G-31). ALFA is the factor by which α is multiplied, or divided, in order to adjust the direction of parameter correction vector. BETA is the factor by which the size of the correction vector is multiplied when the value of α is greater than 1.

The experimental data file can be created independently as an ASCII file with extension *.DAT. The format example of the experimental data input, including variance of each component, time, concentration of each component, and weight of each data point, is shown in the Example of Experimental Data File.

Weighting Factor and Variance Input

The variance (σ^2_i) of experimental data is used in equation G-27 to calculate the weighting factor (w_i) to determine the unbiased weighted sum of squared residuals. The program automatically calculated the variance of each component if the repeated experimental data are available. The input value of variance of each component is simply unity. In case of non-repeated data, the regression can be performed using $\sigma^2_i = 1$ as the first guess. The program generates the estimated variance of each component at the end of analysis. The regression analysis must be repeated using these new estimated variances. The trial-and-error procedure has to be repeated until the good fit is accomplished.

Convergence Criteria

The search in non-linear regression converges if the following equation is satisfied

$$\frac{|SSR_{I-1} - SSR_I|}{SSR_I} < CONV \qquad \text{(G-136)}$$

where

SSR_I = the sum of squared residuals at iteration "I"

$CONV$ = convergence constant

The search also converges if the increment of all parameters satisfy the following equation

$$\left|\frac{\Delta k_{Sj}}{k_{Sj}}\right|, \left|\frac{\Delta K_i}{K_i}\right| < CONV \qquad \text{(G-137)}$$

If the k_{sj} or K_i is equal to zero, the following equation will be used

$$|\Delta k_{Sj}|, |\Delta K_i| < CONV \qquad \text{(G-138)}$$

In the case of *SSR* is zero, *EPS* is an absolute convergence criteria used to eliminate difficulties arising from the overflows. The search converges if the following equation is satisfied

$$SSR_l \leq EPS \tag{G-139}$$

Statistical Analysis

The NLR program also provides a set of four statistical analyses.

1. A linear 95% confidence interval is calculated and a t-test of each parameter is also performed to check if the parameter is significantly different from zero.
2. The correlation matrix of parameters is calculated and the matrix components are tested at the 95% and 99% significance levels to determine the extent of correlation between the parameters.
3. The null hypotheses that the residuals are randomly distributed are tested to ensure the random distribution of deviations between experimental and predicted values
4. Analysis of variance is performed. In case of a repeated experiment, the F-test is applied on the ratio of residual variance to the experimental data variance to determine if more scatter exists than can be explained by experimental error.

Description of NLR Program

The non-linear regression program consists of NLR.FOR as the main program and subroutine programs, JSRKB1.FOR as the integration subroutine, two equation subroutine files, two input files, and three output files.

NLR.FOR

The main program calls all other subroutine programs and performs the non-linear regression analysis.

Subroutine	*Description*
INPUT	input menu, controls the INDATA and INEQU subroutines
INDATA	creates the regression constants and experimental data files
INEQU	to enter the model equations and variational equations
NLR12V	performs the non-linear regression using the Marquardt method, and call other subroutine necessary to the calculation
DATIN	determines the variance of experimental data and the weighting factor
RUNS	performs a two side test at 0.05 significance level
SUMS	calculates the residuals between experimental data and predicted points, and the weighted sum of squared residuals
PHPLA	a matrix inversion routine to determine the inverse of the A^TA matrix
GJLNB	uses the Gauss-Jordan reduction method to obtain the parameter increment vector
SA12V	performs a series of statistical analysis on estimated parameters: - combined residual variance of the data - standard errors and covariances of the parameters - 95% confidence limits of the parameters using the student t-distribution, and significance tests
COMPAR	compares the variance due to the lack-of-fit with the variance due to experimental error, and performs the F-test
FTABL	performs a linear interpolation to determine the distribution coefficients

MUS	calculates the residuals between the group means of the experimental data and the predicted curve
OUTPUT	prints tables of experimental and predicted data, performs the integration with existed parameters, and draws graphs of experimental and predicted data

JSRKB1.FOR

The completed lists and descriptions of all variables used in the JSRKB subroutines are provided in Table G-3.

Subroutine	*Description*
JSRKB	the modified 4th order Runge-Kutta method of integration for liquid phase and surface concentration, and variational equations

RATE_EQ1.FOR

Subroutine	*Description*
EQU	rate equations of liquid phase components and variational equations

EQUD.FOR

Subroutine	*Description*
EQUD	rate equations of liquid phase components and coke formation
EQUI	adsorption equilibrium equations

Other Files

Extension	*Description*
*.CON	constants, regression parameters, initial conditions, and initial guess values
*.DAT	experimental data and weights
*.OUT	calculated profiles of dependent variables
*.PAR	estimated parameters from non-linear regression analysis
*.REP	reintegrated profiles of dependent variables

Table G-1. List of variables for rate equations, variational equations, and adsorption equilibrium equations.

Variable	Program Variable	Variable	Program Variable
k_{S1}	B(2)	C_F	Y(3), YB(3)
k_{S2}	B(1)	C_{FA}	Y(4), YB(4)
$1/K_{S1}$	B(3)	C_{OA}	Y(5), YB(5)
k_{S3}	B(4)	$C_{G\cdot X}$	YS(1)
k_{S4}	B(5)	$C_{H\cdot X}$	YS(2)
k_{S5}/C_X	B(6)	$C_{F\cdot X}$	YS(3)
k_{S6}	B(7)	$C_{FA\cdot X}$	YS(4)
k_{S7}	B(8)	$C_{OA\cdot X}$	YS(5)
K_G	B(9)	dC_G/dt	G(1), GS(1)
K_H	B(10)	dC_H/dt	G(2), GS(2)
K_F	B(11)	dC_F/dt	G(3), GS(3)
K_{FA}	B(12)	dC_{FA}/dt	G(4), GS(4)
K_{OA}	B(13)	dC_{OA}/dt	G(5), GS(5)
C_X	CK, CVK	$dC_{R,H}/dt$	GS(6)
$C_{v,X}$	CV	$dC_{R,FA}/dt$	GS(7)
C_G	Y(1), YB(1)	$dC_{R,OA}/dt$	GS(8)
C_H	Y(2), YB(2)		

Table G-2. List of variables for variational equations.

$\frac{d}{dt}\left(\frac{\partial C_i}{\partial k_j}\right)$	C_G	C_H	C_F	C_{FA}	C_{OA}
k_{S1}	G(6)	G(19)	G(32)	G(45)	G(58)
k_{S2}	G(7)	G(20)	G(33)	G(46)	G(59)
$1/K_{S1}$	G(8)	G(21)	G(34)	G(47)	G(60)
k_{S3}	G(9)	G(22)	G(35)	G(48)	G(61)
k_{S4}	G(10)	G(23)	G(36)	G(49)	G(62)
k_{S5}/C_X	G(11)	G(24)	G(37)	G(50)	G(63)
k_{S6}	G(12)	G(25)	G(38)	G(51)	G(64)
k_{S7}	G(13)	G(26)	G(39)	G(52)	G(65)
K_G	G(14)	G(27)	G(40)	G(53)	G(66)
K_H	G(15)	G(28)	G(41)	G(54)	G(67)
K_F	G(16)	G(29)	G(42)	G(55)	G(68)
K_{FA}	G(17)	G(30)	G(43)	G(56)	G(69)
K_{OA}	G(18)	G(31)	G(44)	G(57)	G(70)

Table G-3. List of variables in subroutine JSRKB.

Variable	*Variable in Program*	*Description*
	A( )	vector of time and predicted concentration of all five components
	AA(,)	matrix of time and predicted concentration of all five components
	AS(,)	matrix of time and predicted surface concentration of all five components and coke formation
$m_{1,i}$, $m'_{1,i}$	AK1( )	parameter # 1 used in the Runge-Kutta method
$m_{2,i}$, $m'_{2,i}$	AK2( )	parameter # 2 used in the Runge-Kutta method
$m_{3,i}$, $m'_{3,i}$	AK3( )	parameter # 3 used in the Runge-Kutta method
$m_{4,i}$, $m'_{4,i}$	AK4( )	parameter # 4 used in the Runge-Kutta method
k_{Sj}, K_i	B( )	model parameters: rate and adsorption equilibrium constants
C_X	CM	acid site concentration
Δt	DX	increment of time
$m_{1,i}$, $m_{1R,i}$	G1( )	parameter # 1 used in the Runge-Kutta method for surface concentration and coke formation
$m_{2,i}$, $m_{2R,i}$	G2( )	parameter # 2 used in the Runge-Kutta method for surface concentration and coke formation
$m_{3,i}$, $m_{3R,i}$	G3( )	parameter # 3 used in the Runge-Kutta method for surface concentration and coke formation
$m_{4,i}$, $m_{4R,i}$	G4( )	parameter # 4 used in the Runge-Kutta method for surface concentration and coke formation
	IQQ	flag parameter for considering coke-blocked acid sites
	IQT	flag parameter for considering coke formation as surface reaction
	LINT	intergration step/number of existing point (LL/NX1)
	LL	number of intergration step

Table G-3. List of variables in subroutine JSRKB (Continued).

Variable	*Variable in Program*	*Description*
	N1	number of all component and coke from all species
	NEQ	number of rate equation and variational equation
	NP	number of model parameter being estimated
	NPOINT	number of repeated experimental point at each reaction time
h	NVF	number of component (dependent variable) being fitted
n_i	NX1	number of existing points for presenting integration result
	RS( )	ratio of coke deposit blocking acid sites (not used)
t_0	XZR	initial value of reaction time
$C_{i\cdot X,t}$, $\left.\frac{\partial C_i}{\partial k_{Sj}}\right\|_t$	YM( )	surface concentration and $\partial C_i/\partial k$ at the beginning of each integration step
$C_{i,t+\Delta t}$, $\left.\frac{\partial C_G}{\partial k_{S2}}\right\|_{t+\Delta t_t}$	YMB( )	liquid phase concentration and $\partial C_i/\partial k$ at the end of each integration step
$C_{i\cdot X,t+\Delta t}$	YMP( )	surface concentration at the end of each integration step
$C_{T,G,t}$	YMT( )	total concentration at the beginning of each integration step
$C_{T,G,t+\Delta t}$	YMPT( )	total concentration at the end of each integration step
$C_{i\cdot X,t}$, $C_{R,i,t}$	YS( )	surface concentration and coke formation at the beginning of each integration step
$C_{i\cdot X,t+\Delta t}$, $C_{R,i,t+\Delta t}$	YS1( )	surface concentration and coke formationat at the end of each integration step
t_f	YZR	final value of reaction time

Program Source Code for the Modified 4th Order Runge-Kutta Method (JSRKB)

```
      SUBROUTINE JSRKB(B,DX,XZR,YZR,RS)
C
C  JSRKB USES STANDARD FOURTH ORDER RUNGE-KUTTA METHOD TO INTEGRATE
C  NEQ SIMULTANEOUS DIFFERENTIAL EQUATIONS.
C     NEQ= NUMBER OF DIFFERENTIAL EQUATIONS
C     LL = NUMBER OF VALUES OF THE INDEPENDENT VARIABLE X
C     A = VECTOR CONTAINING: INDEPENDENT VARIABLE, FIRST DEPENDENT
C     VARIABLE,SECOND DEPENDENT VARIABLE,.....,NEQTH DEPENDENT VARIABLE
C     DX = INCREMENT IN X
C     XZR = INITIAL VALUE OF X
C     YZR = VECTOR OF NEQ INITIAL VALUES OF THE DEPENDENT VARIABLES.
C  SUBROUTINE JSRK CALLS ON SUBROUTINE EQU(NEQ,X,Y,G), WHERE
C     NEQ = NUMBER OF EQUATIONS
C     X = VALUE OF THE DEPENDENT VARIABLE
C     Y = AN NEQ-LONG VECTOR OF VALUES OF THE INDEPENDENT VARIABLES
C     G = AN NEQ-LONG VECTOR OF VALUES OF THE RIGHT HAND SIDE OF THE
C                    GIVEN DIFFERENTIAL EQUATIONS.
C  EQU IS CREATED BY THE NLR PROGRAM WHEN THE EQUATIONS ARE ENTERED
C  EQU HAS DIMENSION Y(*),G(*),B(*)
      DIMENSION AK1(100),AK2(100),AK3(100),AK4(100),YM(100),
     1 YMP(100),G1(100),G2(100),G3(100),G4(100),YS(100),YMB(100),
     1 YMT(100),YMPT(100),YS1(100)
      DIMENSION B(*), YZR(*), RS(*)
      COMMON/ONE/NV,NVF,NP,NPOINT,LL,NX1,LINT,NEQ,NEQP,MTYPE
      COMMON/SIX/N1,IQQ,IQT,CM
      COMMON/SEVEN/A(200000),AA(0:2000,0:10),AS(0:2000,0:10)
      IF(NEQ.GT.500) WRITE(6,118)
      IF(NEQ.GT.500) STOP
118   FORMAT(//,' DIMENSIONS IN JSRKB  EXCEEDED',/' THE NUMBER OF
     1 EQUATIONS TO BE INTEGRATED MUST NOT EXCEED 1000',// )
      NEQP=NEQ+1
      DO 80 L=1,LL
      DO 80 K=1,NEQP
      NPOS= (K-1)*LL + L
      A(NPOS)=0.0
80    CONTINUE
      A(1)=XZR
      AA(1,0) = XZR
      AS(1,0) = XZR
C  EVALUATE DIFFERENTIAL EQUATIONS
      DXD=DX/2.0
      DXDD=DX/6.0
      DO 50 K=1,NEQ
      NPOS= K*LL + 1
      A(NPOS)=YZR(K)
50    CONTINUE
      DO 5 K=1,NV
      YMP(K) = 0.0
      YMPT(K) = YZR(K)
      AA(1,K)=YZR(K)
5     CONTINUE
      DO 555 K=1,N1
      YS(K) = 0.0
      AS(1,K) = 0.0
555   CONTINUE
      DO 100 L=1,LL-1
```

```
      DO 15 K=1,NVF
15    YMB(K) = YMPT(K)-YMP(K)
      CVK = CM
      IF(N1-NVF.LE.0) GOTO 5025
      IF(IQQ.EQ.2) GOTO 5025
      DO 5020 K8=NVF+1,N1
5020  CVK = CVK - RS(K8)*YS(K8)
5025  CALL EQUI(YS,YMB,B,CVK)
      CV =  CVK
      IF(IQT.EQ.2) THEN
      NR = NVF
      ELSE
      NR = N1
      ENDIF
      DO 5030 K9=1,NR
5030  CV = CV - YS(K9)
      XM=A(L)
      DO 3 K = 1,NVF
      YM(K) = YS(K)
      YMT(K) = YMPT(K)
3     CONTINUE
      DO 2 K = NVF+1,NEQ
      NPOS= K*LL + (L)
      YM(K)=A(NPOS)
      YMB(K)=A(NPOS)
2     CONTINUE
      DO 5060 K=1,N1
5060  YS1(K) = YS(K)
      CALL EQU(NEQ,XM,YMB,AK1,B,CV,CVK)
      CALL EQUD(G1,YMB,B,XM,CV,CVK)
      XMP=XM+DXD
      DO 224 K=1,NVF
      YMP(K)=YM(K)+DXD*AK1(K)
      YMPT(K)=YMT(K)+DXD*AK1(K)
      YMB(K)=YMPT(K)-YMP(K)
224   CONTINUE
      DO 4 K=NVF+1,NEQ
      YMB(K)=YM(K)+DXD*AK1(K)
4     CONTINUE
      DO 5090 K3 = 1, N1
      YS(K3) = YS1(K3) + DXD * G1(K3)
5090  CONTINUE
      CALL EQU(NEQ,XMP,YMB,AK2,B,CV,CVK)
      CALL EQUD(G2,YMB,B,XMP,CV,CVK)
      DO 236 K=1,NVF
      YMP(K)=YM(K)+DXD*AK2(K)
      YMPT(K)=YMT(K)+DXD*AK2(K)
      YMB(K)=YMPT(K)-YMP(K)
236   CONTINUE
      DO 6 K=NVF+1,NEQ
      YMB(K)=YM(K)+DXD*AK2(K)
6     CONTINUE
      DO 5130 K4 = 1, N1
      YS(K4) = YS1(K4) + DXD * G2(K4)
5130  CONTINUE
      CALL EQU(NEQ,XMP,YMB,AK3,B,CV,CVK)
      CALL EQUD(G3,YMB,B,XMP,CV,CVK)
      XMP=XM+DX
      DO 248 K=1,NVF
      YMP(K)=YM(K)+DX*AK3(K)
```

```
      YMPT(K)=YMT(K)+DX*AK3(K)
      YMB(K)=YMPT(K)-YMP(K)
248   CONTINUE
      DO 8 K=NVF+1,NEQ
      YMB(K)=YM(K)+DX*AK3(K)
8     CONTINUE
      DO 5170 K5 = 1, N1
      YS(K5) = YS1(K5) + DX * G3(K5)
5170  CONTINUE
      CALL EQU(NEQ,XMP,YMB,AK4,B,CV,CVK)
      CALL EQUD(G4,YMB,B,XMP,CV,CVK)
      A(L+1)=XMP
      DO 20 K=1,NVF
      YMP(K)=YM(K)+DXDD*(AK1(K)+AK4(K)+2.0*(AK2(K)+AK3(K)))
      YMPT(K)=YMT(K)+DXDD*(AK1(K)+AK4(K)+2.0*(AK2(K)+AK3(K)))
      NPOS = K*LL + (L)
      A(NPOS+1) = YMPT(K) - YMP(K)
      AA(L+1,K) = A(NPOS+1)
20    CONTINUE
      AA(L+1,0) = XMP
      DO 10 K=NVF+1,NEQ
      NPOS= K*LL + (L)
      A(NPOS+1)=A(NPOS)+DXDD*(AK1(K)+AK4(K)+2.0*(AK2(K)+AK3(K)))
10    CONTINUE
      DO 5230 K6 = 1, N1
      YS(K6) = YS1(K6)+DXDD*(G1(K6)+G4(K6)+2.0*(G2(K6)+G3(K6)))
      AS(L+1,K6) = YS(K6)
5230  CONTINUE
      AS(L+1,0) = XMP
C
100   CONTINUE
      RETURN
      END
```

Equation Subroutines

RATE_EQ1.FOR

```
      SUBROUTINE EQU(NEQ,X,Y,G,B,CV,CK)
      DIMENSION Y(*),G(*),B(*)
C     13 constant variable
      G(1)=-B(1)*B(9)*CK*Y(1)-B(2)*(B(9)*CK*Y(1)-B(3)*B(11)*CK*Y(3))
      G(2)=B(1)*B(9)*CK*Y(1)+B(4)*B(11)*CK*Y(3)-B(5)*B(10)*CK*Y(2)-
     1 B(6)*B(10)*CK*Y(2)*CV
      G(3)=-B(4)*B(11)*CK*Y(3)+B(2)*(B(9)*CK*Y(1)-B(3)*B(11)*CK*Y(3))
      G(4)=B(6)*B(10)*CK*Y(2)*CV-B(7)*B(12)*CK*Y(4)
      G(5)=B(6)*B(10)*CK*Y(2)*CV-B(8)*B(13)*CK*Y(5)
      G(6)=-B(1)*B(9)*CK*Y(6)-B(2)*B(9)*CK*Y(6)+B(2)*B(3)*B(11)*
     1 CK*Y(32)-B(9)*CK*Y(1)
      G(7)=-B(1)*B(9)*CK*Y(7)-B(2)*B(9)*CK*Y(7)+B(2)*B(3)*B(11)*
     1 CK*Y(33)-B(9)*CK*Y(1)+B(3)*B(11)*CK*Y(3)
      G(8)=-B(1)*B(9)*CK*Y(8)-B(2)*B(9)*CK*Y(8)+B(2)*B(3)*B(11)*
     1 CK*Y(34)+B(2)*B(11)*CK*Y(3)
      G(9)=-B(1)*B(9)*CK*Y(9)-B(2)*B(9)*CK*Y(9)+B(2)*B(3)*B(11)*
     1 CK*Y(35)
      G(10)=-B(1)*B(9)*CK*Y(10)-B(2)*B(9)*CK*Y(10)+B(2)*B(3)*B(11)*
     1 CK*Y(36)
      G(11)=-B(1)*B(9)*CK*Y(11)-B(2)*B(9)*CK*Y(11)+B(2)*B(3)*B(11)*
     1 CK*Y(37)
      G(12)=-B(1)*B(9)*CK*Y(12)-B(2)*B(9)*CK*Y(12)+B(2)*B(3)*B(11)*
     1 CK*Y(38)
      G(13)=-B(1)*B(9)*CK*Y(13)-B(2)*B(9)*CK*Y(13)+B(2)*B(3)*B(11)*
     1 CK*Y(39)
      G(14)=-B(1)*B(9)*CK*Y(14)-B(2)*B(9)*CK*Y(14)+B(2)*B(3)*B(11)*
     1 CK*Y(40)-B(1)*CK*Y(1)-B(2)*CK*Y(1)
      G(15)=-B(1)*B(9)*CK*Y(15)-B(2)*B(9)*CK*Y(15)+B(2)*B(3)*B(11)*
     1 CK*Y(41)
      G(16)=-B(1)*B(9)*CK*Y(16)-B(2)*B(9)*CK*Y(16)+B(2)*B(3)*B(11)*
     1 CK*Y(42)+B(2)*B(3)*CK*Y(3)
      G(17)=-B(1)*B(9)*CK*Y(17)-B(2)*B(9)*CK*Y(17)+B(2)*B(3)*B(11)*
     1 CK*Y(43)
      G(18)=-B(1)*B(9)*CK*Y(18)-B(2)*B(9)*CK*Y(18)+B(2)*B(3)*B(11)*
     1 CK*Y(44)

      G(19)=B(1)*B(9)*CK*Y(6)+B(4)*B(11)*CK*Y(32)-B(5)*B(10)*CK*Y(19)
     1 -B(6)*B(10)*CK*Y(19)*CV+B(9)*CK*Y(1)
      G(20)=B(1)*B(9)*CK*Y(7)+B(4)*B(11)*CK*Y(33)-B(5)*B(10)*CK*Y(20)
     1 -B(6)*B(10)*CK*Y(20)*CV
      G(21)=B(1)*B(9)*CK*Y(8)+B(4)*B(11)*CK*Y(34)-B(5)*B(10)*CK*Y(21)
     1 -B(6)*B(10)*CK*Y(21)*CV
      G(22)=B(1)*B(9)*CK*Y(9)+B(4)*B(11)*CK*Y(35)-B(5)*B(10)*CK*Y(22)
     1 -B(6)*B(10)*CK*Y(22)*CV+B(11)*CK*Y(3)
      G(23)=B(1)*B(9)*CK*Y(10)+B(4)*B(11)*CK*Y(36)-B(5)*B(10)*CK*Y(23)
     1 -B(6)*B(10)*CK*Y(23)*CV-B(10)*CK*Y(2)
      G(24)=B(1)*B(9)*CK*Y(11)+B(4)*B(11)*CK*Y(37)-B(5)*B(10)*CK*Y(24)
     1 -B(6)*B(10)*CK*Y(24)*CV-B(10)*CK*Y(2)*CV
      G(25)=B(1)*B(9)*CK*Y(12)+B(4)*B(11)*CK*Y(38)-B(5)*B(10)*CK*Y(25)
     1 -B(6)*B(10)*CK*Y(25)*CV
      G(26)=B(1)*B(9)*CK*Y(13)+B(4)*B(11)*CK*Y(39)-B(5)*B(10)*CK*Y(26)
     1 -B(6)*B(10)*CK*Y(26)*CV
      G(27)=B(1)*B(9)*CK*Y(14)+B(4)*B(11)*CK*Y(40)-B(5)*B(10)*CK*Y(27)
     1 -B(6)*B(10)*CK*Y(27)*CV+B(1)*CK*Y(1)
```

```
      G(28)=B(1)*B(9)*CK*Y(15)+B(4)*B(11)*CK*Y(41)-B(5)*B(10)*CK*Y(28)
     1 -B(6)*B(10)*CK*Y(28)*CV-B(5)*CK*Y(2)-B(6)*CK*Y(2)*CV
      G(29)=B(1)*B(9)*CK*Y(16)+B(4)*B(11)*CK*Y(42)-B(5)*B(10)*CK*Y(29)
     1 -B(6)*B(10)*CK*Y(29)*CV+B(4)*CK*Y(3)
      G(30)=B(1)*B(9)*CK*Y(17)+B(4)*B(11)*CK*Y(43)-B(5)*B(10)*CK*Y(30)
     1 -B(6)*B(10)*CK*Y(30)*CV
      G(31)=B(1)*B(9)*CK*Y(18)+B(4)*B(11)*CK*Y(44)-B(5)*B(10)*CK*Y(31)
     1 -B(6)*B(10)*CK*Y(31)*CV

      G(32)=(-B(4)*B(11)*CK*Y(32))+B(2)*B(9)*CK*Y(6)-
     1 B(2)*B(3)*B(11)*CK*Y(32)
      G(33)=(-B(4)*B(11)*CK*Y(33))+B(2)*B(9)*CK*Y(7)-
     1 B(2)*B(3)*B(11)*CK*Y(33)+B(9)*CK*Y(1)-B(3)*B(11)*CK*Y(3)
      G(34)=(-B(4)*B(11)*CK*Y(34))+B(2)*B(9)*CK*Y(8)-
     1 B(2)*B(3)*B(11)*CK*Y(34)-B(2)*B(11)*CK*Y(3)
      G(35)=(-B(4)*B(11)*CK*Y(35))+B(2)*B(9)*CK*Y(9)-
     1 B(2)*B(3)*B(11)*CK*Y(35)-B(11)*CK*Y(3)
      G(36)=(-B(4)*B(11)*CK*Y(36))+B(2)*B(9)*CK*Y(10)-
     1 B(2)*B(3)*B(11)*CK*Y(36)
      G(37)=(-B(4)*B(11)*CK*Y(37))+B(2)*B(9)*CK*Y(11)-
     1 B(2)*B(3)*B(11)*CK*Y(37)
      G(38)=(-B(4)*B(11)*CK*Y(38))+B(2)*B(9)*CK*Y(12)-
     1 B(2)*B(3)*B(11)*CK*Y(38)
      G(39)=(-B(4)*B(11)*CK*Y(39))+B(2)*B(9)*CK*Y(13)-
     1 B(2)*B(3)*B(11)*CK*Y(39)
      G(40)=(-B(4)*B(11)*CK*Y(40))+B(2)*B(9)*CK*Y(14)-
     1 B(2)*B(3)*B(11)*CK*Y(40)+B(2)*CK*Y(1)
      G(41)=(-B(4)*B(11)*CK*Y(41))+B(2)*B(9)*CK*Y(15)-
     1 B(2)*B(3)*B(11)*CK*Y(41)
      G(42)=(-B(4)*B(11)*CK*Y(42))+B(2)*B(9)*CK*Y(16)-
     1 B(2)*B(3)*B(11)*CK*Y(42)-B(4)*CK*Y(3)-B(2)*B(3)*CK*Y(3)
      G(43)=(-B(4)*B(11)*CK*Y(43))+B(2)*B(9)*CK*Y(17)-
     1 B(2)*B(3)*B(11)*CK*Y(43)
      G(44)=(-B(4)*B(11)*CK*Y(44))+B(2)*B(9)*CK*Y(18)-
     1 B(2)*B(3)*B(11)*CK*Y(44)

      G(45)=B(6)*B(10)*CK*Y(19)*CV-B(7)*B(12)*CK*Y(45)
      G(46)=B(6)*B(10)*CK*Y(20)*CV-B(7)*B(12)*CK*Y(46)
      G(47)=B(6)*B(10)*CK*Y(21)*CV-B(7)*B(12)*CK*Y(47)
      G(48)=B(6)*B(10)*CK*Y(22)*CV-B(7)*B(12)*CK*Y(48)
      G(49)=B(6)*B(10)*CK*Y(23)*CV-B(7)*B(12)*CK*Y(49)
      G(50)=B(6)*B(10)*CK*Y(24)*CV-B(7)*B(12)*CK*Y(50)
     1 +B(10)*CK*Y(2)*CV
      G(51)=B(6)*B(10)*CK*Y(25)*CV-B(7)*B(12)*CK*Y(51)-B(12)*CK*Y(4)
      G(52)=B(6)*B(10)*CK*Y(26)*CV-B(7)*B(12)*CK*Y(52)
      G(53)=B(6)*B(10)*CK*Y(27)*CV-B(7)*B(12)*CK*Y(53)
      G(54)=B(6)*B(10)*CK*Y(28)*CV-B(7)*B(12)*CK*Y(54)+B(6)*CK*Y(2)*CV
      G(55)=B(6)*B(10)*CK*Y(29)*CV-B(7)*B(12)*CK*Y(55)
      G(56)=B(6)*B(10)*CK*Y(30)*CV-B(7)*B(12)*CK*Y(56)-B(7)*CK*Y(4)
      G(57)=B(6)*B(10)*CK*Y(31)*CV-B(7)*B(12)*CK*Y(57)

      G(58)=B(6)*B(10)*CK*Y(19)*CV-B(8)*B(13)*CK*Y(58)
      G(59)=B(6)*B(10)*CK*Y(20)*CV-B(8)*B(13)*CK*Y(59)
      G(60)=B(6)*B(10)*CK*Y(21)*CV-B(8)*B(13)*CK*Y(60)
      G(61)=B(6)*B(10)*CK*Y(22)*CV-B(8)*B(13)*CK*Y(61)
      G(62)=B(6)*B(10)*CK*Y(23)*CV-B(8)*B(13)*CK*Y(62)
      G(63)=B(6)*B(10)*CK*Y(24)*CV-B(8)*B(13)*CK*Y(63)
     1 +B(10)*CK*Y(2)*CV
      G(64)=B(6)*B(10)*CK*Y(25)*CV-B(8)*B(13)*CK*Y(64)
      G(65)=B(6)*B(10)*CK*Y(26)*CV-B(8)*B(13)*CK*Y(65)-B(13)*CK*Y(5)
```

```
      G(66)=B(6)*B(10)*CK*Y(27)*CV-B(8)*B(13)*CK*Y(66)
      G(67)=B(6)*B(10)*CK*Y(28)*CV-B(8)*B(13)*CK*Y(67)+B(6)*CK*Y(2)*CV
      G(68)=B(6)*B(10)*CK*Y(29)*CV-B(8)*B(13)*CK*Y(68)
      G(69)=B(6)*B(10)*CK*Y(30)*CV-B(8)*B(13)*CK*Y(69)
      G(70)=B(6)*B(10)*CK*Y(31)*CV-B(8)*B(13)*CK*Y(70)-B(8)*CK*Y(5)
      RETURN
      END
```

EQUD.FOR

```
      SUBROUTINE EQUD(G,Y,B,X,CV,CK)
      DIMENSION Y(*),G(*),B(*)
*      8 constant surface rxn model, coke from H, FA, LA
      G(1)=-B(1)*B(9)*CK*Y(1)-B(2)*(B(9)*CK*Y(1)-B(3)*B(11)*CK*Y(3))
      G(2)=B(1)*B(9)*CK*Y(1)+B(4)*B(11)*CK*Y(3)-B(5)*B(10)*CK*Y(2)-
     1 B(6)*B(10)*CK*Y(2)*CV
      G(3)=-B(4)*B(11)*CK*Y(3)+B(2)*(B(9)*CK*Y(1)-B(3)*B(11)*CK*Y(3))
      G(4)=B(6)*B(10)*CK*Y(2)*CV-B(7)*B(12)*CK*Y(4)
      G(5)=B(6)*B(10)*CK*Y(2)*CV-B(8)*B(13)*CK*Y(5)
      G(6)=B(5)*B(10)*CK*Y(2)
      G(7)=B(7)*B(12)*CK*Y(4)
      G(8)=B(8)*B(13)*CK*Y(5)
      RETURN
      END
C
      SUBROUTINE EQUI(YS,YB,B,CVK)
      DIMENSION YS(*),YB(*),B(*)
      YS(1) = YB(1)*B(9)*CVK
      YS(2) = YB(2)*B(10)*CVK
      YS(3) = YB(3)*B(11)*CVK
      YS(4) = YB(4)*B(12)*CVK
      YS(5) = YB(5)*B(13)*CVK
      RETURN
      END
```

Example of Program Data Entry

```
*************************************************************
*                                                           *
*      NONLINEAR REGRESSION USING THE MARQUARDT METHOD      *
*            FOR HETEROGENEOUS REACTION SYSTEM              *
*            COPYRIGHT 1994, A. CONSTANTINIDES              *
*           MODIFIED: AUGUST 1994, K. LOURVANIJ             *
*************************************************************
THIS PROGRAM HAS BEEN MODIFIED FOR A SPECIFIC SYSTEM.
FOR GENERAL CASE, USE THE ORIGINAL-NLR.FOR SOURCE CODE.

GIVE A name FOR THIS PROBLEM (UP TO 8 CHARACTERS LONG).
IT WILL BE USED TO NAME THE FILES WHICH STORE THE MODEL,
DATA, CONSTANTS, AND OUTPUT FOR THIS REGRESSION PROBLEM.
CHANGES MAY BE MADE TO THE STORED INFORMATION BY MAKING
THE APPROPRIATE CHOICES FROM THE MENUS.
ENTER THE name HERE: mcm92

THE PROGRAM CREATES AND USES THE FOLLOWING FILES:

FILE                      CONTENTS
RATE_EQ1.FOR....  MODEL AND VARIATIONAL EQUATIONS.
                  MUST BE COMPILED AND LINKED WITH "NLR.OBJ"
mcm92 .CON  ....  CONSTANTS,INITIAL CONDITIONS, GUESSES
mcm92 .DAT  ....  EXPERIMENTAL DATA AND WEIGHTS
mcm92 .OUT  ....  CALCULATED PROFILES OF VARIABLES
mcm92 .PAR  ....  FITTED PARAMETERS FROM NLR
mcm92 .REP  ....  REINTEGRATED PROFILES OF VARIABLES
MODEL FILE CAN BE EDITED BY USING "MODEL.BAT"
(say "YES" to "Have you previously ...." in
the model input menu).

MAIN MENU:
1     ENTER EQUATIONS, REGRESSION CONSTANTS, AND DATA
2     PERFORM NONLINEAR REGRESSION
3     PRINT OR PLOT THE OUTPUT RESULTS
4     BACK TO THE BEGINNING OF PROGRAM
ENTER YOUR CHOICE (1 - 4):1

INPUT MENU:
1     DESCRIPTION OF THE DATA AND EQUATION FILES
2     ENTER MODEL AND VARIATIONAL EQUATIONS
3     ENTER CONSTANTS AND DATA
4     RETURN TO MAIN MENU
ENTER YOUR CHOICE (1 - 4): 3

EQUATION OPTIONS:
1     MODEL CONTAINS ORDINARY DIFFERENTIAL EQUATIONS
2     MODEL CONTAINS ALGEBRAIC EQUATIONS ONLY
ENTER YOUR CHOICE (1 OR 2):  1

TOTAL NUMBER OF DEPENDENT VARIABLES IN THE SYSTEM:  5
NUMBER OF VARIABLES BEING FITTED TO DATA: 5
TOTAL NUMBER OF PARAMETERS BEING ESTIMATED: 13
NUMBER OF MODEL EQUATIONS (INCLUDING VARIATIONAL): 70
INITIAL VALUE OF INDEPENDENT VARIABLE:    0
FINAL VALUE OF INDEPENDENT VARIABLE:      24
```

```
NUMBER OF INTEGRATION STEPS:  1920
NUMBER OF LOCATIONS OF THE INDEPENDENT VARIABLE
AT WHICH EXPERIMENTAL POINTS CAN EXIST:   25
NUMBER OF INTEGRATION STEPS PER EXPERIMENTAL POINT: 80
MAX # OF EXPERIMENTAL POINTS FOR ANY LOCATION
(REPEATED EXPERIMENTS): 1
NUMBER OF RATE EQUATIONS OF BULK COMPONENTS  AND COKE FORMATION:  8
DO YOU WANT TO ACCOUNT FOR THE EFFECT
OF COKE-BLOCKED SITES (1=Y/2=N)? 2
DO YOU WANT TO CONSIDER COKE FORMATION
AS SURFACE REACTION (1=Y/2=N)? 2
ACTIVE SITE CONCENTRATION:  0.0102

                    REGRESSION OPTIONS
MAXIMUM NUMBER OF ITERATIONS FOR NLR SEARCH:200
PARAMETER CONSTRAINT:
      0 ALLOWS NEGATIVE PARAMETERS
      1 SETS NEGATIVE PARAMETERS TO ZERO
ENTER YOUR CHOICE(0 OR 1):    1
NORMALIZATION:
      0 DOES NOT NORMALIZE SUM OF SQUARES
      1 NORMALIZES SUM OF SQUARES
ENTER YOUR CHOICE(0 OR 1):    0
DO YOU WANT TO NORMALIZE THE INCREMENT OF PARAMETERS
IN EACH ITERATION (1=Y/2=N)? 1
ENTER MARQUARDT CONSTANT (SIGZR):   0.1
ENTER MARQUARDT CONSTANT (ALFA):    10
ENTER MARQUARDT CONSTANT (BETA):    0.5
ENTER NLR CONVERGENCE CONSTANT (CONV):    0.001
ENTER NLR CONVERGENCE CONSTANT (EPS):     0.00001

                    DEBUGING OPTION
THE FOLLOWING INPUT CONTROLS THE AMOUNT OF INFORMATION PRINTED
BY THE PROGRAM (0 GIVES MINIMUM AND 4 GIVES MAXIMUM INFORMATION).
RECOMMENDED VALUE IS 2.
      0 MINIMUM INFORMATION
      2 INTERMEDIATE AMOUNT OF INFORMATION
      4 MAXIMUM AMOUNT OF INFORMATION
ENTER YOUR CHOICE(0, 1, 2, 3, OR 4): 4

ENTER THE NUMBER OF PARAMETERS ASSOCIATED WITH EACH VARIABLE
BEING FITTED.  DO NOT DOUBLECOUNT (i.e., DO NOT COUNT A PARAMETER
TWICE, EVEN IF IT APPEARS IN MORE THAN ONE EQUATION).

NUMBER OF PARAMETERS ASSOCIATED WITH VARIABLE  1: 3
NUMBER OF PARAMETERS ASSOCIATED WITH VARIABLE  2: 3
NUMBER OF PARAMETERS ASSOCIATED WITH VARIABLE  3: 4
NUMBER OF PARAMETERS ASSOCIATED WITH VARIABLE  4: 2
NUMBER OF PARAMETERS ASSOCIATED WITH VARIABLE  5: 2

GIVE THE INITIAL CONDITIONS FOR INTEGRATING THE
DIFFERENTIAL EQUATIONS:

      INITIAL CONDITION FOR EQUATION  1: 0.7416
      INITIAL CONDITION FOR EQUATION  2: 0
      INITIAL CONDITION FOR EQUATION  3: 0
      INITIAL CONDITION FOR EQUATION  4: 0
      INITIAL CONDITION FOR EQUATION  5: 0
      INITIAL CONDITION FOR EQUATION  6: 0
      INITIAL CONDITION FOR EQUATION  7: 0
```

```
      INITIAL CONDITION FOR EQUATION  8: 0
      INITIAL CONDITION FOR EQUATION  9: 0
      :
      :
      INITIAL CONDITION FOR EQUATION 70: 0

GIVE THE INITIAL GUESSES OF THE PARAMETERS

      PARAMETER  1: 4.5
      PARAMETER  2: 8.3
      PARAMETER  3: 0
      PARAMETER  4: 27
      PARAMETER  5: 0
      PARAMETER  6: 1325
      PARAMETER  7: 4.65
      PARAMETER  8: 53
      PARAMETER  9: 0.38
      PARAMETER 10: 1.3
      PARAMETER 11: 0.4
      PARAMETER 12: 0.4
      PARAMETER 13: 2.5

HAVE YOU PREVIOUSLY ENTERED DATA POINTS (Y/N)? y
```

Example of Experimental Data File

MCM92.DAT

```
15
0.005
0      0.741647    1
1      0.705887    1
2      0.682765    1
3      0.672180    1
4      0.642001    1
5      0.604467    1
6      0.576335    1
7      0.538951    1
8      0.506590    1
9      0.469534    1
10     0.447900    1
12     0.418175    1
14     0.382436    1
16     0.326155    1
24     0.264524    1
15
0.005
0      0.000000    1
1      0.009508    1
2      0.011142    1
3      0.017600    1
4      0.025959    1
5      0.038540    1
6      0.044551    1
7      0.048708    1
8      0.063959    1
```

```
9       0.070437    1
10      0.084564    1
12      0.084714    1
14      0.101034    1
16      0.125630    1
24      0.140560    1
15
0.005
0       0.000000    1
1       0.006883    1
2       0.017606    1
3       0.032312    1
4       0.039729    1
5       0.045367    1
6       0.052801    1
7       0.059694    1
8       0.062949    1
9       0.066343    1
10      0.073740    1
12      0.079192    1
14      0.083590    1
16      0.083722    1
24      0.074943    1
15
0.005
0       0.000000    1
1       0.000000    0
2       0.010703    1
3       0.017243    1
4       0.029246    1
5       0.061856    1
6       0.097714    1
7       0.119936    1
8       0.136396    1
9       0.150053    1
10      0.174445    1
12      0.198240    1
14      0.209004    1
16      0.157265    0
24      0.183693    1
15
0.005
0       0.000000    1
1       0.005319    1
2       0.006602    0
3       0.005906    1
4       0.010276    0
5       0.007517    0
6       0.007141    1
7       0.005325    0
8       0.005395    0
9       0.009634    1
10      0.007037    0
12      0.007041    0
14      0.009657    1
16      0.013052    1
24      0.018518    1
```

Example of Program Output

```
************************ CONVERGED *************************

INCREMENT OF PARAMETER IS NORMALIZED

ITERATION =          9   SUM OF SQUARES =   4.136580E-02

Parameter #       Calculated
                  Parameters
    1             .55211E+01

    2             .75096E+01

    3             .17090E-01

    4             .39450E+02

    5             .00000E+00

    6             .24502E+04

    7             .74890E+01

    8             .58888E+02

    9             .36714E+00

   10             .23585E+01

   11             .53726E+00

   12             .74860E+00

   13             .28336E+01

STATISTICAL ANALYSIS OF CONVERGED RESULTS
VARIANCE-COVARIANCE MATRIX: INVERSE OF (A transpose A) TIMES S**2

   1   .3327E+06   .4525E+06  -.2518E+04  -.3448E+07   .4328E+01
       .5501E+08   .9511E+05   .8768E+06  -.2212E+05  -.5295E+05
       .4696E+05  -.9508E+04  -.4219E+05
   2   .4525E+06   .6154E+06  -.3426E+04  -.4690E+07   .2149E+01
       .7482E+08   .1294E+06   .1193E+07  -.3009E+05  -.7202E+05
       .6387E+05  -.1293E+05  -.5739E+05
   3  -.2487E+04  -.3384E+04  -.3332E+02  -.1022E+06   .1053E+01
      -.1242E+07  -.1090E+05   .1013E+06   .1655E+03   .1196E+04
       .1392E+04   .1089E+04  -.4876E+04
   4  -.3376E+07  -.4592E+07  -.1024E+06  -.2605E+09  -.7016E+01
      -.2476E+10  -.2448E+08   .2402E+09   .2245E+06   .2383E+07
       .3547E+07   .2447E+07  -.1156E+08
   5   .4055E+01   .1778E+01   .1051E+01  -.1371E+02   .1098E+02
      -.7080E+03  -.5228E+01  -.1608E+02  -.1206E+00  -.6432E+00
       .1171E+00  -.8651E+00  -.1411E+01
   6   .7616E+08   .1036E+09  -.1140E+07  -.2089E+10  -.5193E+03
       .7548E+12   .3084E+09  -.7374E+10  -.5065E+07  -.7266E+09
       .2845E+08  -.3083E+08   .3548E+09
   7   .2960E+05   .4026E+05  -.7179E+04  -.1636E+08  -.8881E+01
```

	.4810E+09	.1355E+08	.5385E+06	-.1969E+04	-.4630E+06
	.2228E+06	-.1354E+07	-.2591E+05		
8	.3308E+07	.4499E+07	.8457E+05	.2188E+09	.6563E+02
	-.8327E+10	.8592E+07	-.1048E+12	-.2199E+06	.8016E+07
	-.2979E+07	-.8588E+06	.5044E+10		
9	-.2212E+05	-.3009E+05	.1676E+03	.2293E+06	-.1387E+00
	-.3658E+07	-.6324E+04	-.5831E+05	.1471E+04	.3521E+04
	-.3122E+04	.6322E+03	.2806E+04		
10	-.7331E+05	-.9972E+05	.1097E+04	.2011E+07	-.8249E+00
	-.7266E+09	-.2969E+06	.7098E+07	.4875E+04	.6994E+06
	-.2739E+05	.2967E+05	-.3416E+06		
11	.4598E+05	.6254E+05	.1395E+04	.3547E+07	.2586E-01
	.3372E+08	.3334E+06	-.3271E+07	-.3057E+04	-.3245E+05
	-.4831E+05	-.3333E+05	.1574E+06		
12	-.2960E+04	-.4025E+04	.7173E+03	.1635E+07	-.4999E+00
	-.4808E+08	-.1354E+07	-.5382E+05	.1968E+03	.4628E+05
	-.2227E+05	.1354E+06	.2590E+04		
13	-.1592E+06	-.2165E+06	-.4070E+04	-.1053E+08	-.5343E+01
	.4007E+09	-.4134E+06	.5044E+10	.1058E+05	-.3857E+06
	.1434E+06	.4133E+05	-.2427E+09		

DEGREES OF FREEDOM= 53
COMBINED RESIDUAL VARIANCE(S**2)= .7805E-03
STANDARD DEVIATION (S) = .2794E-01

	PARAMETER	STANDARD ERROR	0.95 CONFIDENCE LIMITS	0.95 CONFIDENCE INTERVAL LOWER	UPPER
1	.5521E+01	.5768E+03	.1130E+04	-.1125E+04	.1136E+04
2	.7510E+01	.7845E+03	.1538E+04	-.1530E+04	.1545E+04
3	.1709E-01	.5772E+01	.1131E+02	-.1130E+02	.1133E+02
4	.3945E+02	.1614E+05	.3163E+05	-.3159E+05	.3167E+05
5	.0000E+00	.3314E+01	.6495E+01	-.6495E+01	.6495E+01
6	.2450E+04	.8688E+06	.1703E+07	-.1700E+07	.1705E+07
7	.7489E+01	.3681E+04	.7214E+04	-.7207E+04	.7222E+04
8	.5889E+02	.3238E+06	.6346E+06	-.6345E+06	.6346E+06
9	.3671E+00	.3835E+02	.7517E+02	-.7481E+02	.7554E+02
10	.2359E+01	.8363E+03	.1639E+04	-.1637E+04	.1642E+04
11	.5373E+00	.2198E+03	.4308E+03	-.4303E+03	.4313E+03
12	.7486E+00	.3679E+03	.7212E+03	-.7204E+03	.7219E+03
13	.2834E+01	.1558E+05	.3054E+05	-.3053E+05	.3054E+05

SIGNIFICANCE TEST

	PARAMETER	T-CALCULATED	IS PARAMETER SIGNIFICANTLY DIFFERENT THAN ZERO?
1	.5521E+01	.9572E-02	NO
2	.7510E+01	.9573E-02	NO
3	.1709E-01	.2961E-02	NO
4	.3945E+02	.2444E-02	NO
5	.0000E+00	.0000E+00	NO
6	.2450E+04	.2820E-02	NO
7	.7489E+01	.2035E-02	NO
8	.5889E+02	.1819E-03	NO
9	.3671E+00	.9573E-02	NO
10	.2359E+01	.2820E-02	NO
11	.5373E+00	.2444E-02	NO
12	.7486E+00	.2035E-02	NO
13	.2834E+01	.1819E-03	NO

MEASURED VARIABLE	DEGREES OF FREEDOM	RESIDUAL VARIANCE(S**2)	95% CONFIDENCE LIMIT FOR EACH VARIABLE
1	12	.4403E-03	.4573E-01
2	12	.1267E-02	.7757E-01
3	11	.3842E-03	.4314E-01
4	11	.1503E-02	.8532E-01
5	6	.1994E-04	.1093E-01

RESULTS OF COVARIANCE ANALYSIS
MATRIX OF CORRELATION COEFFICIENTS

1	.1000E+01	.1000E+01	-.7563E+00	-.3704E+00	.2264E-02
	.1098E+00	.4480E-01	.4695E-02	-.1000E+01	-.1098E+00
	.3704E+00	-.4480E-01	-.4695E-02		
2	.1000E+01	.1000E+01	-.7566E+00	-.3704E+00	.8267E-03
	.1098E+00	.4480E-01	.4696E-02	-.1000E+01	-.1098E+00
	.3704E+00	-.4480E-01	-.4696E-02		
3	-.7470E+00	-.7473E+00	-.1000E+01	-.1097E+01	.5505E-01
	-.2477E+00	-.5131E+00	.5422E-01	.7476E+00	.2477E+00
	.1097E+01	.5130E+00	-.5423E-01		
4	-.3627E+00	-.3627E+00	-.1100E+01	-.1000E+01	-.1312E-03
	-.1766E+00	-.4121E+00	.4597E-01	.3627E+00	.1766E+00
	.1000E+01	.4121E+00	-.4597E-01		
5	.2122E-02	.6840E-03	.5494E-01	-.2564E-03	.1000E+01
	-.2459E-03	-.4286E-03	-.1499E-04	-.9487E-03	-.2321E-03
	.1607E-03	-.7095E-03	-.2733E-04		
6	.1520E+00	.1520E+00	-.2274E+00	-.1490E+00	-.1804E-03
	.1000E+01	.9643E-01	-.2621E-01	-.1520E+00	-.1000E+01
	.1490E+00	-.9643E-01	.2621E-01		
7	.1394E-01	.1394E-01	-.3379E+00	-.2753E+00	-.7281E-03
	.1504E+00	.1000E+01	.4519E-03	-.1394E-01	-.1504E+00
	.2753E+00	-.1000E+01	-.4518E-03		
8	.1771E-01	.1771E-01	.4525E-01	.4187E-01	.6117E-04
	-.2960E-01	.7210E-02	-.1000E+01	-.1771E-01	.2960E-01
	-.4187E-01	-.7210E-02	.1000E+01		
9	-.1000E+01	-.1000E+01	.7568E+00	.3704E+00	-.1091E-02
	-.1098E+00	-.4480E-01	-.4696E-02	.1000E+01	.1098E+00
	-.3704E+00	.4480E-01	.4696E-02		
10	-.1520E+00	-.1520E+00	.2273E+00	.1490E+00	-.2976E-03
	-.1000E+01	-.9643E-01	.2621E-01	.1520E+00	.1000E+01
	-.1490E+00	.9643E-01	-.2621E-01		
11	.3627E+00	.3627E+00	.1099E+01	.1000E+01	.3550E-04
	.1766E+00	.4121E+00	-.4597E-01	-.3627E+00	-.1766E+00
	-.1000E+01	-.4121E+00	.4597E-01		
12	-.1395E-01	-.1395E-01	.3378E+00	.2753E+00	-.4100E-03
	-.1504E+00	-.1000E+01	-.4518E-03	.1395E-01	.1504E+00
	-.2753E+00	.1000E+01	.4519E-03		
13	-.1771E-01	-.1771E-01	-.4526E-01	-.4187E-01	-.1035E-03
	.2960E-01	-.7210E-02	.1000E+01	.1771E-01	-.2960E-01
	.4187E-01	.7210E-02	-.1000E+01		

MATRIX OF 0.05 SIGNIFICANCE TEST.
YES MEANS CORRELATION IS SIGNIFICANT:

1	YES	YES	YES	YES	NO	NO	NO	NO	YES	NO	YES	NO	NO
2	YES	YES	YES	YES	NO	NO	NO	NO	YES	NO	YES	NO	NO
3	YES	YES	YES	YES	NO	NO	YES	NO	YES	NO	YES	YES	NO
4	YES	YES	YES	YES	NO	NO	YES	NO	YES	NO	YES	YES	NO
5	NO	NO	NO	NO	YES	NO	NO	NO	NO	NO	NO	NO	NO

6	NO	NO	NO	NO	NO	YES	NO	NO	NO	YES	NO	NO	NO
7	NO	NO	YES	YES	NO	NO	YES	NO	NO	NO	YES	YES	NO
8	NO	NO	NO	NO	NO	NO	NO	YES	NO	NO	NO	NO	YES
9	YES	YES	YES	YES	NO	NO	NO	NO	YES	NO	YES	NO	NO
10	NO	NO	NO	NO	NO	YES	NO	NO	NO	YES	NO	NO	NO
11	YES	YES	YES	YES	NO	NO	YES	NO	YES	NO	YES	YES	NO
12	NO	NO	YES	YES	NO	NO	YES	NO	NO	NO	YES	YES	NO
13	NO	NO	NO	NO	NO	NO	NO	YES	NO	NO	NO	NO	YES

MATRIX OF 0.01 SIGNIFICANCE TEST.
YES MEANS CORRELATION IS HIGHLY SIGNIFICANT:

1	YES	YES	YES	YES	NO	NO	NO	NO	YES	NO	YES	NO	NO
2	YES	YES	YES	YES	NO	NO	NO	NO	YES	NO	YES	NO	NO
3	YES	YES	YES	YES	NO	NO	NO	NO	YES	NO	YES	NO	NO
4	YES	YES	YES	YES	NO	NO	NO	NO	YES	NO	YES	NO	NO
5	NO	NO	NO	NO	YES	NO	NO	NO	NO	NO	NO	NO	NO
6	NO	NO	NO	NO	NO	YES	NO	NO	NO	YES	NO	NO	NO
7	NO	NO	YES	YES	NO	NO	YES	NO	NO	NO	YES	YES	NO
8	NO	NO	NO	NO	NO	NO	NO	YES	NO	NO	NO	NO	YES
9	YES	YES	YES	YES	NO	NO	NO	NO	YES	NO	YES	NO	NO
10	NO	NO	NO	NO	NO	YES	NO	NO	NO	YES	NO	NO	NO
11	YES	YES	YES	YES	NO	NO	NO	NO	YES	NO	YES	NO	NO
12	NO	NO	YES	YES	NO	NO	YES	NO	NO	NO	YES	YES	NO
13	NO	NO	NO	NO	NO	NO	NO	YES	NO	NO	NO	NO	YES

RUNS TEST FOR VARIABLE 1
NUMBER OF POSITIVE RESIDUALS= 12
NUMBER OF NEGATIVE RESIDUALS= 3
NUMBER OF RUNS= 5
Z= -.701
RANDOM AT 95% LEVEL OF CONFIDENCE

RUNS TEST FOR VARIABLE 2
NUMBER OF POSITIVE RESIDUALS= 6
NUMBER OF NEGATIVE RESIDUALS= 8
NUMBER OF RUNS= 2
Z= -3.332
NOT RANDOM AT 95% LEVEL OF CONFIDENCE

RUNS TEST FOR VARIABLE 3
NUMBER OF POSITIVE RESIDUALS= 7
NUMBER OF NEGATIVE RESIDUALS= 7
NUMBER OF RUNS= 2
Z= -3.338
NOT RANDOM AT 95% LEVEL OF CONFIDENCE

RUNS TEST FOR VARIABLE 4
NUMBER OF POSITIVE RESIDUALS= 9
NUMBER OF NEGATIVE RESIDUALS= 3
NUMBER OF RUNS= 4
Z= -1.254
RANDOM AT 95% LEVEL OF CONFIDENCE

RUNS TEST FOR VARIABLE 5
NUMBER OF POSITIVE RESIDUALS= 3
NUMBER OF NEGATIVE RESIDUALS= 4
NUMBER OF RUNS= 3
Z= -1.213
RANDOM AT 95% LEVEL OF CONFIDENCE

Appendix H

Molecular Dimensions

Radius of Hydrogen and Oxygen Atoms

Atom	Van der Waals Radii[a]	Atomic Radii[b]
H	1.2 Å	0.74138 Å
O	1.4 Å	1.20750 Å

[a] *CRC Handbook of Chemistry & Physics*, 59th Edition, p. D-230 (1979)

[b] *American Institute of Physics Handbook*, New York, p. 175, 179 (1972)

Glucose

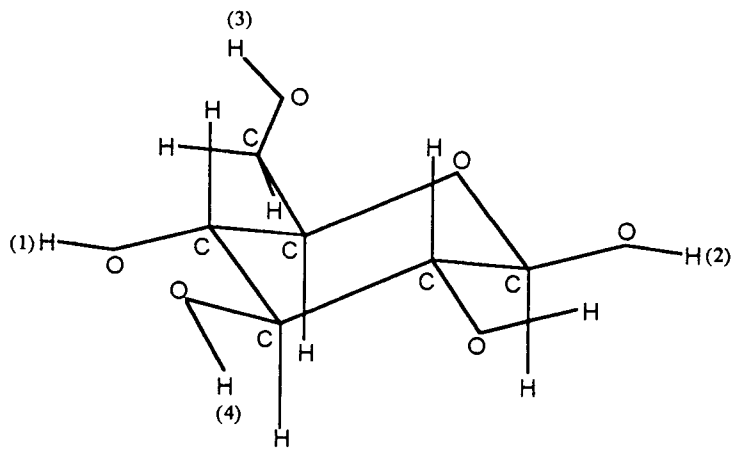

Figure H-1. Glucose molecular structure.

The distance between (1) and (2) is 6.017 Å, and the distance between (3) and (4) is 6.183 Å (calculated by Hyperchem Software). The longest short axis is the length between (1) and (2) including the radius of H, and the long axis is the length between (3) and (4) including the radius of H.

	Van der Waals Radii	Atomic Radii
longest short axis (Å)	6.017 + 2 (1.2) = 8.417	6.017 + 2 (0.741) = 7.500
long axis (Å)	6.183 + 2 (1.2) = 8.583	6.183 + 2 (0.741) = 7.665

Fructose

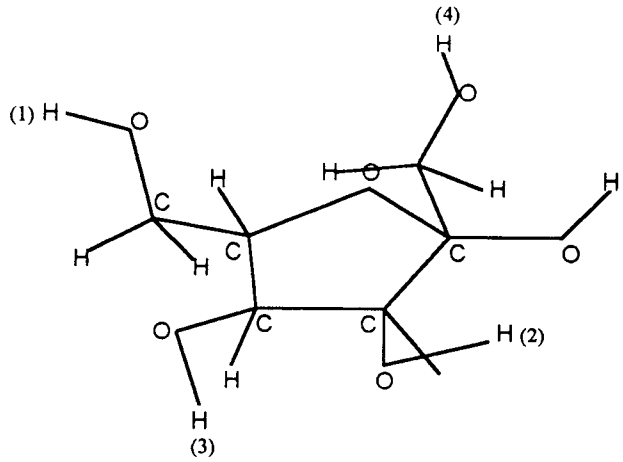

Figure H-2. Fructose molecular structure.

The distance between (1) and (2) is 7.395 Å, and the distance between (3) and (4) is 6.128 Å (calculated by Hyperchem Software). The longest short axis is the length between (3) and (4) including the radius of H, and the long axis is the length between (1) and (2) including the radius of H.

	Van der Waals Radii	Atomic Radii
longest short axis (Å)	6.128 + 2 (1.2) = 8.528	6.128 + 2 (0.741) = 7.610
long axis (Å)	7.395 + 2 (1.2) = 9.795	7.395 + 2 (0.741) = 8.877

HMF

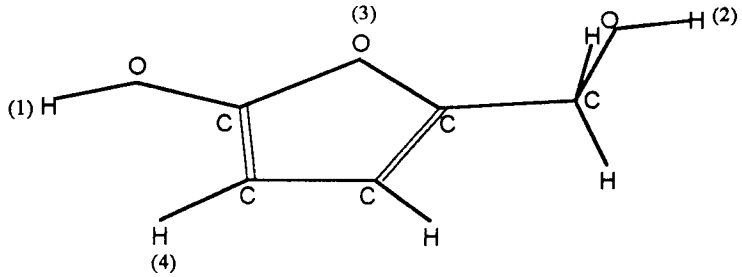

Figure H-3. HMF molecular structure.

The distance between (1) and (2) is 6.922 Å, and the distance between (3) and (4) is 3.284 Å (calculated by Hyperchem Software). The longest short axis is the length between (3) and (4) including the radius of H and O, and the long axis is the length between (1) and (2) including the radius of H.

	Van der Waals Radii	Atomic Radii
longest short axis (Å)	3.284 + 1.2 + 1.4 = 5.884	3.284 + 0.741 + 1.207 = 5.232
long axis (Å)	6.922 + 2 (1.2) = 9.322	6.922 + 2 (0.741) = 8.404

Formic Acid

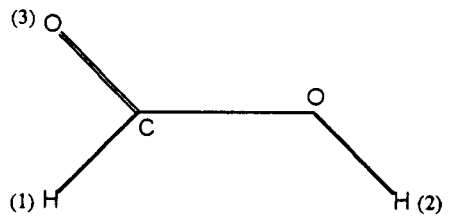

Figure H-4. Formic acid molecular structure.

The distance between (1) and (2) is 2.220 Å, and the distance between (1) and (3) is 1.993 Å (calculated by Hyperchem Software). The longest short axis is the length between (1) and (3) including the radius of H and O, and the long axis is the length between (1) and (2) including the radius of H.

	Van der Waals Radii	Atomic Radii
longest short axis (Å)	1.993 + 1.2 + 1.4 = 4.593	1.993 + 0.741 + 1.207 = 3.941
long axis (Å)	2.220 + 2 (1.2) = 4.620	2.220 + 2 (0.741) = 3.702

4-Oxopentanoic Acid

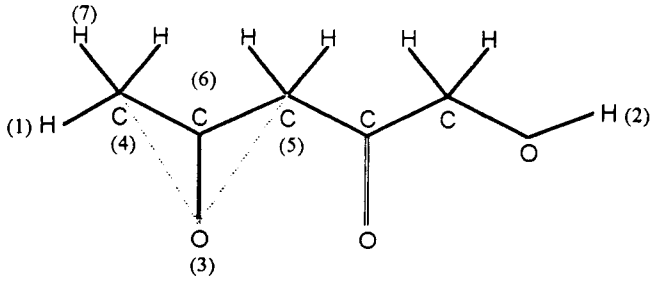

Figure H-5. 4-Oxopentanoic acid molecular structure.

The distance between (1) and (2) is 7.874 Å, the distance between (3) and (4) is 2.377 Å, the distance between (4) and (5) is 2.633 Å, and the distance between (4) and (7) is 1.09 Å (calculated by Hyperchem Software). The distance between (3) and (6) for triangle (3)(4)(5) is 1.980 Å. The longest short axis is the sum of the length between (3) and (6), and the length between (4) and (7) including the radius of H and O, and the long axis is the length between (1) and (2) including the radius of H.

	Van der Waals Radii	Atomic Radii
longest short axis (Å)	3.070 + 1.2 + 1.4 = 5.670	3.070 + 0.741 + 1.207 = 5.018
long axis (Å)	7.874 + 2 (1.2) = 10.274	7.874 + 2 (0.741) = 9.356

Appendix I

Diffusion Coefficient Measurement

The effective diffusion coefficient ($D_{G,e}$) of aqueous glucose within Al-pillared montmorillonite (APM) was measured by a liquid chromatography technique (Awum et al., 1988 and Ma et al., 1988). The detailed experimental procedures and data analysis used in this measurement are given by Netrabukkana (1994).

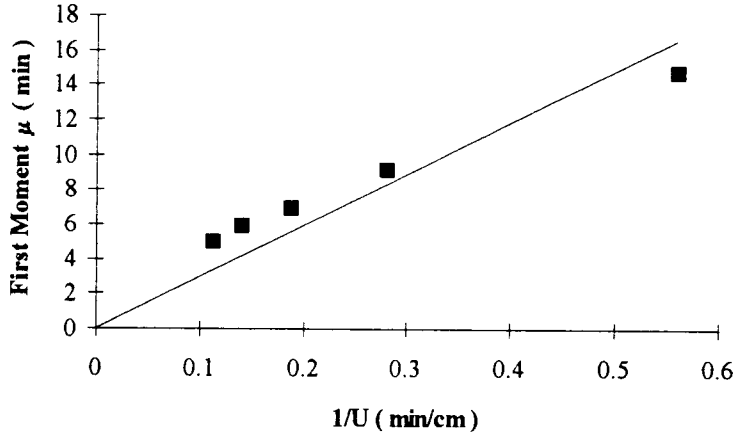

Figure I-1. First moment of glucose diffusion in packed column of APM catalyst (measurement # 1).

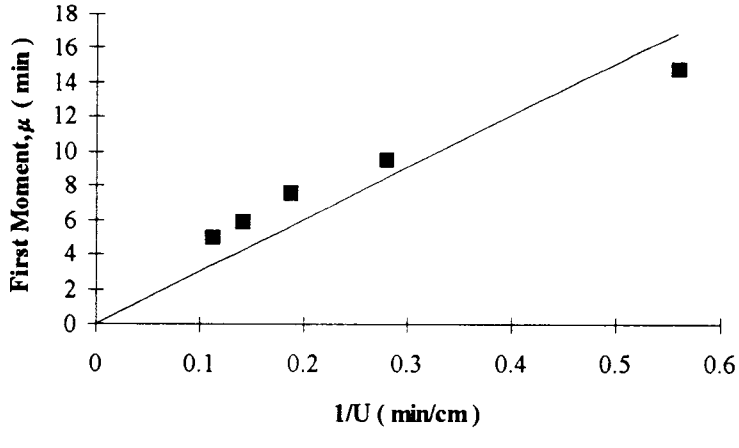

Figure I-2. First moment of glucose diffusion in packed column of APM catalyst (measurement # 2).

Table I-1. Least square fit of the first moment of glucose diffusion within APM catalyst (measurement # 1).

1/Interstitial velocity 1/U (min/cm)	Corrected first moment μ (min)
0.559	14.886
0.279	9.190
0.186	6.974
0.139	6.040
0.111	5.112

Regression Statistics	
Multiple R	0.890
R Square	0.792
Adjusted R Square	0.542
Standard Error	1.782
Observations	5.000

	Coefficients	Standard Error	t Stat
Intercept	0.000	-	-
X Variable 1	29.783	2.639	11.286

Table I-2. Least square fit of the first moment of glucose diffusion within APM catalyst (measurement # 2).

1/Interstitial velocity 1/U (min/cm)	Corrected first moment μ (min)
0.559	14.936
0.279	9.638
0.186	7.603
0.139	5.964
0.111	5.020

Regression Statistics	
Multiple R	0.871
R Square	0.758
Adjusted R Square	0.508
Standard Error	1.937
Observations	5.000

	Coefficients	Standard Error	t Stat
Intercept	0.000	-	-
X Variable 1	30.328	2.868	10.575

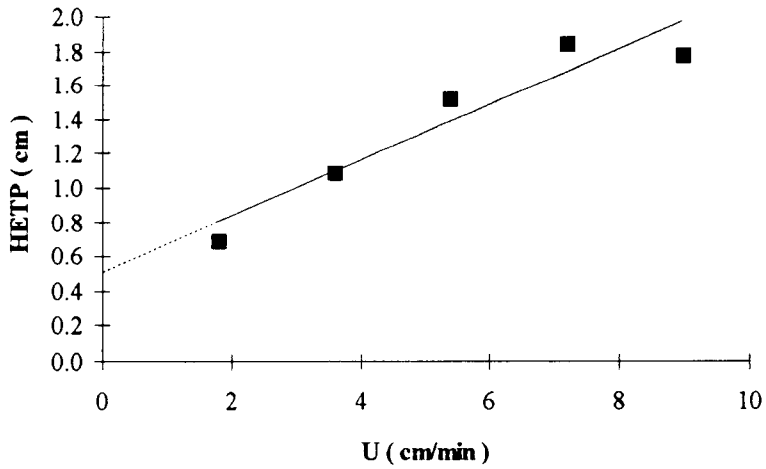

Figure I-3. HETP of glucose diffusion in packed column of APM catalyst (measurement # 1).

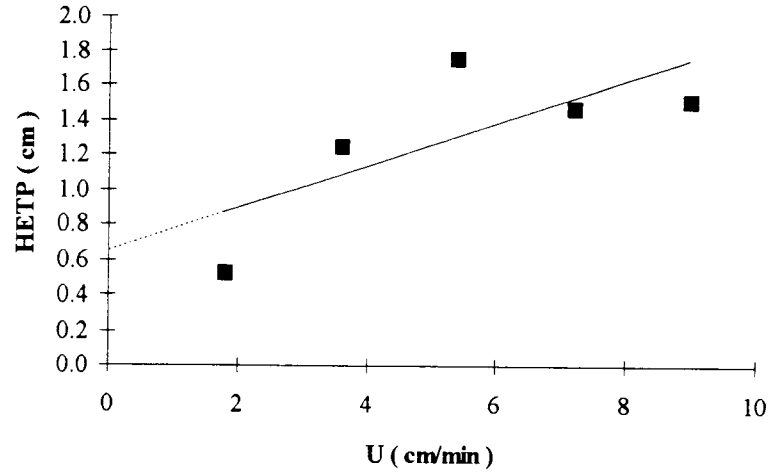

Figure I-4. HETP of glucose diffusion in packed column of APM catalyst (measurement # 2).

Table I-3. Least square fit of the HETP of glucose diffusion within APM catalyst (measurement # 1).

Interstitial velocity U (cm/min)	Corrected second moment σ^2 (min)^2	HETP (cm)
1.790	15.374	0.694
3.590	9.265	1.097
5.380	7.448	1.531
7.170	6.743	1.849
8.970	4.669	1.786

Regression Statistics	
Multiple R	0.949
R Square	0.900
Adjusted R Square	0.867
Standard Error	0.179
Observations	5.000

	Coefficients	Standard Error	t Stat
Intercept	0.511	0.187	2.727
X Variable 1	0.164	0.031	5.198

Table I-4. Least square fit of the HETP of glucose diffusion within APM catalyst (measurement # 2).

Interstitial velocity U (cm/min)	Corrected second moment σ^2 (min)^2	HETP (cm)
1.790	11.841	0.531
3.590	11.706	1.260
5.380	10.231	1.770
7.170	5.270	1.482
8.970	3.854	1.529

Regression Statistics	
Multiple R	0.740
R Square	0.548
Adjusted R Square	0.397
Standard Error	0.368
Observations	5.000

	Coefficients	Standard Error	t Stat
Intercept	0.649	0.386	1.682
X Variable 1	0.124	0.065	1.906

Table I-5. Effective diffusion coefficient ($D_{G,e}$) of aqueous glucose within APM catalyst at 30°C.

	Effective Diffusion Coefficient $D_{G,e}$ (cm^2/sec)	$D_{G,e}/D_G$
measurement # 1	2.46×10^{-9}	0.0003
measurement # 2	$3.23 \times$ [illegible]$^{-9}$	0.0005
Average	2.84×10^{-9}	0.0004

Appendix J

Mass Transfer Resistance Determination

External Mass Transfer Resistance

Mass Transfer Coefficient Estimation

The relative velocity between the particles and the liquid in a slurry reactor is low, because the particles are so small that they tend to move with liquid. In agitated slurries, the relative velocity is due primarily to the shearing action induced by the stirrer blades. The correlation of the mass transfer coefficient (k_c) as a function of mixing speed and particle size is based on the Kolomogoroffs' theory of isotropic turbulence. The Reynolds' number (Re) is defined in terms of the energy dissipation rate.

The energy dissipation rate (ω) described by Smith (1981) can be estimated by

$$\omega = \frac{N_p \rho_L N^3 D_I^5}{W} \tag{J-1}$$

$$N_p = \frac{P}{\rho_L N^3 D_I^5} \cong 10 \tag{J-2}$$

where:

D_I	impeller diameter, cm
ρ_L	density of liquid, g/cm^3
N	impeller speed, rps
W	mass of liquid in slurry, g
N_p	power number
P	power input, erg/s

The Eddy size (ζ) is defined as

$$\zeta = \left(\frac{\nu^3}{\omega}\right)^{1/3} \tag{J-3}$$

If $\zeta > d_p$:

$$Re = \left(\frac{\omega \cdot d_p^4}{\nu^3}\right)^{1/2} \tag{J-4}$$

If $\zeta < d_p$: $$Re = \left(\frac{\omega \cdot d_p^4}{\nu^3}\right)^{1/3} \quad \text{(J-5)}$$

The mass transfer coefficient (k_c) for convective flow around a spherical particle (Cussler, 1984) is given by

$$Sh = \frac{k_c d_p}{D_G} = 2.0 + 0.6(Re)^{1/2}\left(\frac{\nu}{D_G}\right)^{1/3} \quad \text{(J-6)}$$

The molecular diffusivity of glucose in water (D_G) is estimated by the Hayduk and Laudie correlation

$$D_G = 13.26 \times 10^{-5}\, \mu_L^{-1.14}\, V_G^{-0.589} \quad \text{(J-7)}$$

where ν kinemetic viscosity, cm^2/s

d_p particle diameter, cm

μ_L viscosity of liquid at reaction temperature, cp

V_G molar volume of glucose, cm^3/mol

Significance of External Mass transfer Resistance

External mass transfer resistance is evaluated by the ratio of glucose conversion rate to convective mass transfer rate (γ) as described by Petersen (1965)

$$\gamma = \frac{k_{app} d_p}{6 k_c} \quad \text{(J-8)}$$

where k_{app} is an apparent reaction rate constant.

The external mass transfer resistance is not the limiting process if $\gamma << 1$.

Table J-1. Properties of water at 130 to 170°C.

Temperature (°C)	ρ_L (g/cm^3)	ν (cm^2/s)	μ_L (cp)	D_G (cm^2/s)
130	0.930	0.002513	0.236	3.25×10^{-5}
150	0.911	0.002255	0.208	3.75×10^{-5}
170	0.892	0.001997	0.181	4.41×10^{-5}

Table J-2. Apparent rate constant of reaction of 12% wt glucose.

Catalyst	130°C	150°C	170°C
HY-zeolite	n/a	0.256	n/a
APM	0.0738	0.313	0.752
MCM-41	0.0172	0.096	0.349

Table J-3. Estimation of k_C and γ for HY-zeolite catalyst.

	150°C	
rpm	k_C (cm/s)	γ
200	0.076	3.70×10^{-07}
400	0.094	2.98×10^{-07}
600	0.108	2.59×10^{-07}
800	0.120	2.33×10^{-07}
1000	0.131	2.15×10^{-07}
1200	0.140	2.00×10^{-07}
1400	0.149	1.88×10^{-07}

Table J-4. Estimation of k_C and γ for APM catalyst.

	130°C		150°C		170°C	
rpm	k_C (cm/s)	γ	k_C (cm/s)	γ	k_C (cm/s)	γ
200	0.074	9.37×10^{-08}	0.084	3.51×10^{-07}	0.096	7.31×10^{-07}
400	0.913	7.59×10^{-08}	0.103	2.85×10^{-07}	0.118	5.96×10^{-07}
600	0.105	6.62×10^{-08}	0.118	2.49×10^{-07}	0.135	5.22×10^{-07}
800	0.116	5.98×10^{-08}	0.130	2.25×10^{-07}	0.149	4.72×10^{-07}
1000	0.126	5.51×10^{-08}	0.141	2.08×10^{-07}	0.162	4.36×10^{-07}
1200	0.135	5.14×10^{-08}	0.151	1.94×10^{-07}	0.173	4.07×10^{-07}
1400	0.143	4.85×10^{-08}	0.161	1.83×10^{-07}	0.184	3.84×10^{-07}

Table J-5. Estimation of k_C and γ for MCM-41 catalyst.

	130°C		150°C		170°C	
rpm	k_C (cm/s)	γ	k_C (cm/s)	γ	k_C (cm/s)	γ
200	0.070	2.50×10^{-08}	0.080	1.23×10^{-07}	0.092	3.88×10^{-07}
400	0.087	2.01×10^{-08}	0.098	9.91×10^{-08}	0.113	3.15×10^{-07}
600	0.100	1.75×10^{-08}	0.113	8.64×10^{-08}	0.129	2.75×10^{-07}
800	0.111	1.58×10^{-08}	0.125	7.80×10^{-08}	0.143	2.49×10^{-07}
1000	0.121	1.46×10^{-08}	0.136	7.18×10^{-08}	0.155	2.29×10^{-07}
1200	0.129	1.36×10^{-08}	0.145	6.70×10^{-08}	0.166	2.14×10^{-07}
1400	0.137	1.28×10^{-08}	0.154	6.31×10^{-08}	0.177	2.02×10^{-07}

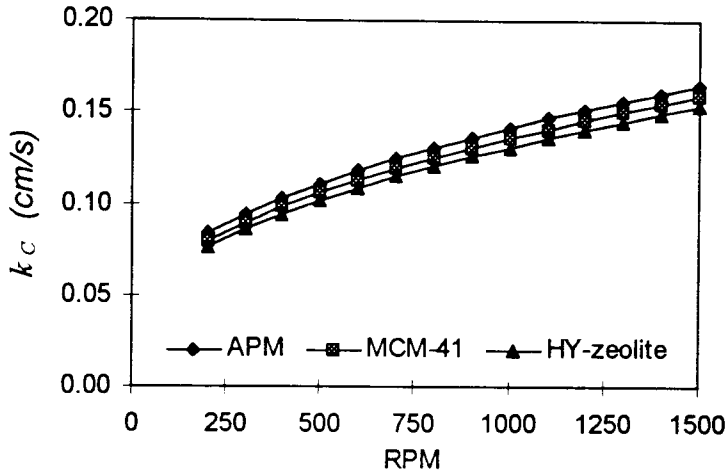

Figure J-1. Mass transfer coefficient (k_C) vs. mixing speed for HY-zeolite, APM, and MCM-41 catalysts at 150°C.

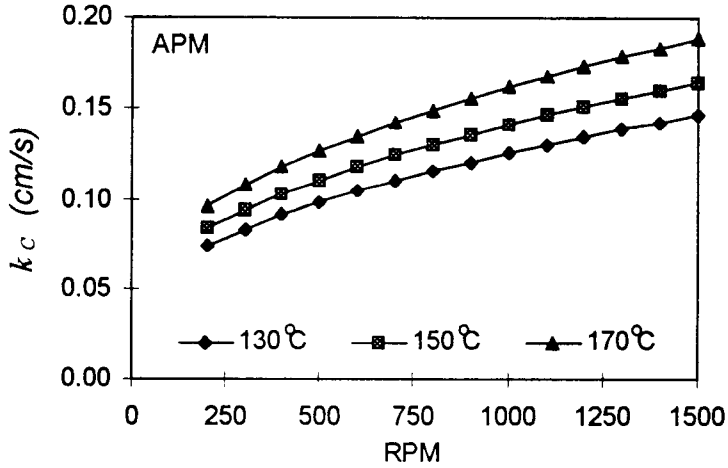

Figure J-2. Mass transfer coefficient (k_C) vs. mixing speed for APM from 130 to 170°C.

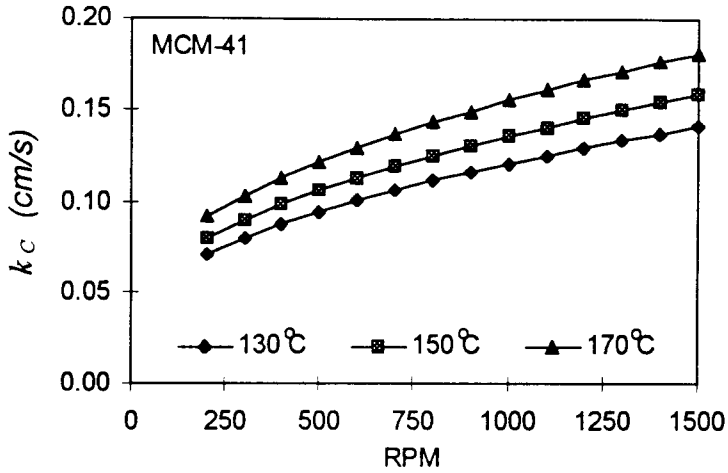

Figure J-3. Mass transfer coefficient (k_C) vs. mixing speed for MCM-41 from 130 to 170°C.

Internal Mass Transfer Resistance

Weisz and Prater Development (Petersen, 1965)

The apparent reaction rate of pseudo-homogeneous reaction is defined as

$$r_{i,app} = \rho_p S r_{i\cdot X} \eta \tag{J-9}$$

where $r_{i,app}$ pseudo-homogeneous reaction rate (apparent rate), mol/cm^3-s

ρ_p density of catalyst particle, g/cm^3

S specific internal surface area, cm^2/g

$r_{i\cdot X}$ surface reaction rate, mol/cm^2-s

η effectiveness factor

The generalized Thiele modulus (Φ_T) is given by

$$\Phi_T = \frac{V_p}{A_p}\sqrt{\frac{\rho_p \cdot S \cdot r_{i\cdot X}}{D_{i,e} \cdot C_{i,p}}} \tag{J-10}$$

where V_p volume of catalyst particle, cm^3/g

A_p external surface area of particle, cm^2/g

$D_{i,e}$ effective diffusivity, cm^2/s

$C_{i,p}$ concentration at pore mouth, mol/cm^3

From equations J-9 and J-10, the Weisz modulus (Φ_W) can be obtained by

$$\Phi_W = \frac{r_{i,app}\left(V_p/A_p\right)^2}{D_{i,e} \cdot C_{i,p}} = \Phi_T^2 \cdot \eta \tag{J-11}$$

Significance of Internal Mass transfer Resistance

If $\eta \rightarrow 1.0$, the resistance from diffusion process is very small and $\Phi_T \leq 1/3$. Therefore, it can be determined from equation (J-11) that for no pore diffusion effect, $\Phi_W < 0.15$, whereas for a strong pore diffusion effect, $\Phi_W > 7$, as described by Levenspiel, 1972. The Weisz modulus was developed regardless of reaction order. Since η for all reaction orders are nearly coincident at $\Phi_T \leq 1/3$. It is valid even though it was derived from a first order reaction.

For the diffusion-reaction of glucose with molecular-sieve catalysts, the Weisz modulus is applied with the assumptions that the catalyst particle is spherical, no external

mass transfer resistance, and the apparent reaction rate of glucose is pseudo-homogeneous reaction. Therefore

$$r_{G,app} = k_{app} C_G \tag{J-12}$$

$$C_G = C_{G,p} \tag{J-13}$$

$$V_p/A_p = d_p/6 \tag{J-14}$$

where k_{app} apparent rate constant, 1/s

d_p particle diameter, cm

C_G liquid phase concentration of glucose, mol/L

The Weisz modulus for this particular system is given by

$$\Phi_W = \frac{k_{app}\left(d_p/6\right)^2}{D_{G,e}} \tag{J-15}$$

The diffusion resistance is not a limiting process if $\Phi_W < 0.15$.

Table J-6. Estimation of Φ_W for HY-zeolite, APM, and MCM-41 catalysts from 130 to 170°C.

Catalyst	d_p (μm)	$D_{G,e}$ (cm^2/s)	Φ_W 130°C	Φ_W 150°C	Φ_W 170°C
HY-zeolite	23.70	1.77×10^{-9}	n/a	0.00627	n/a
APM	20.27	2.83×10^{-9}	0.00083	0.00351	0.00843
MCM-41	22.00	1.71×10^{-8}	0.00004	0.00021	0.00076

Appendix K

Reactions of HMF and 4-Oxopentanoic Acid with HY-zeolite

Materials

0.5 % wt. of HMF aqueous solution

0.1 % wt. of 4-oxopentanoic acid aqueous solution

HY-zeolite catalyst powder

Reaction Procedures

1. Load 3 g of either HMF or 4-oxopentanoic acid solution into micro reactor vials. Total number of eight vials are required.
2. Load 0.17 g of HY-zeolite powder into each reactor vial from the previous step. Total number of four vials with catalyst are required. (0.17 g catalyst/3 g solution = 10 g catalyst/170 g solution).
3. Put a magnetic stirrer in each reactor vial, then tighten a vial cap.
4. Place all eight vials in a Pierce heating/stirrer module.
5. Insert a thermocouple, connected to a temperature display unit, into a slot on the vial block of the heating/stirrer module.
6. Set a heater switch to "HIGH" position, then set the "HIGH" temperature controller knob to obtain a desired temperature and the stirrer speed controller knob to a desired mixing speed.
7. Remove two reactor vials, one with catalyst and one without catalyst, every 6 h reaction time. The last pair of vials will be removed at 24 h reaction time.
8. Sample analysis in each vials are similar to the organic acid analysis described by Lourvanij and Rorrer (1993).

HMF Reaction Analysis

Materials

HMF weight: 0.25 g

Distilled water weight: 43.35 g

Catalyst: H-Y zeolite

Catalyst weight: 0.17 g

Internal standard: Butyric Acid, 18.006 mg
myo-Inositol, 90.072 mg

Process Parameters

Reaction temperature: 130°C

Total reaction time: 24 h

Table K-1. Reactions of HMF with HY-zeolite catalyst at 130°C.

Time (h)	% moles of HMF (with catalyst) Experiment # 1	% moles of HMF (without catalyst) Experiment # 1	% moles of HMF (with catalyst) Experiment # 2	% moles of HMF (without catalyst) Experiment # 2
0.0	100.00	100.00	100.00	100.00
6.0	20.39	95.29	18.97	87.51
12.0	24.68	93.68	18.03	85.48
18.0	18.57	88.29	15.61	83.63
24.0	16.58	72.74	15.27	76.23

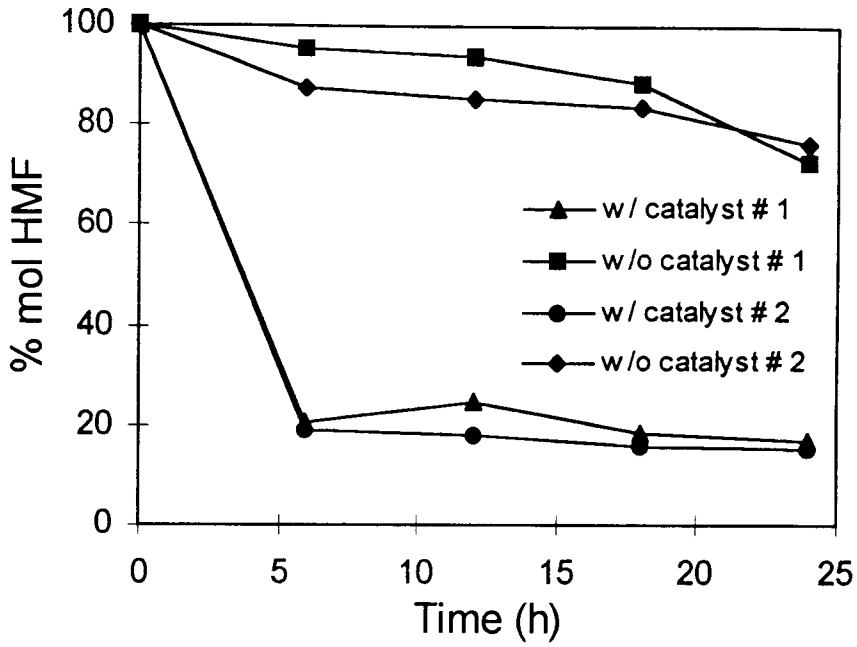

Figure K-1. HMF conversion vs. reaction time at 130°C for HY-zeolite catalyst.

4-Oxopentanoic Acid Reaction Analysis

Materials

4-oxopentanoic acid weight: 0.54 g

Distilled water weight: 50.04 g

Catalyst: H-Y zeolite

Catalyst weight: 0.17 g

Internal standard: Butyric Acid, 18.006 mg

myo-Inositol, 90.072 mg

Process Parameters

Reaction temperature: 130°C

Total reaction time: 24 h

Table K-2. Reactions of 4-oxopentanoic acid with HY-zeolite catalyst at 130°C.

Time (h)	% moles of 4-oxopentanoic acid (with catalyst) Experiment # 1	% moles of 4-oxopentanoic acid (without catalyst) Experiment # 1	% moles of 4-oxopentanoic acid (with catalyst) Experiment # 2	% moles of 4-oxopentanoic acid (without catalyst) Experiment # 2
0.0	100.00	100.00	100.00	100.00
6.0	38.12	87.42	41.11	92.26
12.0	37.38	85.78	35.95	86.16
18.0	41.39	91.22	34.22	85.86
24.0	37.56	87.91	29.30	87.72

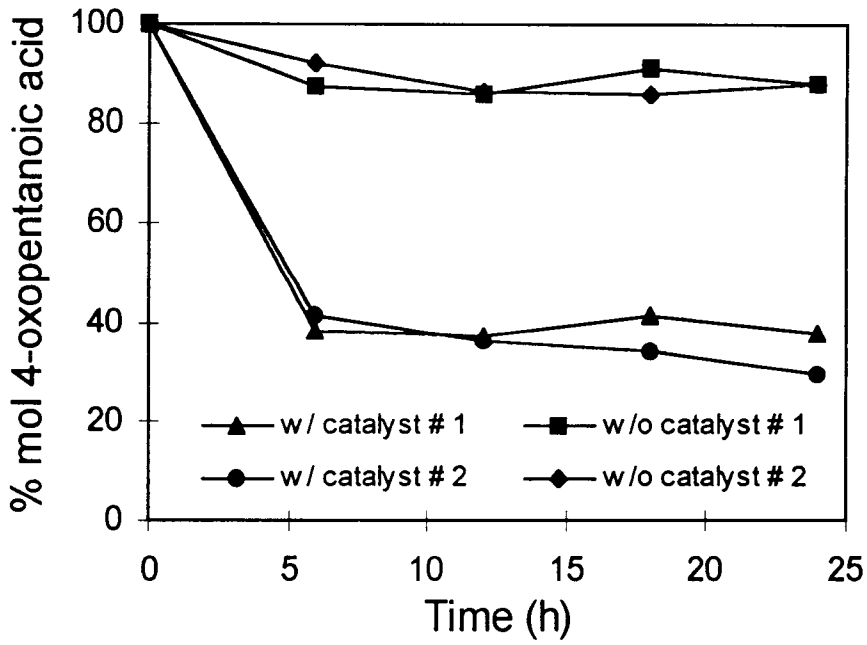

Figure K-2. 4-oxopentanoic acid conversion vs. reaction time at 130°C for HY-zeolite catalyst.

Appendix L

Reactions of Glucose with Bentonite

Introduction

Bentonite is any clay mineral that predominantly consists of smectite clay, montmorillonite. The remainder of bentonite contents is a mixture of mineral impurities and various other clay minerals, depending on geological origin. Therefore, the bentonite properties are mainly represented by montmorillonite properties (Diddams, 1992).

Bentonite used in this reaction study with glucose has the empirical formula of $Na[Si_{69.78}Al_{21.25}Mg_{4.94}Ca_{2.12}K_{0.39}O_{180.16}Fe_{27.5}]$, BET surface area of 87.0 ± 0.22 m^2/g, and acid activity of 0.20 mmol H^+/g.

Reaction Analysis

Materials

(D)-Glucose weight: 20.03 g

Distilled water weight: 150.03 g

Catalyst: Astraben 10, bentonite clay

Catalyst weight: 10.0124 g

Internal standard: Butyric Acid, 18.391 mg
myo-Inositol, 75.001 mg

Process Parameters

Reaction temperature: 130°C

Mixing speed: 300 rpm

Total reaction time: 24 h

Pressure: 30-60 psi

Table L-1. Reactions of glucose with bentonite clay at 130°C.

Time (h)	Glucose (mol/L)	HMF (mol/L)	Fructose (mol/L)	Formic Acid (mol/L)	4-Oxopentanoic Acid (mol/L)
0.0	0.7570	0.0000	0.0000	0.0000	0.0000
1.0	0.6607	0.0028	0.0479	0.0000	0.0000
2.0	0.6717	0.0034	0.0489	0.0000	0.0000
3.0	0.6619	0.0031	0.0580	0.0000	0.0000
4.0	0.6429	0.0040	0.0663	0.0000	0.0000
5.0	0.6293	0.0062	0.0708	0.0000	0.0000
6.0	0.6164	0.0086	0.0669	0.0000	0.0000
7.0	0.6152	0.0107	0.0662	0.0000	0.0000
8.0	0.5945	0.0133	0.0766	0.0000	0.0000
9.0	0.5920	0.0153	0.0713	0.0000	0.0000
10.0	0.5852	0.0181	0.0699	0.0000	0.0000
12.0	0.5768	0.0211	0.0750	0.0000	0.0000
14.0	0.5716	0.0262	0.0735	0.0000	0.0000
16.0	0.5571	0.0310	0.0687	0.0000	0.0000
24.0	0.5238	0.0357	0.0741	0.0000	0.0000

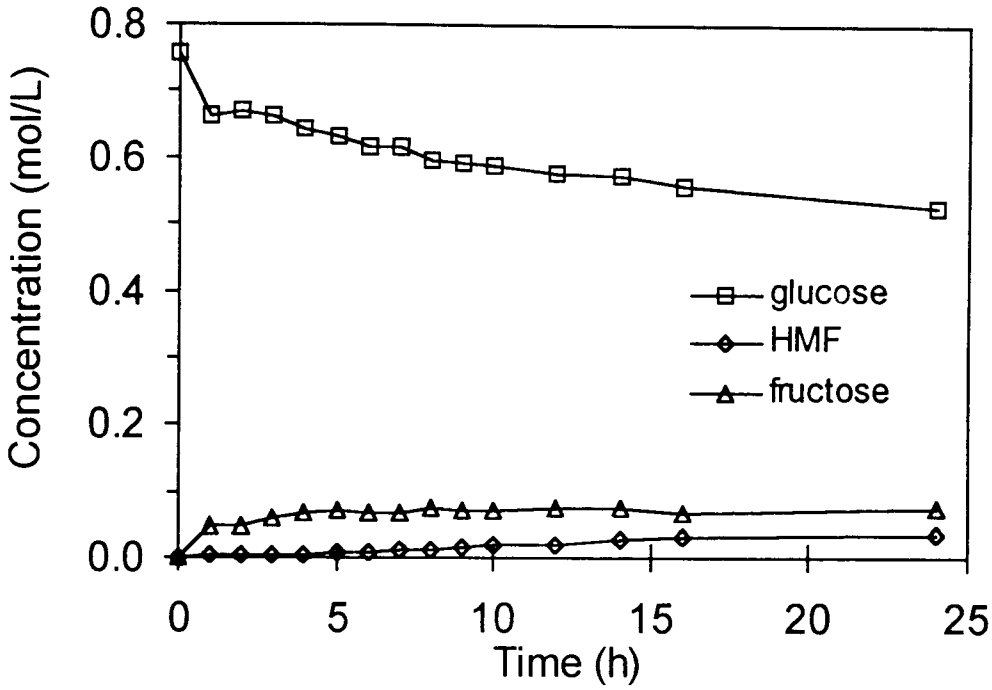

Figure L-1. Glucose conversion and product distribution vs. reaction time at 130°C for bentonite clay.

Reference

Diddams, P. 1992. Inorganic Supports and Catalysts - an Overview. In *Solid Supports and Catalysts in Organic Synthesis*, ed. K. Smith, 24. New York: Ellis Horwood and PTR Prentice Hall.

Appendix M

Reactions of Fructose with HY-zeolite

Reaction Analysis

Materials

(D)-Fructose weight: 20.01 g

Distilled water weight: 150.07 g

Catalyst: HY-zeolite

Catalyst weight: 5.0051 g

Internal standard: Butyric Acid, 19548 mg
Manitol, 60.039 mg

Process Parameters

Reaction temperature: 150°C

Mixing speed: 400 rpm

Total reaction time: 24 h

Pressure: 30-60 psi

Table M-1. Reactions of fructose with HY-zeolite at 150°C.

Time (h)	Fructose (mol/L)	HMF (mol/L)	Glucose (mol/L)	Formic Acid (mol/L)	4-Oxopentanoic Acid (mol/L)
0.0	0.7359	0.0000	0.0000	0.0000	0.0000
1.0	0.6365	0.0000	0.0000	0.0599	0.0085
2.0	0.5340	0.0279	0.1026	0.0500	0.0093
3.0	0.2247	0.0570	0.0690	0.2080	0.0089
4.0	0.1227	0.0483	0.0632	0.2953	0.0095
5.0	0.0391	0.0630	0.0252	0.3159	0.0288
6.0	0.0241	0.0644	0.0184	0.2794	0.0203
7.0	0.0158	0.0568	0.0125	0.3190	0.0175
8.0	0.0119	0.0513	0.0104	0.2883	0.0264
9.0	0.0071	0.0437	0.0066	0.2656	0.0244
10.0	0.0000	0.0362	0.0041	0.2561	0.0227
12.0	0.0000	0.0223	0.0012	0.2236	0.0209
14.0	0.0000	0.0183	0.0000	0.2108	0.0257
16.0	0.0000	0.0089	0.0000	0.2155	0.0201
24.0	0.0000	0.0000	0.0000	0.1904	0.0247

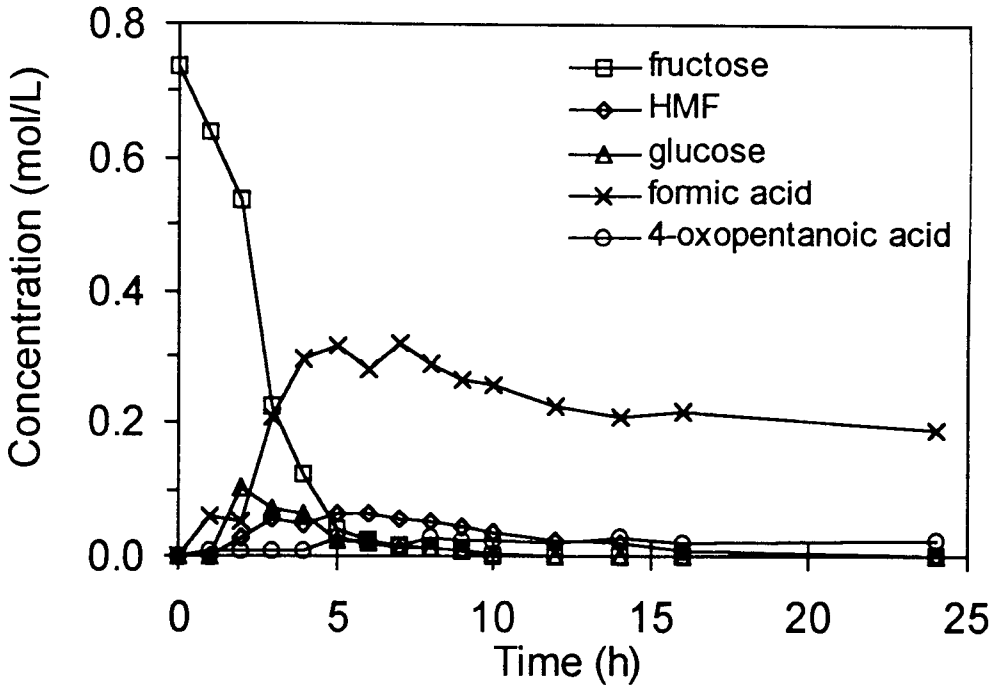

Figure M-1. Fructose conversion and product distribution vs. reaction time at 130°C for HY-zeolite catalyst.

Appendix N

Estimated Model Parameters for Pillared Clay Catalysts

Table N-1. Estimated model parameters at 130 to 170°C for the HM catalyst.

Temperature (°C)	130	150	170
k_{S1} (1/h)	0.378	3.309	6.781
k_{S2} (1/h)	1.463	7.903	7.954
$1/K_{S1}$	2.385	4.840	2.887
k_{S3} (1/h)	1.278	0.194	5.251
k_{S4} (1/h)	11.830	0.000	0.779
k_{S5} (1/h)	24.600	45.923	39.782
k_{S6} (1/h)	0.000	3.378	8.178
k_{S7} (1/h)	0.000	15.724	24.056
K_G (L/mol-h)	0.629	0.743	0.874
K_H (L/mol-h)	0.192	0.504	1.253
K_F (L/mol-h)	0.758	0.731	1.404
K_{FA} (L/mol-h)	0.000	0.679	0.818
K_{OA} (L/mol-h)	0.000	2.602	1.158

Table N-2. Estimated model parameters at 130 to 170°C for the CPM catalyst.

Temperature (°C)	130	150	170
k_{S1} (1/h)	2.556	6.897	13.085
k_{S2} (1/h)	5.895	21.922	25.059
$1/K_{S1}$	2.685	2.333	2.003
k_{S3} (1/h)	0.000	1.453	10.974
k_{S4} (1/h)	5.359	8.656	18.682
k_{S5} (1/h)	11.531	21.695	21.452
k_{S6} (1/h)	0.000	3.213	1.499
k_{S7} (1/h)	24.833	12.532	3.426
K_G (L/mol-h)	0.955	1.090	1.344
K_H (L/mol-h)	1.885	1.201	1.821
K_F (L/mol-h)	0.949	1.103	1.567
K_{FA} (L/mol-h)	0.000	0.321	0.300
K_{OA} (L/mol-h)	2.483	0.627	0.571

Table N-3. Estimated model parameters at 130 to 170°C for the FPM catalyst.

Temperature (°C)	130	150	170
k_{S1} (1/h)	1.095	9.062	43.430
k_{S2} (1/h)	5.118	21.872	0.746
$1/K_{S1}$	0.261	2.341	0.000
k_{S3} (1/h)	9.172	14.521	0.000
k_{S4} (1/h)	22.158	18.955	62.402
k_{S5} (1/h)	30.148	46.767	50.997
k_{S6} (1/h)	0.000	0.000	0.000
k_{S7} (1/h)	30.829	62.387	0.000
K_G (L/mol-h)	0.732	1.252	1.597
K_H (L/mol-h)	2.023	2.944	2.437
K_F (L/mol-h)	0.866	1.187	0.000
K_{FA} (L/mol-h)	0.000	0.000	0.000
K_{OA} (L/mol-h)	1.522	3.076	0.000